DYNAMICS AND MOTION REGULATION OF A FIVE-LINK BIPED ROBOT WALKING IN THE SAGITTAL PLANE

BY

XIUPING MU

A Thesis

Submitted to the Faculty of Graduate Studies

In Partial Fulfillment of the Requirements

For the Degree of

DOCTOR OF PHILOSOPHY

Department of Mechanical and Manufacturing Engineering

The University of Manitoba

Winnipeg, Manitoba

Canada

THE UNIVERSIT OF MANITOBA

FACULTY OF GRADUATE STUDIES

*****

COPRIGHT PERMISSION

DYNAMICS AND MOTION REGULATION OF A FIVE-LINK BIPED ROBOT WALKING IN THE SAGITTAL PLANE

BY

XIUPING MU

A Thesis/Practicum submitted to the Faculty of Graduate Studies of The University of Manitoba in partial fulfillment of the requirement of the degree of

DOCTOR OF PHILOSOPHY

Abstract

Five-link biped has been developed for decades with advantages of its simplicity in modeling and adequacy in representing typical bipedal locomotion. However, establishment of modeling and control for the five-link biped has not been achieved satisfactorily. This thesis presents a systematic study of the dynamics and control of five-link biped walking on level ground.

Firstly, the dynamic model of a complete gait cycle in the sagittal plane is developed, which includes the single support phase, double support phase and impact. A novel kinematic model has been constructed for the five-link biped by modifying the conventional definition of certain physical parameters of the system and it has greatly simplified the derivation procedure and the final form of the dynamic equations. A general model to describe the impact dynamics of planar multi-link robotic collisions is also formulated and solved for cases when the Jacobian matrices are either full-ranked or rank-deficient.

Next, a systematic method is proposed for synthesizing a cyclic biped gait allowing for adjustments to various ground conditions. A method of formulating the compatible trajectories with time polynomial functions for the hip and the swing leg end tip motion is first provided and the joint angle profiles are determined accordingly. Based on the dynamic formulation and motion planning, the sliding mode control law is developed, for the first time, to regulate the motion during the double support phase where the biped is treated as a redundant manipulator. The stability and the robustness of the controller are also investigated, and its effectiveness is demonstrated by computer simulations.

Finally, the impact dynamics and its effects on the contact events of a five-link biped walking are studied. A parametric analysis is performed to correlate the type of impact with certain gait parameters and the results are presented in graphical form in the parameter space. Through the parametric analysis, the regions are identified, for the first time in literature, where none of the single or double impact can occur or both types of impact may occur. These results reveal important physical insights into the mechanisms of biped impact and facilitate motion planning and motion regulation such that desired gait with prescribed contact events can be produced.

The work enables us to gain an in-depth understanding of dynamics and control of bipedal locomotion. It also serves as a stepping stone to the study of the mechanics of human walking and to the development of biped robots. The formulation and methodology developed here can not only benefit the research on biped systems, but also make contributions to the analysis of many multi-link serial chain robotic systems.

Acknowledgements

First and foremost, I would like to express my deepest thanks to my supervisor, Dr. Christine Q. Wu for giving me the opportunity to pursue doctoral studies. Thank you for providing continuous guidance, stimulating suggestions, patience and encouragement that helped me throughout the course of my research and writing of this thesis.

My sincere appreciation goes to the members of my advisory committee members, Dr. Nariman Sepehri, Dr. Steve Onyshko and Dr. Abba Gumel, for their careful review, comments and suggestions with regard to this thesis. Thanks to Dr. A.B. Thornton-Trump, for providing me with the suggestions at the early stage of my research. I also wish to thank Dr. Qingjin Peng, for teaching me one of my favorite courses and providing me much help during my study. Thanks also to Dr. Hooshang Hemami, the external examiner of the thesis examination committee.

I thank my fellow students in the Nonlinear Systems Research Laboratory for valuable discussions. To those whose names are not listed your supports did not go unnoticed.

Finally, I wish to thank my husband for his ubiquitous love, support and many sacrifices during my study. I also thank my mother, my father, my sisters and their families for their infinite love and support. I could not have accomplished my goals without any of them.

Table of Contents

List of Figures

List of Tables

Chapter 1

Introduction

1.1 General Background

1.1.1 Motivations

The main applications of study of biped locomotion systems may be in the following aspects: to have better understanding of motion of natural physiological systems from biological or biodynamical point of view; to construct prosthetic appliances for disabled people or amputees; and to design humanoid robots to perform onerous labor work or hazardous tasks (Hemami *et al.* 1973).

From a scientific perspective, researchers study legged systems with the similarities to animal or human locomotion to better understand the principles of locomotion in biological systems. From a practical perspective, devices and mechanisms can be built with legged characteristics to perform various gait patterns. On one hand, by studying the characteristics of biped locomotion, one can design and manufacture artificial limbs or part of limbs as prostheses for humans. On the other hand, one can build walking mechanisms as alternatives to wheeled vehicles with the recognized mobility advantages such as moving on rough terrain. Especially with the development and availability of powerful computers and microprocessors, biped robots may be built to fulfill various kinds of tasks which are in hazardous environments for humans, or perform onerous or reiterative labor work which are degrading to humans. Thus, it is of great significance to study biped locomotion.

1.1.2 Preliminary Remarks

Theoretical and applied studies of biped locomotion have focused on dynamic modeling, motion planning, motion control and walking stability (Hemami *et al.* 1973, Shih 1996). Biped locomotion has been studied using knowledge of classic dynamics, robotics, control theory, etc. For the last two decades, research on biped locomotion has been actively put into practice by making a legged robot capable of walking and running with advanced technologies (Honda Motor Co. 2004).

The present difficulties to construct a highly mobile and dynamically stable biped locomotion stems from a lack of a complete dynamic model to describe the biped motion and the deficiency of a reliable control algorithm to perform the biped locomotion with system uncertainties and environment disturbances. First, development of an artificial mechanism to duplicate anthropomorphic type locomotion is a very complicated and difficult problem. This is not only because of the complexity to describe a solid mathematical model with high non-linearity due to multi-degrees of freedom (DOF) and coupling of the mechanical structure, but also because of the diversity of biped walking patterns for various purposes and ground conditions. Second, as the biped system requires highly dynamic stability in locomotion, the control problem of a biped is more difficult than that of the industrial manipulators which may be described as problems of positioning end-effectors. Also the naturally tipping over unstable tendency and the collision phenomenon due to heel strike make the control problem extremely difficult.

The study of biped locomotion is still incomplete. A lot of work needs to be done in biped modeling, motion planning and stability control. To study biped locomotion, one should choose the model structure as simple as possible, as long as its performance

satisfies the requirements from researcher's interests. A practical biped robot may be built based on a considerably simplified version of human being, such as allowing the biped walking on only a flat horizontal ground within the sagittal plane, but should have some basic features of human walking, such as allowing both feet on the ground with a certain period of time (Mitobe *et al.* 1997). Actually this feature which is often mentioned as double support is crucial in keeping biped walking stably and in a wide range of speed (Sonoda *et al.* 1997). However, double leg support phase is quite often ignored in literature due to the difficulty of motion regulation. Another feature of human walking, impact (heel strike), should also be considered in biped modeling. Biped impact during walking not only brings system angular velocity discontinuities, but also dictates the forthcoming contact event of the lower limbs with the ground, i.e., either a single support phase (SSP) or a double support phase (DSP), or slippage of the foot/feet following impact. This information is crucial for motion planning and regulation, however the related literature is sparse.

In motion planning, systematic methods, other than experimental methods, have been developed to synthesize the biped gait. Basically, there are two distinct approaches in designing the desired joint angle profiles. One is using parametric formulations that prescribe the biped motion by generating a set of objective functions to solve biped joint angle profiles (Hurmuzlu, 1993a). The other is using numerical approximation to generate the joint angle profiles by polynomial functions or periodic spline interpolation, etc (Shih 1997, Cabodevila and Abba 1997, Chevalleraeau and Aoustin 2001, Huang *et al.* 2001). For the first method, desirable joint angle profiles for continuous and steady walking must also satisfy some additional conditions, such as repeatable gait, no scuffling

and no hyperextensions at knee joints. These extra conditions impose restrictions on the selection of objective functions, initial conditions and associate gait parameters, and can make the synthesis of biped gait extremely challenging. The second method overcomes these disadvantages and can be used satisfactorily to design biped joint angle profiles for control purposes. However, the computing load may be high for large bipedal systems and the selection of the polynomials may impose undesirable features to the joint angle profiles (Chevalleraeau and Aoustin 2001). Moreover, some basic requirements for desired joint angle profiles, such as providing smooth trajectories and maintaining stable walking, have not been considered thoroughly in previous literature.

Biped control is another difficult problem since motion of multiple-DOF biped robot is highly nonlinear. Firstly, the system parameter uncertainties and the environment disturbances sometimes may greatly affect the control performance. Secondly, motion of a biped system in the DSP can be described as the motion of a dynamic system under holonomic constraints which make the control problem much complicated. Lastly, the main purpose to control a biped is to maintain dynamically stable walking, and thus the stability is also an important problem under consideration for motion planning and regulation. Robust control, especially sliding mode control, has been successfully applied to biped SSP to remove the system uncertainties and stabilize the system, however in previous literature it has not been applied to the DSP due to aforementioned problems.

All of the above facts motivate the ongoing research on biped robots. In the following parts, the progress of recent biped research is briefly highlighted and the important aspects of this thesis work are outlined.

1.2 Literature Survey

Researchers have long been interested in studying movable robots. Those robots can be designed with wheels or with legs for different uses. Wheeled robots have higher stability and are easier to control. Legged robots are much more difficult to control but have higher mobility than wheeled robots, especially when climbing stairs, stepping across or jumping over obstacles or walking on uneven surfaces. Those legged robots can be distinguished as hopper (one leg), biped (double legs), quadruped (four legs), hexapod (six legs), etc. MIT Leg Laboratory have built and implemented various walking/jumping/running machines having one to four legs (Raibert and Brown 1984, Raibert 1986). The first legged robot built in MIT is a planar hopper with a small foot, which achieved balance and dynamic stability in jumping locomotion. Such one-legged robots can provide theoretical and practical guide in modeling and regulation of multi-legged robots. In 1984 MIT built a quadruped which can run by trotting using gait generalization of one-leg algorithms. Such robots were studied and built by other researchers. Francois (1998) addressed the problem of control and stability of a planar hopper which could be central to a better understanding of the potentials and limitations of legged locomotion.

Generally speaking, the more legs a robot has, the more stable walking can be realized, the more complex controllers are needed (Sonoda *et al.* 1997). In all those legged robots/machines, the biped draws much attention to researchers. Biped is a class of walking robots that imitates human locomotion. Biped robot research is centered in Japan and the United States. Waseda University has been one of the leading research institutes for anthropomorphous robots and has developed a series of biped walkers since

1972. Miura and his colleagues in Tokyo University have developed five types of bipeds since 1980 and all of them are statically unstable but can perform a dynamically stable walking with suitable control (Miura and Shimoyama 1984). Honda Motor Corp. (2004) has developed several legged robots that are autonomous in terms of energy and computation. Their latest biped robot ASIMO with more human-friendly design was developed in 2000. In United States, a series of walking or running biped robots have been built in MIT Leg Laboratory since 1985 (Raibert 1986). Recently, an anthropomorphous biped robot "Johnnie" is currently being developed at the University of Munich (Gienger *et al.* 2001). Nowadays, various human-shaped robots are being developed that can fulfil certain tasks and be well-suited for operating within specific environments (Kagami *et al.* 2001).

Biped study can be used for both research and practical purposes. The main purpose to study biped is to obtain stable locomotion with desired gait using an appropriate control law. Many biped studies focus on dynamic modeling, motion planning and motion regulation. The following sections give the detailed literature information about these topics.

1.2.1 Dynamic Modeling

Dynamic modeling is a complicated problem that requires knowledge of classic mechanics, nonlinear mathematics and dynamics. The major problem to fully describe a locomotion system that imitates human walking is associated with a large number of DOFs and the highly coupled nonlinearities involved in the dynamic system, e.g., for natural human walking, more than 20-DOFs may be involved (Golliday and Hemami 1977). Description of such a system would lead to great dynamic complexity. Studies of

such complex systems require certain simplifications. Therefore, the first task to study bipedal locomotion is to select a mechanical model with few DOFs to keep the equations of motion at a manageable level and yet reasonably describe the motion of interest.

Numerous approaches to study human/biped locomotion simplify the dynamic model of the system to that of an inverted pendulum (Chow and Jacobson 1971, 1972, Hemami *et al.* 1973, Hemami and Golliday 1977, Hemami *et al.* 1978, Hemami, and Katbab 1982, Muira 1984, Kajita and Tanie 1991, Wu, *et al.* 1998). Inverted pendulum may be considered as the simplest model to represent a biped locomotion system. An inverted pendulum model can be studied to solve problems of simple periodic locomotion and posture stability of a biped system. As is pointed out by Wu *et al.* (1996, 1998), one aspect in the study of human locomotion is to investigate the unstable equilibrium of the trunk about the upright position and to find the control law that human uses during walking, while the human trunk, in a simplified form, can be modeled as an inverted pendulum with up to three degrees of rotational freedom. Chow and Jacobson (1971) modeled human upper body as an inverted pendulum with the prescribed base point moving only in the vertical direction. Hemami (1980) used a control system approach to study bipedal locomotion by using an inverted pendulum model and the system was stabilized by position and rate feedback. Muira (1984) worked on the biped stability by using an inverted pendulum and developed two biped robots that could walk in a dynamically stable mode. Kajita and Tanie (1991) presented a dynamic biped locomotion on rugged terrain using a linear inverted pendulum model. Wu *et al.* (1998) studied a base-excited (in 3D space) inverted pendulum with two degrees of rotational freedom to predict major features of upper body dynamics and stability.

However, the single inverted pendulum model seems too simple to describe biped locomotion completely. Some researchers made a further assumption that the biped motion can be thought of being oscillatory like a pendulum for the swing leg and like an inverted pendulum for the supporting leg (Kajita *et al.* 1992, Cabodevila and Abba 1997). The model to describe bipedal locomotion has then increased to 2-DOF and brought the idea of using a two-link double inverted-pendulum model (Golliday and Hemami 1976, Hemami and Camana 1976, Hemami 1978, Hurmuzlu and Moskowitz 1986, Wu and Swain 2002). Hurmuzlu and Moskowitz (1986) developed a mathematical model of a double inverted-pendulum locomotion system and studied the stability and the role of impact in the motion. Yi (1999) proposed a controller for passive ankle joints modeled as a two-link inverted pendulum with one actuator and tested on the nine-link target robot, SD-2 at the Ohio State University. However, even one inverted pendulum is inherently unstable, the trajectory of the robot's center of gravity depends significantly on maintaining the stable walking gait and is difficult to vary the speed during walking because the biped walking cycle is determined by the inverted pendulum model natural frequency (Mitobe *et al.* 1995).

In the following research since late 1970s, biped system has been developed from 3-DOF up to 9-DOF. Three-link biped was studied/built by Hemami and Wyman (1979a and 1979b), Hurmuzlu and Moskowitz (1987a), Miura and Shimoyama (1984), etc., but the mechanical structure is not the same. Hemami and Wyman (1979a and 1979b), Hurmuzlu and Moskowitz (1987a) established three-link biped model as one upright trunk and two lower limbs, like an inversed "Y" shape. Miura and Shimoyama (1984) developed two types 3-DOF bipeds, Biped-1 and Biped-2. Each of them has two lower

limbs representing the legs and a link located at the pitch axis representing the hip—looks like a "Π" shape. Four-link bipedal model was studied by Hurmuzlu and Moskowitz (1987b), Pandy and Zajac (1990), Iqbal *et al.* (1993). Their kinematic structures are similar to Miura's three-link biped, except one more element representing the upper body.

A general five-link biped is modeled with a torso and two legs, each leg consisting of a thigh and a shank. Such a five-link biped model has the advantage that it has sufficiently few DOFs to establish the mathematical model of its motion yet still has enough DOFs to adequately describe the motion which can imitate a simplest human-like locomotion. Thus, such a model has received most attention and found in much literature (Hemami and Farnsworth 1977, Ceranowicz 1980, Hurmuzlu 1993a and 1993b, Tzafestas, *et al.* 1996, Cabodevila 1997, Hardt and Mann 1999, Lum *et al.* 1999, Chi and Shih 2000, Wu and Chan 2002, Ma and Wu 2002).

For the five-link biped model, although feet are not included, much may be modeled in ways which do not increase the DOFs to the system by assuming that the massless feet are included (Hurmuzlu 1993a). For example, two of the main contributions of the feet are the introduction of ankle torques and the lift-off force produced as the heel comes off of the ground besides the supporting and cushioning purpose (Hardt and Kreutz-Delgado 1999). Actually, it is possible to introduce ankle torques in the dynamic model by treating those as input torques at the tips of the limbs in contact with ground without mass feet. Also, the lift-off force to the feet can be replaced by instantaneous impulsive force or constraint forces at the tip of the supporting leg (Hardt and Kreutz-Delgado 1999).

Bipeds with more than five links describe more accurate locomotion but increase the complexity. Like adding two more links to a five-link biped, representing two feet, the biped system becomes 7-DOF. Onyshko and Winter (1980) studied human locomotion using such a seven-link biped model. Shih (1996) has addressed the dynamic and control problems with such a model. Huang (2001) also described a method for motion planning of a seven-link biped model and tested on a 12-DOF biped robot. Eight-link biped has been found in Koopman's work (1995). Nine-link biped is a rather complicated model to describe human walking and usually has been implemented as walking robots, found in Furusho and Sano (1990), Zheng and Shen (1990), and Tagawa and Yamashita (1981).

Besides the choice of DOFs affecting the establishment of the biped dynamic model, various kinds of walking patterns and configurations require different modeling approaches. Such complicated motion includes the 3-dimentional walking (Raibert 1986, Pandy and Berme 1989), stopping/standing (Reisinger and Moskowitz 1999), running and jumping (Caux and Zapata 1999), jogging (Gienger *et al.* 2001), turning (Kane and Scher 1970, Chen *et al.* 1986), side-stepping (Goddard *et al.* 1983) and side-to-side swaying (Iqbal *et al.* 1993).

Hemami and Wyman (1979a, b) presented a method of modeling and control of dynamic systems including holonomic constraints and applied to a three-link biped locomotion using non-reduced state space. Based on the derived constraint forces as explicit functions of the state and the input, a general model is presented to apply to both the constraint case and unconstraint cases. The unconstraint cases correspond to the single support case. The constraint case is when both limbs are in contact with the ground, i.e., the DSP. The SSP has been widely studied because of its simple and periodic

nature and possibility to describe a biped walking cycle. The DSP can be applied to the biped model as a state indicating an instantaneous period of time (Hemami and Farnsworth 1977, Chevallereau *et al.* 1998), or the case during which the biped is moving forward with the contact points unchanged (Mitobe *et al.* 1997, Sonoda *et al.* 1997, Huang *et al.* 2001). Hemami (1980) proposed a feedback on-off model of biped dynamics where the internal and external forces acting on the biped system are unified as constraint forces which are functions of state and inputs. When any constraint is satisfied, its feedback loop which includes the force is on and when the constraint is violated the feedback loop is off. For this model, the original dimension of the system is maintained at all times. When the constraints are applied, the motion of the system is limited to subspaces of a larger state space, but for sensing and control the entire state is available at all times. This model shows a way to deal with transitions from one constrained configuration to another.

Another issue related to biped dynamic modeling is impact. Impact occurs naturally during biped locomotion as a result of the collision or contact of the free end of the limb with the environment. The velocities of the biped body and limbs will be subject to an instantaneous change before and after impact. Some previous bipedal locomotion research focuses primarily on the SSP while ignoring the events of impact and transfer of support (switching due to phase change). Some studies deliberately ignored impact (Chow and Jacobson 1971, Hardt and Mann 1980). Some studies assumed zero tip velocities at heel strike so that the impulsive forces occurring at heel strike can be avoided (Kajita and Tanie 1991, Channon *et al.* 1992). Other approaches have established elastic heel model to study impact (Hemami and Farnsworth 1977, Khandelwal and

Frank 1974, Hatze 1981). As mentioned by Zheng and Hemami (1984), this kind of walk implies a high level of consciousness that humans do not ordinarily practice when walking, even with elastic heel an impact phenomenon still persists. In Zheng and Hemami's (1984, 1985) work, impact problems were studied and modeled. The impact model was established by a correlation between the velocity changes and the magnitude of the impulsive forces by an infinitesimal time integration of the dynamic equation with swing tip touchdown constraints. The prerequisite for the solution of their model is that the Jacobian matrix must be full-ranked (Zheng and Hemami 1985). According to the model, conclusions were drawn that impact may cause large internal impulsive forces to the body and the magnitude of the impulse is related to different postures before impact. Tzafestas *et al.* (1996) applied this method to deduct the velocity changes for a five-link planar biped impact.

Furusho and Sano (1990) derived a mathematical model for nine-link biped locomotion with single support, instantaneous double support and "touchdown" phase. The "touchdown" phase is a biped collision phenomenon. In solving the dynamics, they used Lagrange's impulsive equation to get the angular velocities of each link just after touchdown as functions of those velocities before touchdown. This method actually has no difference from Zheng and Hemami's (1984) work and gives the same results in the end, both of which are from Lagrangian mechanics point of view.

Hurmuzlu and Moskowitz (1986) introduced both impact and switching in two-link biped locomotion system and addressed the role of impact and switch in the stability and progression of bipedal locomotion. They indicated that the swing-leg impact with the ground enabled the system to avoid certain unstable trajectories and therefore was the

major factor of a contribution to stable locomotion. Their work on impact and switching continued with the application to 3-link (Hurmuzlu and Moskowitz 1987a), 4-link (Hurmuzlu and Moskowitz 1987b) and 5-link (Hurmuzlu 1993a, 1993b, Chang and Hurmuzlu 1993) bipeds. In their work, however, the impact dynamics was solved by applying the principle of the conservation of linear and angular impulse and momentum. The equations were derived in the Cartesian coordinate system and this approach can be considered to be in the category of Newtonian mechanics. This was a different approach from Zheng and Hemami's work. One of the advantages is that the impulsive forces at both contact ends in horizontal and vertical directions can be solved simultaneously. Moreover, two categories of impact—single and double impact were clearly defined, such that a single impact is followed by a SSP while the double impact is followed by a DSP. The dynamic equations describing each impact event were introduced with a general form.

To sum up, the contributions to biped dynamic modeling made in recent studies can be described as four main aspects: an inverted pendulum has been presented as the simplest model to investigate biped locomotion and posture stability; a general five-link biped has been modeled to adequately describe the motion which can imitate a basic human locomotion; more complicated biped models have been developed to describe accurate locomotion which imitate various human walking patterns; one of the important phenomena of biped locomotion—impact event has been considered and introduced to biped dynamic modeling. However, there also exist some problems in biped dynamic modeling. Firstly, for the most popular five-link biped, an important feature—DSP has been received less attention in previous literature. DSP exists in natural human walking

and can provide for more stable locomotion (Mitobe *et al.* 1997, Huang *et al.* 2001). Thus it should be considered in biped dynamics. Secondly, although impact dynamics has been outlined and modeled in previous literature, it has not been found in detailed formulation regarding the two categories of impact (single and double impact). Other major problems include the fact that the current biped dynamic formulations are more complicated than those of robot manipulators. The conventional kinematic model needs improving such that the dynamic equations can be derived efficiently with the model. A complete biped model including a SSP, a DSP and impact should be studied in detail to perform more accurate biped locomotion.

1.2.2 Motion Planning

For a biped robot to progress in a desired direction, it is natural to have one leg supported on ground while the other moves forward. However, formulation of such walking patterns for a biped is not a simple task. It results in many problems, such as balance, stability and control difficulties. The approach used to synthesize the biped gait depends, so to speak, on the inclination of the researchers.

Most early studies did not consider a systematic method to design the biped walking patterns. For example, Zarrugh and Radcliffe (1979) have investigated the biped walking pattern by recording human kinematic data. Furusho and Masubuchi (1986) have developed several walking patterns for a biped robot based on numerical and experimental approaches. Vukobratovic *et al.* (1990) have studied biped locomotion by using human walking data to prescribe the motion of the lower limbs. Methods using computer recording or analysis of gait data were developed for the design and control of biped locomotion. Thornton-Trump and Daher (1975) have devised a method using

computer analysis of gait data to determine the translational and angular accelerations of the limbs during normal locomotion and this work has produced a guide to the design of stable external polycentric knee joints. Hemami and Farnsworth (1977) have studied posture and gait stability of a planar five-link biped tested by simulation. Computer-television recording of angles and angular velocities of all primary segments of a human in normal walking was taken and used as reference input to the system in order to generate torques for such locomotion. Onyshko and Winter (1980) have used the measured data of joint moments and applied them to the link segment model to produce a desired walking cycle for a seven-link biped. They have shown that a normal human walking cycle can be achieved and, with minor modification, typical gait patterns could also be achieved. As pointed out by Hurmuzlu (1993a), since a practical walking machine would be considerably simpler than human, the validity of mimicking the dynamics of a system without a good knowledge of its internal structure and its strategies is questionable.

Systematic methods for biped gait synthesis are developed by recent researchers. Hurmuzlu (1993a, 1993b) developed a parametric formulation that ties together the constraint functions and joint angle profiles. The constraint functions are cast in terms of coherent physical characteristics of gait, which has been used to generate the joint angle profiles of a 5-link biped during a SSP. Four quantities were used to characterize the motion of biped, including step length, progress speed, maximum step height and stance knee bias. Comparing with earlier locomotion literature, Humuzlu's method fills the gap in the design of walking machines regarding the specification of objective functions. However, to have continuous and repeatable gait, the postures at the beginning and end of

each step have to be identical. This requires a proper selection of specific initial conditions, constraint functions and their associated gait parameters. Ma and Wu (2002) developed a general necessary and sufficient condition for repeatable gait when the highest order of the differential equations among the constraint equations is one. This condition provides a guideline for selecting constraint functions and their associated gait parameters in the context of producing repeatable gait based on Humuzlu's method. However, finding repeatable gait when constraint equations involve higher order differential equations still remained unsolved. The restriction of creating repeatable gait and the lack of rules for selecting proper initial angles, constraint functions and their gait parameters have severely limited the applications of Hurmuzlu's method.

The above problem such as the selection of proper initial conditions to generate repeatable gait can be remedied by using numerical methods by approximating the joint angle profiles through Fourier's series expansion (Cabodevila and Abba 1997), time polynomial function (Red 2000, Chevallereau and Aoustin 2001), or periodic spline interpolation (Shih 1997, Huang *et al.* 2001). One advantage of such techniques is that extra constraints, such as repeatability of gait, can be easily included by adding the coefficients to the polynomials. Disadvantages include that the computing load is high for large bipedal systems and the improper selection of the polynomials may impose undesirable features to the joint angle profiles (Chevallereau and Aoustin 2001).

Aside from the requirements of geometric configurations and kinematic characteristics, a biped robot model must be built to maintain stable locomotion. To keep biped walking forward, either static or dynamic gait, must be considered. By the explanation of terminology described by McCown-McClintick and Moskowitz (1998),

static biped walking occurs when the biped center of gravity remains over the stance foot area as the swinging leg moves, while the dynamic walking is faster and does not depend on the center of gravity placement for stability. Early literature was found for building biped walking pattern based on static stability requirement (Zheng and Shen 1990, Kato 1984, Miura and Shimoyama 1984). Static stability requirement is not enough to adapt wide range of biped walking speed. Dynamically stable walking criterion chosen for biped locomotion was well accepted in the latest studies (Kajita and Tanie 1991, Channon *et al.* 1992, McCown-McClintick and Moskowitz 1998, Chevallereau *et al.* 1998, 1999, Huang 2001), including much faster dynamic patterns like running (Raibert 1986, Caux and Aapata 1999, Chevallereau and Aoustin 2001). To maintain dynamically stable walking, methods (Shil 1990, Hirai *et al.* 1998, Huang 2001) have been proposed for synthesizing walking patterns based on the concept of zero moment point (ZMP) (Vukobratovic 1973). The ZMP is defined as the point on the ground about which the sum of all the moments of the active forces equals zero. If the ZMP is within the convex hull of all contact points between the feet and the ground, the bipedal robot can walk stably. In Shil's (1990) and Hirai's (1998) work, the ZMP trajectory was first designed and the hip motion and joint angle profiles are then derived. In Huang's (2001) work, however, the constraints of parameters, which can produce different types of foot motion to adapt to ground conditions were first formulated, and then methods were introduced to generate biped trajectories with the largest ZMP stability margin.

Also, there are many investigations to focus on low energy trajectories in synthesising biped walking patterns. Energy minimization for biped locomotion becomes a promising topic. Channon *et al.* (1992), Rostami and Bessonnet (1998), Roussel *et al.* (1998),

Chevallereau *et al.* (1998, 2001) have proposed various methods of gait generation by minimizing the cost function of energy consumption, but their cost functions are different. Channon (1992) generated the motions of hip and feet of a planar seven-link biped during a regular step by third-order polynomial functions, the coefficients of which are obtained by numerically minimizing an energy cost function. Chevallereau and Aoustin (2001) introduced an optimal cyclic gait for a non-ankle-torque five-link biped walking and running by defining each of the four joint angles a fourth-order polynomial function. The coefficients of the polynomials were chosen to optimize some criteria (maximal advance velocity, minimal torque and minimal energy) and to insure cyclic motion of the biped.

When designing the biped gait, most of previous work (Shil 1991, Seo and Yoon 1994, Chevallereau and Aoustin 2001) formulated the joint angle profiles. Chow and Jacobson (1971) studied the optimal biped locomotion and first drew attention to the hip motion and suggested that the hip trajectory be synthesized prior to joint angle profile design because the hip motion plays an important role of walking stability. Channon (1992) and Huang *et al.* (2001) adopted this idea and synthesized walking patterns for seven-link bipedal robots. One advantage of this approach that the authors did not mention is that the hip joint divides the biped into three sub-systems—an upper body and two lower legs and thus the approach can simplify the gait synthesis procedure.

Clearly, the literature has addressed the superiority of systematic formulations to experimental approaches in gait generation and various systematic methods have been developed in recent studies for biped joint profile design. Two classic approaches, parametric formulation and numerical approximation have both their advantages and

disadvantages. In the survey of prevailing literature dealing with biped motion planning, a thorough consideration with some basic requirements for desired joint angle profiles, such as providing smooth trajectories, minimizing impact effect and maintaining stable walking, considering a full gait cycle with both single and double leg support phase, was not well received in previous literature.

1.2.3 Motion Control

In early studies, a biped system was often linearized about the upright position. Based on the linearized system, linear feedback stability control laws were used so that the equilibrium point was stable under disturbances (Golliday and Hemami 1976, Hemami and Wyman 1979a, Hemami 1980, Ceranowicz 1980). Since the biped system is highly nonlinear, linear control laws are not suitable to handle such systems. To fulfill the various requirements for biped regulation, non-linear controls are often used.

Vukobratovic, who has done one of the most extensive studies of biped locomotion, concluded that the way to settle a control problem in multivariable systems is to decompose the system. Accordingly, an adequate control of the system should be organized on the principle of hierarchy in compliance with the aim of the tasks (Vukobratovic and Juricic 1969). A natural division of such control was outlined as decision-making level, algorithmic level and dynamic level. Miyazaki and Arimoto (1980), Furusho and Masubuchi (1986, 1987), Furusho and Sano (1990), Borovac *et al.* (1989), Shih (1996) ever realized biped motion control by hierarchical structures. Other control strategies often used for biped motion regulation include neural network control (Kawato *et al.* 1987 and 1988, Dinneen and Hemami 1993, Hu *et al.* 1999) and hybrid

control (Chevallereau *et al.* 1998, Song *et al.* 1999, Park and Chung 2000, Silva and Machado 2001), etc.

Biped walking was generally implemented by nonlinear control algorithms due to its highly nonlinear dynamics. Hemami and Camana (1976) used a nonlinear feedback control in a simple model of a locomotion system to produce postural stability and to construct desired periodic trajectories. Based on their work, one can see the effectiveness for de-coupling, periodic motion and stability. Mitobe *et al.* (1995) also utilized such a nonlinear feedback controller to control the position and velocity of the biped center of gravity. Computed torque control is a classical nonlinear control based on the feedback linearization technique, i.e., using a control law with the structure similar to that of the system's dynamic model to eliminate the nonlinearities involved in the model and with error signals as feedback input for a better track of the reference trajectories. Mitobe *et al.* (1997) controlled the motion of a 4-DOF biped robot during the DSP and applied the computed torque control algorithm to the system. In their work, the position of center of gravity of the trunk is formulated as the reduced space independent generalized coordinate, and the control problem is defined as a trajectory tracking problem which the motion of the trunk center of gravity is controlled to track a desired trajectory.

In the control of biped system locomotion, uncertainties regarding the values of parameters and the imprecision of the dynamic model usually exist. To face this problem, two main techniques namely robust control and adaptive control are available in dealing with such systems. Adaptive control is an approach to estimate the uncertain parameters on-line based on the measured signals and to use the estimated parameters in the control input computation (Slotine and Li 1991). The effectiveness of this control technique was

investigated by Yang and Shahabuddin (1994) in the five link biped model. Robust control utilizes control design methodologies to retain assurance of system performance in spite of model inaccuracies and changes (Dorf and Bishop 1998). Robust sliding mode control has received much attention because of its high insensitivity to parameter variations and external disturbances (Slotine and Sastry 1983, Slotine 1984). Chang and Hurmuzlu (1993) derived a sliding mode control law that eliminates the reaching phase and provided a mechanism to directly influence the tracking errors in a planar five-link biped during the SSP. Park and Kim (2001) applied the sliding mode control to solve the stable dynamic walking of a 3D 14-DOF biped robot. Tzafestas *et al.* (1996) applied a sliding mode control algorithm to a five-link biped walking during the SSP and compared with computed torque control. The experimental results showed that sliding mode control is considerably superior to computed torque control in the presence of parameter uncertainties.

Another challenge in biped motion regulation is the control of biped walking with constraints. Motion of a biped in the DSP can be described as motion of the system under holonomic constraints as the contact position between the feet and ground are fixed. These constraints introduce two difficulties in motion regulation. One is that the generalized coordinates used in the SSP are no longer independent. Another difficulty is that the constraint forces are not provided *a priori* but are among the unknowns of the system, which must be obtained from the solution one seeks (Goldstein 1980). Control of constrained dynamic systems with application to 3-link biped model was studied by Hemami and Wyman (1979a, 1979b), Hemami (1980). In their work, the constraint forces were computed as functions of the generalized coordinate system with the states of

angles and angular velocities. The constraint forces were then used as control inputs to maintain or to deliberately violate the constraints between constrained and free motion. The control problem was solved in non-reduced space. Mitobe *et al.* (1997) proposed a control method to a 4-DOF biped robot during the DSP. The position in the Cartesian system of the biped center of gravity was selected as the independent generalized coordinates which belong to reduced-space. A computed torque control law was utilized to stabilize the independent generalized coordinates and the constraint forces. Sonoda *et al.* (1997) introduced an approach to a 4-link biped control utilizing redundancy in the DSP. They considered the biped robot during the DSP as a redundant manipulator, and set a general acceleration reference formulation to each joint given by a performance function with null space vector, which decides robot's configuration. By choosing the performance function of the null space input in compliance with the aim of desired task, various configurations control of the robot can be realized.

From review of prevailing literature it can be concluded that the nonlinear control strategies have been widely used in biped locomotion and motion regulation of the SSP has been well established. As the robust control techniques, especially sliding mode control, were successfully applied to biped locomotion with single support, good performance can be achieved in the presence of parameter uncertainties. However, control of the DSP is still not satisfactory. The constraints involved in the DSP introduce difficulties for motion regulation. These difficulties can be solved by introducing a set of independent generalized coordinates to describe the constrained system and to eliminate the constraint forces (Goldstein 1980). However, although theoretically speaking the choice of the proper set of independent coordinates can be chosen arbitrarily, some

selections of such a reduced state space coordinate system may result in extreme difficulty in transformation. Also, if the related transformation matrix is not square and thus is not invertible, it may cause challenges in controller design. Accordingly, robust sliding mode techniques were not found in controlling the five-link biped DSP. These problems need to be solved in biped motion control.

1.2.4 Biped Stability and Contact Event Study

Biped motion must satisfy stability requirements. Vukobratovic *et al.* (1970) introduced the general stability of all legged machines into three categories: body stability; body path stability; and stationary gait stability. They are described as follows: (*i*) The biped is considered body stable if there exists a closed region R which encloses the undisturbed trajectory of the three earth angles (body angular orientations with respect to earth) and the altitude (distance between the system body's center of gravity and the ground) such that if the machine is disturbed by a disturbance, the trajectory returns to the region R as time becomes infinite. (*ii*) The path of the biped body in space is considered stable if the average velocity vector returns towards its original direction and magnitude after a disturbance. (*iii*) A stationary gait stability is considered stable if the characteristic factors (parameters to describe the gait, such as average constant forward velocity, stride, cycle time, etc.) of the undisturbed system represented by a k-vector g lie within a volume v_0 and if after a disturbance, the vector g_n returns and remains within v_0. These stability theorems, especially the third one, gait stability, are widely used in biped locomotion study and design.

Early work on stability of biped models was restricted to small deviations about vertical stance (Vukobratovic 1970, Golliday and Hemami 1976, Hemami and Golliday

1977, Hemami and Cvetkovic 1977). Lyapunov stability theory was used to analyze the biped posture stability. Hemami and Wyman (1979) proposed a modeling and control method to constrained dynamic systems with application to a three-link biped based on Lyapunov's linearization method. Feedback linearization and pole-assignment techniques can be attempted for the control of such nonlinear systems. Hemami and Cvetkovic (1977) used Lyapunov's direct method for estimating the region of the stability and transient time of two biped models and designed the nonlinear on-off feedback controller using their constructed Lyapunov function. Wu *et al.* (1998) presented a methodology of Lyapunov stability control to achieve the upright balance of a base-excited inverted pendulum with two degrees of rotational freedom. A piecewise continuous controller which guarantees the solution trajectories to be arbitrarily close to the upright position was designed based on Lyapunov theories and then the system stability was traded off with a weaker one by smooth functions to prevent chattering of control torques. The robustness analysis shows that the system stability is not sensitive to the variation of the physical parameters and base point movement measurements as long as the measured base point accelerations are overestimated. This work provided a solid framework in the study of posture stability and control of biped movement.

To ensure the dynamic stability and to prevent the tipping over of a biped, several criteria for the evaluation and control of the system are raised, such as center of pressure (CoP) (Marchese *et al.* 2001, Silva and Machado 2001), foot rotation indicator (FRI) (Goswami 1999), force-angle stability measure (Paradopoulos and Rey 1996), and zero moment point (ZMP) (Vokobratovic and Stepanenko 1973). Vokobratovic and Stepanenko (1973) first raised the idea of ZMP and it is the most popular criterion in the

study of biped dynamic walking. ZMP criterion has been used in biped controller design (Vanel and Gorce 1997, Stojic and Chevallereau 2000), and in gait synthesis (Shih *et al.* 1990; 1996; Huang *et al.* 1997, Chi and Shih 2000). It plays an important role in the analysis and design of biped dynamic locomotion.

Another factor to affect walking stability is biped contact event (SSP/DSP or slippage of foot/feet) due to impact. Impact interrupts the continuous movement and indicates the forthcoming contact phases or slippage of the foot (feet). The type of impacts (single or double impact) and its associated contact event occurring after impact are determined by the nature of physics of the biped systems and the environment. Research on impact in the context of biped contact event is relatively limited. A distinguished work related to the biped contact event can be found in Hurmuzlu (1993). In his work, a parametric analysis was carried out to correlate the outcome of the contact between the lower limbs and the ground with the gait parameters associated with the objective functions. Results for the single and double impact regions without slipping were presented. However, the results of the parametric study were restricted to his objective functions.

Overall, present stability theories and methodologies have provided solid framework in the study and analysis of biped posture stability and control stability. Biped parametric analysis with the type of impact and its associated contact event provides important information in selecting parameters for desired gait design and facilitating motion regulation such that a stable walking can be obtained. However, such study has been fairly limited.

1.3 Objectives and Scope of this Thesis

The five-link biped mathematical model has been worked on for decades with advantages of its simplicity in modeling and adequacy in representing typical legged-locomotion. However, establishment of modeling and control for the five-link biped has not been achieved satisfactorily. For example, a detailed model and robust sliding mode control of a DSP has not been found in previous five-link biped study. Also, although the prediction of the forthcoming contact event associated with the pre-impact parameters is found to provide critical information for motion planning and motion regulation, it has not been studied thoroughly. Furthermore, the dynamic equations in previous work are complex and lengthy. Especially, it is extremely difficult to conduct a contact event study through previously introduced impact solutions. Thus, the goal of this thesis is to contribute to the development of dynamic modeling and motion regulation of a five-link biped locomotion system walking in the sagittal plane by solving these challenges.

The first objective is to develop the mathematical model that describes a detailed planar biped walking motion. An improved kinematic model is also required to simplify the modeling procedure and final equations. Toward this goal, a complete dynamic model including a SSP, a DSP, impact and switching due to phase change is developed with a modified kinematic model by treating the biped system as an open-loop series chain. A general form of impact model is also developed and solved regardless of the rank of the Jacobian matrix. The simplicity of the entire dynamic equations facilitates the control design and contact event study.

The second objective is to provide a strategy for biped motion planning and motion regulation. Firstly, to present a systematic methodology for synthesizing biped gait

trajectories for control purposes. A desirable biped gait should perform a cyclic and steady walking and allow adjusting to various ground conditions. Also it should not be too complicated for synthesis. Secondly, to develop a strategy for motion regulation with a robust control algorithm based on sliding mode techniques applied to biped DSP. The chattering problem should be avoided and the system stability must be guaranteed insensitively to the variation of biped system physical parameters. To fulfil these requirements, the motion of the trunk and hip is planned and regulated for the DSP where the biped is considered as a redundant system.

The third objective is to conduct a parametric study to correlate the type of contact events with certain gait parameters via impact effects. Firstly, the explicit solutions for impulses and post-impact angular velocities are derived and examined from the impact dynamics. Secondly, a correlation of the contact events with certain biped system parameters and gait parameters via impact effects is investigated. The key parameters are selected based on the explicit solutions from the impact model, which are not restricted by specific objective functions. Lastly, the results are provided in graphical form to show the relationship among the locomotion parameters and specific contact regions. The parametric analysis provides important information to facilitate motion planning and regulation of stable walking.

1.4 Thesis Organization

The remainder of this thesis is as follows. Chapter 2 develops a complete dynamic model for the five-link planar biped locomotion, including a SSP, a DSP, impact and switching due to phase exchange. A general impact model is also developed for multi-link rigid body collisions and a method is provided to solve the impact equations. Chapter

3 contains the gait synthesis of the planar five-link biped walking on level ground. The compatible trajectories of the hip and the swing limb are first designed, and the joint angle profiles are then calculated which will be used as reference input for motion regulation. Chapter 4 is devoted to the motion control for biped walking. Main objective is the motion regulation of the biped DSP. The sliding mode control techniques are employed to biped locomotion. The stability and the robustness of the controller are investigated, and its effectiveness is demonstrated by computer simulations. Chapter 5 investigates the impact phenomenon and its effects on the contact events of five-link biped walking on level ground. A parametric study is performed to correlate the type of impact with certain gait parameters and the results are presented in graphical form in the parameter space. The conclusions and recommended future work are outlined in Chapter 6.

Chapter 2

Dynamic Modeling

2.1 Introduction

It is sufficient to study the posture or simple movement like swaying by employing a mechanical model with double inverted-pendulum (Hurmuzlu and Moskowitz 1986, Wu and Swain 2002) or three-link (Hemami and Wyman 1979a, 1979b) biped locomotion system. But such a model is not enough to have better understanding of biped walking. Generally speaking, many of the essential characteristics of sagittal human walking can be presented with a five-link planar biped model (Hemami and Farnsworth 1977, Hurmuzlu 1993a, 1993b, Tzafestas *et al.* 1996).

The biped locomotion with single foot support can be considered as an open-loop kinematic chain model (Vukobratovic and Ekalo 1973). The dynamic equations to describe such a biped SSP can be derived using standard procedure of Lagrangian formulation. Motion of a biped in the DSP can be thought as the movement of a robot under holonomic constraints where its model can be developed by Lagrangian formulation with constraint conditions (Hemami and Wyman 1979a, 1979b).

The main objective of this chapter is to develop a complete planar five-link biped walking model. The kinematic model of a planar five-link biped robot is described in Section 2.2. The dynamic equations of the five-link biped locomotion with both the SSP, the DSP, impact and switching due to phase change are derived in Section 2.3. The impact dynamics representing a general multi-link collision problem is thoroughly

discussed and derived in Section 2.4. For the first time, the impact dynamics is investigated when the Jacobian matrix is rank-deficient. The presented generalized impact equation and its explicit solution can be applied conveniently to the biped collision problems and provide significant insight into the impact dynamics for biped locomotion.

Nomenclatures

The nomenclatures of the biped model is given below:

m_i mass of link i

l_i length of link i

d_i distance from the mass center of link i to joint i (refer to Figure 2.1)

I_i moment of inertia of link i about the axis passing through the center of mass of link i and perpendicular to the sagittal plane

θ_i angle of link i about the vertical, ccw for "+"

q_{i-1} relative angle between links: $q_{i-1}=\theta_{i-1}-\theta_i$, $q_i=1,2...5$

(x_b, y_b) the coordinate of the supporting point B

(x_e, y_e) the coordinate of the tip of the swing limb E

τ_0 control torque at the ankle of the stance limb

τ_1 control torque at the knee of the stance limb

τ_2 control torque at the hip connecting the torso and the stance limb

τ_3 control torque at the hip of the swing limb

τ_4 control torque at the knee of the swing limb

$a_i = \begin{cases} 0 & \text{when i} = 3; \\ 1 & \text{when i} \neq 3; \end{cases}$ i=1,2...5. a_i is a constant number used in dynamic model.

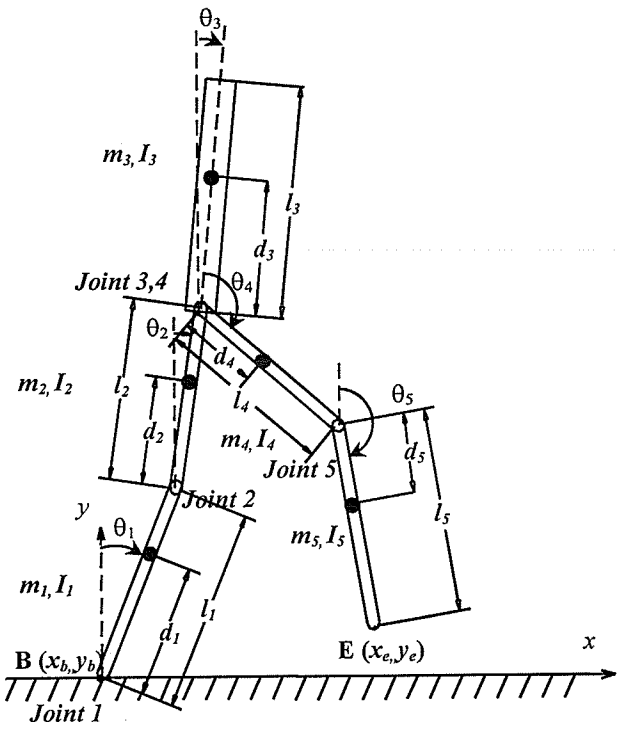

Figure 2.1 A planar five-link biped model

2.2 Five-Link Biped Kinematic Model

The biped under study consists of five links: a torso and two identical lower limbs with each limb having a thigh and a shank. Also the biped has two hip joints, two knee joints, and two ankles at the tips of the lower limbs. There is an actuator located at each joint and all of the joints are considered rotating only in the sagittal plane and friction free. Massless feet are assumed to simplify the modeling. Although the dynamics of the feet is neglected, it is assumed that the biped can apply torque at the ankles (Hurmuzlu 1993). During the DSP, a torque is applied at the leading ankle whereas the rear ankle does not possess a torque but can rotate through the knee torque and the effect of gravity (Chi and Shih 2000). The friction between the tip and the ground is assumed sufficient to prevent slippage during walking.

Figure 2.1 depicts a schematic representation of this biped model. Each link of the biped has an associated mass m, moment of inertia I, length l and the location of its center of mass d. As the two legs are symmetric, the mass, moment of inertia and length of the two thighs and two shanks should be identical. In most previous five-link biped study (Hemami and Farnsworth 1977, Furusho and Masubuchi 1986, 1987, Furusho and Sano 1990, Seo and Yoon 1995, Tzafestas *et al.*1996, Lum *et al.* 1999, Chan 2000), the location of mass center d and the physical angle θ representing the orientation of each link has been defined by treating the system as symmetric. In Figure 2.1, the biped system has been considered as a successive open loop of kinematic chain from the support point to the free ends, as robot manipulators. With such a series kinematic chain model, the dynamic equations can be derived more conveniently, the final forms of the dynamic equations can be significantly simplified and consequently the computation and programming will also be simplified. The comparison of the dynamic equations using the modified definitions in kinematics and the conventional ones is outlined in Section 2.3.5 to show the superiority of this modified model.

According to the relationship between the links shown in Figure 2.1, the position and velocity of the tip of swing limb are formulated as:

$$\begin{aligned} x_e &= \sum_{i=1}^{5}\left(a_i l_i \sin\theta_i\right) + x_b, \\ y_e &= \sum_{i=1}^{5}\left(a_i l_i \cos\theta_i\right) + y_b, \\ \dot{x}_e &= \sum_{i=1}^{5}\left(a_i l_i \dot{\theta}_i \cos\theta_i\right) + \dot{x}_b, \\ \dot{y}_e &= -\sum_{i=1}^{5}\left(a_i l_i \dot{\theta}_i \sin\theta_i\right) + \dot{y}_b. \end{aligned} \tag{2.1}$$

The position and velocity of the center of mass of link i are formulated as:

$$
\begin{aligned}
x_{ci} &= \sum_{j=1}^{i-1}\left(a_j l_j \sin\theta_j\right) + d_i \sin\theta_i + x_b, \\
y_{ci} &= \sum_{j=1}^{i-1}\left(a_j l_j \cos\theta_j\right) + d_i \cos\theta_i + y_b, \\
\dot{x}_{ci} &= \sum_{j=1}^{i-1}\left(a_j l_j \dot{\theta}_j \cos\theta_j\right) + d_i \dot{\theta}_i \cos\theta_i + \dot{x}_b, \\
\dot{y}_{ci} &= -\sum_{j=1}^{i-1}\left(a_j l_j \dot{\theta}_j \sin\theta_j\right) - d_i \dot{\theta}_i \sin\theta_i + \dot{y}_b.
\end{aligned}
\tag{2.2}
$$

Equations (2.1) and (2.2) will be used to derive the dynamic equations, detailed in the following section.

2.3 Dynamic Model of Biped Walking

The differential equations of the dynamic motion of the five-link biped are derived using Lagrangian formulation and Newton-Eular formulation. In this section, the biped motion is modeled with five parts: SSP, DSP, single/double impact, switching due to the phase change, and transformation of dynamic model for purpose of applying joint torques instead of generalized torques.

The potential energy P (assume $P=0$ at ground level) of the five-link biped model is:

$$
P = \sum_{i=1}^{5} P_i = \sum_{i=1}^{5} m_i g y_{ci} = \sum_{i=1}^{5}\left\{ m_i g \cdot \left[\sum_{j=1}^{i-1}\left(a_j l_j \cos\theta_j\right) + d_i \cos\theta_i \right] \right\}, \tag{2.3}
$$

and the kinetic energy is

$$
K = \sum_{i=1}^{5} K_i = \sum_{i=1}^{5}\left(\frac{1}{2} m_i v_{ci}^2 + \frac{1}{2} I_i \dot{\theta}_i^2 \right) = \sum_{i=1}^{5}\left[\frac{1}{2} m_i (\dot{x}_{ci}^2 + \dot{y}_{ci}^2) + \frac{1}{2} I_i \dot{\theta}_i^2 \right]. \tag{2.4}
$$

where $\frac{1}{2} m_i v_{ci}^2$ and $\frac{1}{2} I_i \dot{\theta}_i^2$ are translational kinetic energy and rotational kinetic energy, respectively. And for each link, the kinetic energy is solved in detailed form as:

$$
\begin{aligned}
K_i = {} & \frac{1}{2}\{I_i + m_i d_i^2\}\dot{\theta}_i^2 + \frac{1}{2} m_i \left[\sum_{j=1}^{i-1}\left(a_j l_j \dot{\theta}_j \cos\theta_j\right) \right]^2 + \frac{1}{2} m_i \left[\sum_{j=1}^{i-1}\left(a_j l_j \dot{\theta}_j \sin\theta_j\right) \right]^2 \\
& + m_i d_i \dot{\theta}_i \left\{ \sum_{j=1}^{i-1}\left[a_j l_j \dot{\theta}_j \cos(\theta_i - \theta_j) \right] \right\}
\end{aligned}
\tag{2.5}
$$

The kinetic energy and potential energy will be employed in the Lagrange formula to solve the dynamic equations for the SSP and the DSP.

2.3.1 Single Support Phase

The SSP is characterized by a stance limb in contact with the ground and the other limb swinging from the rear to the front. This phase begins with the tip of the swing limb leaving the ground and terminates with the swing limb touching the ground. The contact point between the stance limb tip and the ground are fixed in the fixed frame. The Lagrangian equation of the motion of the SSP can be expressed as

$$\frac{d}{dt}\left(\frac{\partial K}{\partial \dot{q}_i}\right)-\frac{\partial K}{\partial q_i}+\frac{\partial P}{\partial q_i}=Q_i, \tag{2.6}$$

where q_i and Q_i represent the generalized coordinates and generalized forces. Substituting Equations (2.3)-(2.5) into the Lagrange Equation (2.6) gives the desired biped model (see Appendix I for detail). The Lagrange dynamic model describing the motion of the biped in the SSP can be written as a vector equation

$$D(\theta)\ddot{\theta}+H(\theta,\dot{\theta})\dot{\theta}+G(\theta)=T_\theta, \tag{2.7}$$

where $D(\theta)$ is the 5×5 positive definite and symmetric inertia matrix, $H(\theta,\dot{\theta})$ is the 5×5 matrix related to centrifugal and Coriolis terms, $G(\theta)$ is the 5×1 matrix of gravity terms, θ, $\dot{\theta}$, $\ddot{\theta}$, T_θ are the 5×1 vectors of generalized coordinates, velocities, accelerations and torques, respectively. The detailed forms of D, H, G in Equation (2.7) are presented as follows:

$$D_{ij}=p_{ij}\cos(\theta_i-\theta_j), \tag{2.8a}$$

$$H_{ij}=p_{ij}\sin(\theta_i-\theta_j)\dot{\theta}_j, \tag{2.8b}$$

$$G_i = g_i \sin\theta_i , \tag{2.8c}$$

where $i, j=1,2...5$, p_{ij} and g_i are inertial terms defined as

$$p_{ij} = \begin{cases} I_i + m_i d_i^2 + a_i\left(\sum_{k=i+1}^{5} m_k\right) l_i^2 & j = i \\ a_i m_j d_j l_i + a_i a_j\left(\sum_{k=j+1}^{5} m_k\right) l_i l_j & j > i \\ p_{ji} & j < i \end{cases},$$

$$g_i = m_i d_i g + a_i\left(\sum_{k=i+1}^{5} m_k\right) l_i g .$$

Note that using the open-loop kinematic chain model, the detailed final form of the dynamic Equations (2.8) is much simplified as compared with the conventional form as typically shown in previously published articles (Furusho and Masubuchi 1986 and 1987, Tzafestas *et al.* 1996). The comparison of the detailed forms of the equation with conventional ones will be discussed in Section 2.3.5 and Appendix III.

2.3.2 Double Support Phase

In the DSP, both limbs are in contact with the ground while the body can move forward slightly. This phase begins with the front limb touching the ground and ends with the rear limb taking off the ground (see Figure 2.2). As both of the contact points between the lower limbs and the ground are fixed during the DSP, there exists a set of holonomic constraint equations:

$$\Phi(\theta) = \begin{pmatrix} f_1 \\ f_2 \end{pmatrix} = \begin{pmatrix} x_e - x_b - L \\ y_e - y_b \end{pmatrix} = \begin{pmatrix} \sum_{i=1}^{5} (a_i l_i \sin\theta_i) - L \\ \sum_{i=1}^{5} (a_i l_i \cos\theta_i) \end{pmatrix} = 0 . \tag{2.9}$$

where L is the distance of the tips of the two lower limbs and is a constant in each step. The Lagrangian equation of motion during the DSP is

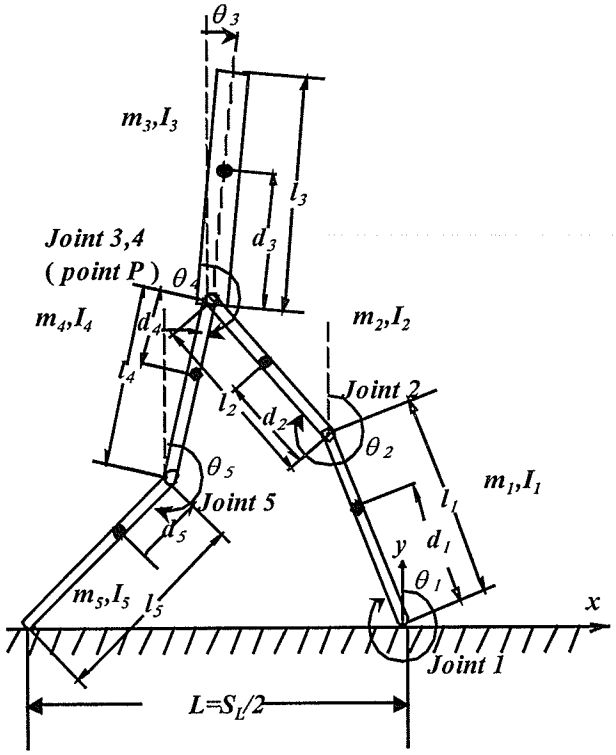

Figure 2.2 Biped model in double support phase

$$\frac{d}{dt}\left(\frac{\partial K}{\partial \dot{q}_i}\right)-\frac{\partial K}{\partial q_i}+\frac{\partial P}{\partial q_i}=Q_i+\frac{\partial \Phi}{\partial q}\lambda, \tag{2.10}$$

where λ is the vector of Lagrange multipliers, $(\partial\Phi/\partial q)\lambda$ represents the constraint forces. Substituting Equations (2.3)-(2.5) into (2.9) and (2.10), the dynamic model to describe the DSP is solved as

$$D(\theta)\ddot{\theta}+H(\theta,\dot{\theta})\dot{\theta}+G(\theta)=J^T(\theta)\lambda+T_\theta, \tag{2.11}$$

where D, H, G, T_θ are the same as in Equation (2.7), λ is a 2×1 vector of Lagrange multipliers, and J is the 2×5 Jacobian matrix: $J=\partial\Phi/\partial\theta$. The dynamic model describing the DSP can be written as

$$\begin{cases} D(\theta)\ddot{\theta} + N(\theta,\dot{\theta}) = J^T(\theta)\lambda + T_\theta & \text{(2.12a)} \\ \Phi(\theta) = 0 & \text{(2.12b)} \end{cases}$$

where and hereafter $N = H(\theta,\dot{\theta})\dot{\theta} + G(\theta)$.

As a dynamic system under holonomic constraints, a set of independent generalized coordinates is possible to be found to formulate the dynamic equations which can describe the constraint system without using the terms of constrained forces (Goldstein 1980, Mitobe *et al*, 1997). In the present studied five-link biped DSP, the set of independent generalized coordinates should be chosen in R^3. In the DSP as the two tips are fixed on the ground, the motion of the biped system can be fully described by the hip and trunk motion. It is natural to think of selecting the hip position and the trunk orientation as the independent generalized coordinates, i.e., let the independent generalized coordinates be $p \in R^{3\times 1}$: $\underline{p} = (x_h \quad y_h \quad \theta_3)^T$, where $(x_h, \quad y_h)$ is the coordinate of hip position. Note that p is a function of θ:

$$p(\theta) = \begin{pmatrix} l_1 \sin\theta_1 + l_2 \sin\theta_2 \\ l_1 \cos\theta_1 + l_2 \cos\theta_2 \\ \theta_3 \end{pmatrix}. \qquad \text{(2.13)}$$

Differentiating Equation (2.13) twice with respect to time, yields

$$\dot{p} = R\dot{\theta}, \qquad \text{(2.14)}$$

$$\ddot{p} = \dot{R}\dot{\theta} + R\ddot{\theta}, \qquad \text{(2.15)}$$

where $R = \dfrac{\partial p}{\partial \theta} \in R^{3\times 5}$. Combining Equations (2.12), (2.13) and (2.14), (2.15) yields

$$\begin{pmatrix} R \\ J \end{pmatrix}\dot{\theta} = \begin{pmatrix} \dot{p} \\ 0 \end{pmatrix}, \qquad \text{(2.16)}$$

$$\begin{pmatrix} R \\ J \end{pmatrix}\ddot{\theta} = \begin{pmatrix} \ddot{p} \\ 0 \end{pmatrix} - \begin{pmatrix} \dot{R} \\ \dot{J} \end{pmatrix}\dot{\theta}. \tag{2.17}$$

It is obvious that $\begin{pmatrix} R \\ J \end{pmatrix} \in R^{5\times 5}$ is a full-rank matrix, thus is invertible. Thus, $\dot{\theta}$ and $\ddot{\theta}$ can be described as explicit functions of $\dot{p}$ and $\ddot{p}$. Combining (2.16), (2.17) and the DSP dynamic model from Equation (2.11), finally,

$$\begin{pmatrix} \ddot{p} \\ 0 \end{pmatrix} = \begin{pmatrix} \dot{R} \\ \dot{J} \end{pmatrix}\begin{pmatrix} R \\ J \end{pmatrix}^{-1}\begin{pmatrix} \dot{p} \\ 0 \end{pmatrix} + \begin{pmatrix} R \\ J \end{pmatrix}D^{-1}(T-N) + \begin{pmatrix} R \\ J \end{pmatrix}D^{-1}J^{T}\lambda. \tag{2.18}$$

Writing Equation (2.18) as

$$\begin{pmatrix} \ddot{p} \\ 0 \end{pmatrix} = S_a\begin{pmatrix} \dot{p} \\ 0 \end{pmatrix} + S_b(T-N) + S_c\lambda, \tag{2.19}$$

where $S_a = \begin{pmatrix} S_{a11,3\times 3} & S_{a12,3\times 2} \\ S_{a21,2\times 3} & S_{a21,2\times 2} \end{pmatrix} = \begin{pmatrix} \dot{R}\begin{pmatrix} R \\ J \end{pmatrix}^{-1} \\ \dot{J}\begin{pmatrix} R \\ J \end{pmatrix}^{-1} \end{pmatrix}$, $S_b = \begin{pmatrix} S_{b1,3\times 5} \\ S_{b2,2\times 5} \end{pmatrix} = \begin{pmatrix} RD^{-1} \\ JD^{-1} \end{pmatrix}$,

$S_c = \begin{pmatrix} S_{c1,3\times 2} \\ S_{c2,2\times 2} \end{pmatrix} = \begin{pmatrix} RD^{-1}J^{T} \\ JD^{-1}J^{T} \end{pmatrix}$. Note that S_{c2} is an invertible matrix. Equation (2.19) can be expressed as

$$\begin{cases} \ddot{p} = S_{a11}\dot{p} + S_{b1}(T-N) + S_{c1}\lambda & \text{(2.20a)} \\ 0 = S_{a21}\dot{p} + S_{b2}(T-N) + S_{c2}\lambda & \text{(2.20b)} \end{cases}$$

The difference between the Equations (2.20) and the conventional ones (2.11) is that in Equations (2.20) the constraint force term λ is separated from the second derivative vector $\ddot{p}$, and thus it can be first solved from (2.20b) and then used as known factor into (2.20a), finally,

$$\ddot{p} = B\dot{p} + C(T-N), \tag{2.21}$$

where $B = S_{a11} - S_{c1}S_{c2}^{-1}S_{a21}$, $C = S_{b1} - S_{c1}S_{c2}^{-1}S_{b2}$.

Equation (2.21) will be used as the dynamic model of five-link biped during the DSP to facilitate motion control shown in Chapter 4.

2.3.3 Biped Impact

Impact happens in an infinitesimal period of time as the swing limb collides with the ground and the joint velocities will be subject to a sudden jump resulting from this impact event. It is frequently assumed that biped impact is with rigid-to-rigid body point contact, perfectly plastic and occurs instantaneously* (Zheng and Hemami 1984, Hurmuzlu and Chang 1992, Hurmuzlu 1993a, Tzafestas *et al.* 1996).

The impact event can be specified as single impact and double impact. Single impact happens between two consecutive SSPs. The stance limb does not receive external impulses from the environment during single impact (Tzafestas *et al.* 1996, Gienger *et al.* 2001). When the single impact is completed, the leading swing leg touches the ground and receives all the ground reaction force and impulse force. Double impact happens between the SSP and the DSP (Hurmuzlu 1993a, Furusho and Sano 1990). When the swing leg comes into contact with the ground, impact occurs while the stance limb is still on the ground. Both lower limbs receive external impulse forces from the environment during double impact.

It should be noted that although the biped walking cycle includes a SSP and a DSP in the present study, one can not assume or guarantee that a double impact must occur between each phase change. This is because the following support phase results from the

* The term 'instantaneously' means that the impact happens in a very short period of time.

type of impact, whereas the type of impact is dictated by the system parameters and states prior to impact. If the controllers can not track the reference trajectories perfectly, the system states may deviate from the desired ones, and different states immediately before impact can lead to different type of contact events. Thus, both single impact and double impact should be considered and modeled in this work.

In this section, the double impact and single impact equations are solved using Newtonian impulse theory of the principle of the conservation of linear and angular impulse and momentum. An assumption is made before deriving the equations that the joints are frictionless and the impulse moment at each joint is negligible during impact.

The free-body diagram of link i during impact is shown in Figure 2.3. P_i and $P_{(i+1)}$ are the impulses to link i at joint i and $i+1$ respectively. The impulse and impulse moment equations for link i can be written as

$$m_i \Delta\dot{x}_{ci} = m_i \left[\Delta\dot{x}_b + \sum_{j=1}^{i-1} \left(a_j l_j \cos\theta_j \Delta\dot{\theta}_j \right) + d_i \cos\theta_i \Delta\dot{\theta}_i \right] = P_{iX} - P_{(i+1)X}, \qquad (2.22a)$$

$$m_i \Delta\dot{y}_{ci} = m_i \left[\Delta\dot{y}_b - \sum_{j=1}^{i-1} \left(a_j l_j \sin\theta_j \Delta\dot{\theta}_j \right) - d_i \sin\theta_i \Delta\dot{\theta}_i \right] = P_{iY} - P_{(i+1)Y}, \qquad (2.22b)$$

$$I_i \Delta\dot{\theta}_i = P_{(i+1)X}(a_i l_i - d_i)\cos\theta_i + P_{iX} d_i \cos\theta_i - P_{(i+1)Y}(a_i l_i - d_i)\sin\theta_i - P_{iY} d_i \sin\theta_i, \qquad (2.22c)$$

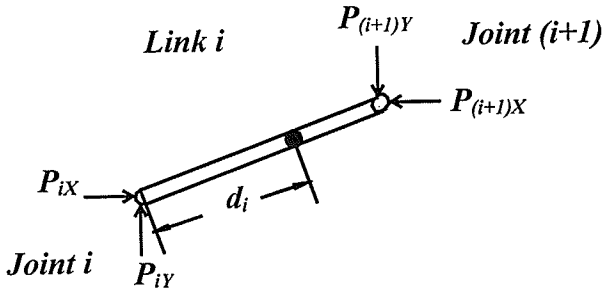

Figure 2.3 Free body diagram of a biped link at the instant of impact

where $\Delta\dot{x}_{ci}$, $\Delta\dot{y}_{ci}$ and $\Delta\dot{x}_b$, $\Delta\dot{y}_b$ are the horizontal and vertical velocity changes at the gravity center of link i and stance limb tip, respectively. Equation (2.22) will be used to derive the double and single impact models as follows. The conditions for the validity of the solutions are also investigated.

2.3.3.1 Double Impact

During double impact, there are impulsive forces between the contact points of the two limbs and the ground. The velocities of both contact points immediately after double impact are zero. The two contact tips should neither lift up nor slip on the ground. Thus in Equation (2.22), $\Delta\dot{X}_b = \begin{bmatrix}\Delta\dot{x}_b & \Delta\dot{y}_b\end{bmatrix}^T = \underline{0}$. The corresponding equations describing double impact can be derived as the following matrix form (refer to Appendix II for detailed derivation)

$$\begin{pmatrix} W & J^T \\ J & \underline{0}_{2\times 2} \end{pmatrix}\begin{pmatrix} \Delta\dot{\theta} \\ P_I \end{pmatrix} = \begin{pmatrix} \underline{0}_{5\times 1} \\ -J\dot{\theta}^- \end{pmatrix}, \tag{2.23a}$$

where W is a 5×5 lower-triangular matrix in the following detailed form

$$W_{ij} = \begin{cases} I_i - m_i d_i (a_i l_i - d_i) & j = i \\ -\left[a_i m_j d_j l_i + a_j m_i (a_i l_i - d_i) l_j + a_i a_j \left(\sum_{k=j+1}^{i-1} m_k \right) l_i l_j \right] \cos(\theta_i - \theta_j) & j < i \\ 0 & j > i \end{cases} \tag{2.23b}$$

J is the Jacobian matrix:

$$J = \frac{\partial f_i}{\partial \theta_j} : \begin{pmatrix} f_1 \\ f_2 \end{pmatrix} = \begin{pmatrix} \sum_{i=1}^{5} (a_i l_i \sin\theta_i) - \frac{1}{2} S_L \\ \sum_{i=1}^{5} (a_i l_i \cos\theta_i) \end{pmatrix} = \underline{0}, \tag{2.23c}$$

where f_i denotes the contact constraint functions, S_L is the step length. $P_I = \begin{bmatrix} P_{IX} & P_{IY} \end{bmatrix}^T$ represents the impulses at the contact point of the left limb (trailing limb), shown as point

B in Figure 2.1. The advantage of Equations (2.23) over Hurmuzlu's (1993) double impact equation is that in Equation (2.23a), the coefficient matrix is partitioned into four submatrices, and each of the submatrices can be presented in an explicit and simple form which is due to the improved kinematic model. This makes it possible to derive the explicit solutions for $\Delta\dot{\theta}$ and P_l separately. Equation (2.23) can be rewritten as

$$\begin{cases} W\Delta\dot{\theta} + J^T P_l = 0 & \text{(2.24a)} \\ J\Delta\dot{\theta} = -J\dot{\theta}^- & \text{(2.24b)} \end{cases}$$

Since W is a lower-triangular inertial matrix which is invertible, Equation (2.24a) can be written as

$$\Delta\dot{\theta} = -W^{-1}J^T P_l . \tag{2.25}$$

Substituting Equation (2.25) into (2.24b) yields

$$JW^{-1}J^T P_l = J\dot{\theta}^- . \tag{2.26}$$

Note that J is full ranked and W is an invertible matrix so that $JW^{-1}J^T$ is invertible. Thus, the impulse at the tip of the trailing limb can be solved as

$$P_l = (JW^{-1}J^T)^{-1}J\dot{\theta}^- , \tag{2.27}$$

and the changes of angular velocities are derived as

$$\Delta\dot{\theta} = -W^{-1}J^T(JW^{-1}J^T)^{-1}J\dot{\theta}^- . \tag{2.28}$$

Furthermore, the impulses at the contact point of the right limb (swing limb before impact, or leading limb) can be solved from Equations (2.22) as follows:

$$P_r = V\Delta\dot{\theta} - P_l , \tag{2.29a}$$

where $V = V(\theta^-) \in R^{2\times 5}$ defined by

$$V_{ij} = \left[m_j d_j + \left(\sum_{k=j+1}^{5} m_k \right) (a_j l_j) \right] \left[b_i \cos\theta_j + (b_i - 1)\sin\theta_j \right], \quad i = 1,2; j = 1,2..5, \text{ (2.29b)}$$

$b_i=1$ if $i=1$ and $b_i=0$ if $i=2$. As $\dot{X}_e^- = \begin{bmatrix} \dot{x}_e^- & \dot{y}_e^- \end{bmatrix}^T = (\partial f_i / \partial \theta_j)\dot{\theta}^- = J\dot{\theta}^-$, where $\dot{X}_e^-$ denotes the velocity of the swing tip immediately before impact, the dynamic equations to describe double impact can be expressed using the term of swing tip velocity immediately before impact, as follows:

$$\begin{cases} \dot{\theta}^+ = -W^{-1}J^T(JW^{-1}J^T)^{-1}\dot{X}_e^- + \dot{\theta}^- & \text{(2.30a)} \\ P_l = (JW^{-1}J^T)^{-1}\dot{X}_e^- & \text{(2.30b)} \\ P_r = -(I + VW^{-1}J^T)(JW^{-1}J^T)^{-1}\dot{X}_e^- & \text{(2.30c)} \end{cases}$$

The detailed forms of W, J and V are shown in Equations (2.23b), (2.23c) and (2.29b) respectively. The validity of solutions to Equations (2.30) is dependent on the following three conditions (Hurmuzlu 1993):

$$1) \quad P_{lY} > 0, \text{ (2.31a)}$$

$$2) \quad \frac{|P_{lX}|}{|P_{lY}|} < \mu, \text{ (2.31b)}$$

$$3) \quad \frac{|P_{rX}|}{|P_{rY}|} < \mu, \text{ (2.31c)}$$

where μ is the coefficient of friction between the contact points and the ground. Inequality (2.31a) should be satisfied since the trailing limb is assumed to remain on the ground during and after double impact. Inequalities (2.31b) and (2.31c) represent the no-slip impact conditions at the contact points of the limbs with the ground. The theoretical basis of the frictional impulse can be found in Whittaker (1944).

2.3.3.2 Single Impact

Immediately before single impact the trailing limb tip is not in contact with the ground but its velocity is assumed to be zero (Tzafestas *et al.* 1996). During single impact there is no impulsive force at the trailing limb tip, i.e., for Equations (2.22), $[P_{IX} \quad P_{IY}]^T = \underline{0}$. The corresponding equations representing the single impact are derived as the following matrix form

$$\begin{pmatrix} W & U \\ J & I_{2\times 2} \end{pmatrix} \begin{pmatrix} \Delta\dot{\theta} \\ \Delta\dot{X}_b \end{pmatrix} = \begin{pmatrix} \underline{0}_{5\times 1} \\ -J\dot{\theta}^- \end{pmatrix}, \tag{2.32a}$$

where W is the same matrix as in Equation (2.23b), J is the Jacobian matrix expressed by Equation (2.23c), I is a 2×2 unit matrix, and U is a 5×2 matrix related with the system parameters taking the form:

$$U_{ij} = \left[-m_i(a_i l_i - d_j) - \left(\sum_{k=1}^{i-1} m_k \right)(a_i l_i) \right] \left[b_j \cos\theta_i + (b_j - 1)\sin\theta_i \right], \quad i = 1,2..5; j = 1,2 \tag{2.32b}$$

where $b_j=1$ if $j=1$ and $b_j=0$ if $j=2$. The derivation procedure is similar to that of double impact model shown in Appendix II, and is abbreviated here. Equation (2.32a) can be rewritten as

$$\begin{cases} W\Delta\dot{\theta} + U\Delta\dot{X}_b = 0 & (2.33a) \\ J\Delta\dot{\theta} + \Delta\dot{X}_b = -J\dot{\theta}^- = -\dot{X}_e^- & (2.33b) \end{cases}$$

Eliminating $\Delta\dot{X}_b$ from Equations (2.33) yields

$$(W - UJ)\Delta\dot{\theta} = U\dot{X}_e^- . \tag{2.34a}$$

As W, U and J are well-defined matrices related with system inertial terms using the series chain model, the coefficient matrix $(W - UJ)$ can be calculated as

$$(W-UJ)_{ij}=\begin{cases} I_i+m_i(a_il_i-d_i)^2+\left(\sum_{k=1}^{i-1}m_k\right)a_il_i & j=i \\ -\left[m_i(a_il_i-d_i)a_jl_j+\left(\sum_{k=1}^{i-1}m_k\right)a_il_ia_jl_j\right]\cos(\theta_i-\theta_j) & j>i \\ \left[\left(\sum_{k=1}^{j}m_k\right)a_il_ia_jl_j-m_jd_ja_il_i\right]\cos(\theta_i-\theta_j) & j<i \end{cases} \quad (2.34b)$$

It is obvious that (*W-UJ*) is full-ranked and thus is invertible. Finally the angular velocity changes, the trailing tip velocity changes and the impulses during single impact are

$$\Delta\dot{\theta}=(W-UJ)^{-1}U\dot{X}_e^-, \quad (2.35a)$$

$$\Delta\dot{X}_b=-J\Delta\dot{\theta}-\dot{X}_e^-, \quad (2.35b)$$

$$P_S=m_{sum}\Delta\dot{X}_b+V\Delta\dot{\theta}. \quad (2.35c)$$

Where m_{sum} is the summation of the mass of all links, P_S is the external impulse at the collision tip for single impact. As is previously assumed that $\dot{X}_b^-=\underline{0}$, the explicit solutions to the single impact model—the post-impact angular velocity, the trailing tip velocity and the collision tip impulses are derived as

$$\begin{cases} \dot{\theta}^+=(W-UJ)^{-1}U\dot{X}_e^-+\dot{\theta}^- & (2.36a) \\ \dot{X}_b^+=-\left[I+J(W-UJ)^{-1}U\right]\dot{X}_e^- & (2.36b) \\ P_S=\left[(V-m_{sum}J)(W-UJ)^{-1}U-m_{sum}I\right]\dot{X}_e^- & (2.36c) \end{cases}$$

where *W*, *J*, *V* and *U* are shown in detail by Equations (2.23b), (2.23c), (2.29b) and (2.32b) respectively. Equation (2.36) is another form of Equation (2.35). One observes that $\Delta\dot{\theta}$, $\dot{X}_b^+$ and P_{SI} are linear functions of $\dot{X}_e^-$ and none of them is dependent on $\dot{\theta}_3^-$ and $\dot{X}_h^-$. This is in accordance with that of double impact. The single impact model described by Equation (2.36) is valid with the satisfaction of the following two conditions (Hurmuzlu 1993):

$$1)\quad \dot{y}_b^+ > 0, \tag{2.37a}$$

$$2)\quad \frac{|P_{SX}|}{|P_{SY}|} < \mu . \tag{2.37b}$$

Inequalities (2.33) and (2.37) can be utilized to explore how the forthcoming contact events are associated with the system states prior to impact. The detailed analysis will be given in Chapter 5.

Remark

Since the single and double impact equations are derived from a series rigid body chain model, these impact equations can be easily extended to other multi-link rigid body chains and the efficiency of the derivation procedure can be improved with this kinematic chain model.

2.3.4 Switching and Transformation

During biped locomotion, when the swing limb contacts the ground, the roles of the swing and the stance side members will be exchanged and this leads to discontinuity in the mathematical model. The role of the stance and swing limb need to be exchanged. The physical link displacements and velocities do not actually change but the members of the biped link, which are used in the dynamic modeling, need re-labelling. The overall result of the generalized coordinates and velocities immediately before and after the switch can be written by a transformation equation as follows:

$$\begin{pmatrix} \theta^+ \\ \dot{\theta}^+ \end{pmatrix}_{switch} = \begin{pmatrix} T & \underline{0}_{5\times5} \\ \underline{0}_{5\times5} & T \end{pmatrix} \begin{pmatrix} \theta^- \\ \dot{\theta}^+_{impact} \end{pmatrix} + \Pi , \tag{2.38}$$

where $T = \begin{pmatrix} 0 & 0 & 0 & 0 & 1 \\ 0 & 0 & 0 & 1 & 0 \\ 0 & 0 & 1 & 0 & 0 \\ 0 & 1 & 0 & 0 & 0 \\ 1 & 0 & 0 & 0 & 0 \end{pmatrix}$, $\Pi = [\pi \quad \pi \quad \pi \quad \pi \quad \pi \quad 0 \quad 0 \quad 0 \quad 0 \quad 0]^T$,

$\begin{pmatrix} \theta^- \\ \dot{\theta}^+_{impact} \end{pmatrix}$ and $\begin{pmatrix} \theta^+ \\ \dot{\theta}^+ \end{pmatrix}_{switch}$ are the state space vectors specifying the coordinates and the velocities immediately before and after the switch from the SSP to the DSP.

To facilitate the control procedure, the equations of motion (2.7) and (2.11) need to be formulated in terms of the relative angles between jointed links as

$$D_q(q)\ddot{q} + H_q(q,\dot{q}) + G_q(q) = T_q, \tag{2.39}$$

$$D_q(q)\ddot{q} + H_q(q,\dot{q}) + G_q(q) = T_q + J_q^T \lambda, \tag{2.40}$$

where $T_q = [\tau_0 \quad \tau_1 \quad \tau_2 \quad \tau_3 \quad \tau_4]$, each entry representing the joint torque to each joint, $q = [q_0 \quad q_1 \quad q_2 \quad q_3 \quad q_4]^T$, representing the joint angles. A transformation can be found to express q by θ:

$$q = M_{q\theta} \cdot \theta, \tag{2.41}$$

where $M_{q\theta}$ is a transformation matrix from θ to q:

$$M_{q\theta} = \begin{pmatrix} 1 & 0 & 0 & 0 & 0 \\ 1 & -1 & 0 & 0 & 0 \\ 0 & 1 & -1 & 0 & 0 \\ 0 & 0 & 1 & -1 & 0 \\ 0 & 0 & 0 & 1 & -1 \end{pmatrix}.$$

Clearly, there is a relation between the segment torques and joint torques

$$T_{\theta i} = \sum_{j=1}^{5} \tau_{j-1} \frac{\partial q_{j-1}}{\partial \theta_i} = \sum_{j=1}^{5} \tau_{j-1} (M_{q\theta})_{ji}. \tag{2.42}$$

Equation (2.42) can be written as a vector form to transform segment torques into joint torques:

$$T_\theta = (T_q^T M_{q\theta})^T = M_{q\theta}^T T_q, \tag{2.43}$$

or $T_q = (M_{q\theta}^T)^{-1} \cdot T_\theta$, the transformation from joint torques to segment torques. In order to solve the coefficient matrix terms for Equation (2.39) and (2.40), subtitute (2.41) and (2.43) into (2.7) and (2.11), the following transformation forms can be determined,

$$D_q = (M_{q\theta}^{-1})^T D_\theta(\theta(q)) M_{q\theta}^{-1}, \tag{2.44a}$$

$$H_q = (M_{q\theta}^{-1})^T H(\theta(q), \dot{\theta}(\dot{q})) M_{q\theta}^{-1} \dot{q}, \tag{2.44b}$$

$$G_q = (M_{q\theta}^{-1})^T G_\theta(\theta(q)), \tag{2.44c}$$

$$J_q = J_\theta(\theta(q)) M_{q\theta}^{-1}. \tag{2.44d}$$

Similarly, Equation (2.21) is transformed to

$$\ddot{p} = B(q)\dot{p} + C(q)(T_q - N(q)), \tag{2.45}$$

where

$$B(q) = B(R(q), D_q, J_q), \tag{2.46a}$$

$$C(q) = C(\theta(q)) M_{q\theta}^T, \tag{2.46b}$$

$$N(q) = (M_{q\theta}^{-1})^T N(\theta(q)). \tag{2.46c}$$

Thus, Equations (2.44) and (2.46) can be conveniently applied to dynamic model (2.39), (2.40) and (2.45) when motion control is implemented.

2.3.5 Simplicity of the Dynamic Equations in Comparison with Conventional Work

The biped presented above is derived using a kinematic model shown in Figure 2.1 (SSP) and Figure 2.2 (DSP). This structure denotes that it has been treated as an open

loop kinematic chain resembling a robot manipulator starting from the supporting point to the free end of the swing limb and the trunk. Each labelled link is considered as a vector originating from its starting joint (the joint connecting the link to the previous one) to the end joint (the joint connecting the link to the next one). Accordingly, the location of mass center is measured from the mass center of each link to its starting joint, and the segment angle is also measured from the vertical axis through the starting joint to each link counter-close-wise (refer to Figure 2.4a). This kinematic defination may not show much superiority until it is compared with other biped literature (Tzafestas *et al.*1996, Lum *et al.* 1999, Chan 2000). Most of the previous work treated the biped as a symmetric multi-link system and their definition in kinematic model mainly emphasized this feature (see Figure 2.4b). However their kinematic defination leads to an extremely complicated derivation and irregular expression in dynamic equations. Their work has also been duplicated in Appendix III to demonstrate the simplicity of this modified defination.

To be specific, the dynamic equations derived in this work are compared with those conventional ones. The position and velocity of the mass center of each link expressed by Equation (2.2) using the modified kinematic defination is identical to (A13) (refer to Appendix III) in conventional work (Tzafestas *et al.*1996); the derivation of dynamic model using Lagrange formulation with Equations (2.3) and (2.5) are identical to the complicated Equations (A14); and (A1)-(A4) in this work are identical to (A15)-(A18) in previous work. The final forms of dynamic model (2.7) in Section 2.4.1 are also found significantly simplified than those in conventional work shown in Appendix III. Applying the series kinematic chain model also shows superiority in the expression of joint angles (Equation 2.41) and the derivation of the single/double impact (in Section 2.4.3) as well

as the transformation matrices (in Section 2.4.4). As the final forms of the whole dynamic model are simplified, the computation and programming are accordingly simplified and are less prone to mistakes.

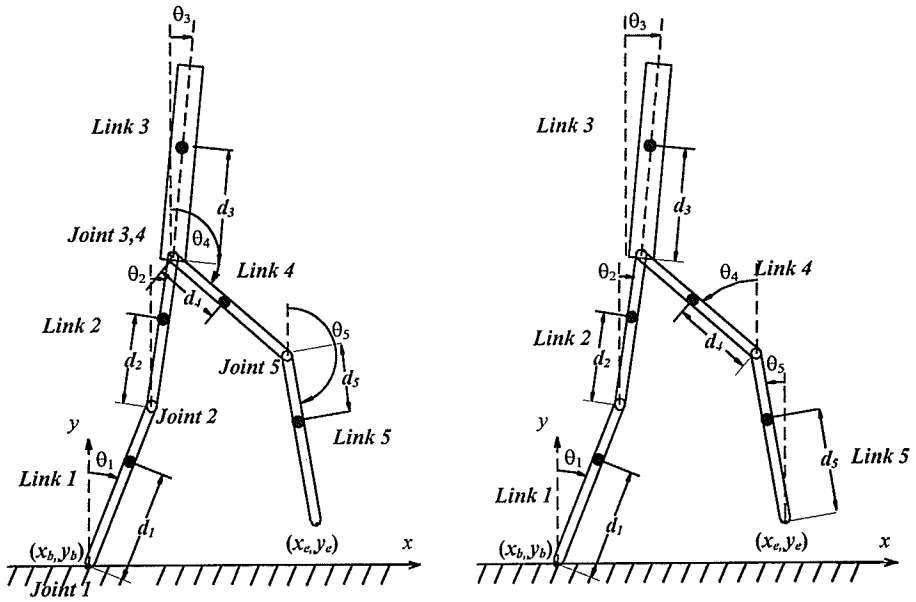

(a) Mode in this work (b) Model in conventional work

Figure 2.4 Comparison with the Kinematic model of a 5-link biped

2.4 Impact Dynamics of Planar Multi-Link Rigid Body Systems

As is previously mentioned that Zheng and Hemami (1984, 1985) have developed a method to solve the angular velocity changes of a robotic system due to impact by integrating the dynamic equations with contact constraints over an infinitesimal impact time period. Their work has been used widely to both biped robots and robot manipulators (Tzafestas *et al.* 1996, Lum *et al.* 1999, Chan 2000, Abo-Shanab and Sepehri 2001). Since their proposed impact equation resulted from the system Lagrangian dynamics prior to impact, one can take advantages of the existing dynamic model to

directly obtain the post impact velocities. However, as pointed out by the authors (Zheng and Hemami 1995), their solutions to the impact model are valid provided that the Jacobian matrices are full-ranked. Rank-deficient Jacobian matrices occur in the impact dynamics of some typical robot collision problems. The causes of rank-deficient Jacobian matrices may come from redundancy or dependence of contact constraint equations. Such circumstance can be found in both biped system and mobile robot impact problems. No method has been found for solving impact dynamic problems when the Jacobian matrix is rank-deficient.

The work in this section is to extend Zheng and Hemami's (1984, 1985) impact model such that the impact dynamic equations can be partially solved when the Jacobian matrix is rank-deficient. The results can benefit the development of both biped robot and robotic manipulators with impact. The proposed method consists of two parts. Firstly, the dynamic equations of impact are reformulated, which can model both cases of full-ranked and rank-deficient Jacobian matrices. The post impact velocities and impulses can be solved directly from the impact equations if the Jacobian matrices are full-ranked. However, rank-deficient Jacobian matrices lead to indetermined solutions of the post impact velocities and impulses since the number of independent equations is lower than the number of unknowns. Thus secondly, a method is developed to solve the impact equations by transforming the rank-deficient Jacobian matrices into their row-equivalent matrices, which contains a full-ranked sub-matrix and a null sub-matrix. By employing the full-ranked sub-matrix, the post impact velocities can be solved explicitly without extra equations and a set of linear equations with unknown impulses can be obtained where the impulses can only be solved if extra equations for impulses are provided. Proof

is given that the solution of the post impact velocities is unique regardless of the rank of the Jacobian matrix. During the whole formulation, an m-link planar rigid body system is utilized instead of directly modeling the five-link biped impact dynamics for generality. Examples are presented at last to demonstrate the application of the proposed model and solution scheme.

2.4.1 Formulation of a General Impact Model

As mentioned in Section 2.3.3, an impact model that has often been used in robot impact problems is that the impact is with point contact, perfectly plastic and occurs instantaneously (Zheng and Hemami 1984, Hurmuzlu and Chang1992). Such an impact model is appealing in that it significantly simplifies the analysis of the collision process. The validity of the model has also been discussed in (Hurmuzlu and Chang 1992, Hurmuzlu 1993). Since the collision is plastic and occurs instantly, the configuration of the robot remains constant during the collision and the collision tips do not leave the contact surface after impact. Although simultaneous collisions of independently moving objects seem nongeneric, the collision at multiple objects jointed by one another of a system is common in practice (Marghitu and Hurmuzlu 1995, Ivanov 1995, Chatterjee and Ruina 1998). Figure 2.5 represents the diagram of the contact problem of a planar *m*-link robotic system with multiple collision points. Prior to collision, point b on the robot is stationary on the environment at B, which is termed a supporting point. Impact occurs when each of the end tips e_i $(i=1,2,...,k)$ on the robot strikes the environment simultaneously at point E_i, which is termed a collision point. The origin of the world coordinate system is at B throughout the following derivation.

The dynamic equation describing the motion of the system before impact is given as

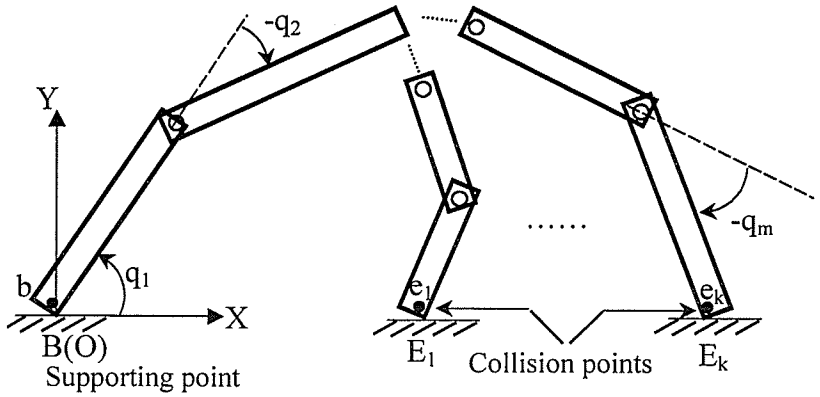

Figure 2.5 A planar m-link rigid body chain collisions

$$D(q)\ddot{q} + H(q,\dot{q})\dot{q} + G(q) = \tau\,, \tag{2.47}$$

where D and $R \in R^{n\times n}$; G and q, $\dot{q}$, $\ddot{q}$ and $\tau \in R^n$, referring to Equation (2.7) for each representation. Here n denotes the system degrees of freedom prior to impact. According to Lagrange 's impulsive equation (Goldsmith 1960),

$$\Delta\left(\frac{\partial K}{\partial \dot{q}_i}\right) = Q_i,\quad i = 1,2...n, \tag{2.48}$$

which is an integration of Lagrange formulation with respect to time over the impact period $\Delta t = t_1 - t_0$ by carrying out the limiting process $\Delta t \to 0$, where K is the kinetic energy of the system, $\Delta(\partial K/\partial \dot{q}_i)$ represents the change in the momentum component $\partial K/\partial \dot{q}_i$, Q_i represents the generalized impulses resulting from the generalized impact force $Q_{\delta i}$: $Q_i = \lim_{\Delta t\to 0}\int_{t_0}^{t_0+\Delta t} Q_{\delta i}\,dt = Q_{\delta i}\Delta t$. Thus, (2.47) is integrated over the impact time period $\Delta t = t_1 - t_0$ and carrying out the limiting process $\Delta t \to 0$ at the onset of the collision:

$$\lim_{\Delta t\to 0}\int_{t_0}^{t_0+\Delta t} D\ddot{q}dt + \lim_{\Delta t\to 0}\int_{t_0}^{t_0+\Delta t}\left(H\dot{q} + G - \tau\right)dt = \lim_{\Delta t\to 0}\int_{t_0}^{t_0+\Delta t} Q_\delta dt = Q\,. \tag{2.49}$$

The second term of the left-hand side, $\lim_{\Delta t \to 0} \int_{t_0}^{t_0+\Delta t} (H\dot{q} + G - \tau)dt$, is equal to zero, because the positions, velocities and control input remain finite. Therefore (2.49) become

$$D(\dot{q}^+ - \dot{q}^-) = Q, \tag{2.50}$$

where $\dot{q}^+$ and $\dot{q}^-$ represent the angular velocities immediately before and after impact, respectively. The impact equation (2.50) is different from Zheng and Hemami's (1984) work in that in their work, the impact dynamic equation was directly solved under the condition that the Jacobian matrix must be full-ranked. If the Jacobian matrix is rank-deficient, the changes in the angular velocities and the impulses can not be solved. In the present formulation, the right-hand side of Equation (2.50) does not include the Jacobian matrix. Thus (2.50) can be used regardless of the ranks of Jacobian matrices. However, to solve the generalized impulses Q, D'Alembert's principle is applied to the system at collision, which is written as

$$\delta q \cdot \{D\ddot{q} + H\dot{q} + G - \tau - Q_\delta\} = 0. \tag{2.51}$$

The virtual work done by the force Q_δ in the virtual displacement δq is (Pestel and Thomson 1968)

$$\delta w = \delta q \cdot Q_\delta, \tag{2.52}$$

whereas it is also the resultant virtual work done by the external impact forces at the collision tips, $F_{\delta e} = [F_{\delta e1X} \quad F_{\delta e1Y} \quad \ldots \quad \ldots \quad F_{\delta ekX} \quad F_{\delta ekY}]^T$, in the virtual displacements, $\delta X_e = [\delta x_{e1} \quad \delta y_{e1} \quad \ldots \quad \ldots \quad \delta x_{ek} \quad \delta y_{ek}]^T$:

$$\delta w = \delta X_e \cdot F_{\delta e}, \tag{2.53}$$

where $F_{\delta e}$ and X_e are $2k \times 1$ vectors of the external impact forces and coordinates at the collision tips and k is the number of the collision points. By transformation, X_e can be expressed in terms of the generalized coordinates q:

$$X_e = [f_1(q) \quad f_2(q) \quad \cdots \quad \cdots \quad f_{2k-1}(q) \quad f_{2k}(q)]^T . \tag{2.54}$$

Thus $\delta X_e = J\delta q$, where J is the Jacobian matrix: $J = \partial f_i / \partial q_j$. Equation (2.53) can be written as

$$\delta w = \delta X_e \cdot F_{\delta e} = (J\delta q)^T F_{\delta e} = (\delta q)^T J^T F_{\delta e} = \delta q \cdot \left(J^T F_{\delta e}\right). \tag{2.55}$$

Combining (2.52) and (2.55),

$$Q_\delta = J^T F_{\delta e} . \tag{2.56}$$

Thus, the generalized impulse over the infinitesimal period of time Δt is

$$Q = J^T F_e , \tag{2.57}$$

where F_e represents the external impulses at collision tips: $F_e = F_{\delta e}\Delta t$. Thus (2.50) can be rewritten as

$$D(\dot{q}^+ - \dot{q}^-) = J^T F_e . \tag{2.58}$$

For multiple rigid-body collision problems, several authors adopt one of the two conditions at each supporting point that (*i*) the normal velocity is kept zero and there is a non-negative impulse, or, (*ii*) there is a zero impulse and the post collision normal velocity is non-negative (see. e.g. Hurmuzlu and Chang 1992, Marghitu and Hurmuzlu 1995 and the references therein). Since by assumption the collision points on the system rest at the same position of the contact points on the environment after impact, the following equation of contact constraint exists:

$$f(q^+) - X_E = 0 , \tag{2.59}$$

where X_E is the vector of coordinates of the collision points on the environment and is a constant vector. Differentiating (2.59) with respect to time yields

$$J\dot{q}^+ = 0. \tag{2.60}$$

Combining (2.58) and (2.60), the impact equation becomes

$$\begin{cases} D\dot{q}^+ - J^T F_e = D\dot{q}^- & \text{(2.61a)} \\ J\dot{q}^+ = 0 & \text{(2.61b)} \end{cases}$$

or in the matrix form

$$\begin{bmatrix} D & -J^T \\ J & 0 \end{bmatrix} \begin{bmatrix} \dot{q}^+ \\ F_e \end{bmatrix} = \begin{bmatrix} D\dot{q}^- \\ 0 \end{bmatrix}. \tag{2.62}$$

This model is applicable to all multi-link systems with perfect plastic collisions. Equation (2.62) is solved in the following section.

2.4.2 Solutions to the Impact Model

In order to solve Equation (2.62), two cases may arise: (*i*) Jacobian matrix J is full-ranked and the post impact velocity $\dot{q}^+$ and the external impulse F_e can be solved explicitly, and (*ii*) Jacobian matrix J is rank-deficient, which causes matrix $\begin{bmatrix} D & -J^T \\ J & 0 \end{bmatrix}$ to be rank-deficient and there are infinite solutions to (2.62). The two cases are solved separately as follows.

2.4.2.1 Full-Ranked Jacobian Matrix

When the contact constraint conditions are independent and not redundant, the Jacobian matrix J is full-ranked. By multiplying both sides of (2.61a) by JD^{-1} and combining with (2.61b), one has

$$(JD^{-1}J^T)F_e = -J\dot{q}^-. \tag{2.63}$$

Since J and D are full-ranked matrices, the coefficient matrix $(JD^{-1}J^T)$ is invertible. Thus,

$$F_e = (JD^{-1}J^T)^{-1}(-J\dot{q}^-).$$

Note that $\dot{X}_e^- = J\dot{q}^-$. Equation (2.62) will then be solved as

$$\begin{cases} F_e = (JD^{-1}J^T)^{-1}(-\dot{X}_e^-) & \text{(2.64a)} \\ \dot{q}^+ = \dot{q}^- + D^{-1}J^T(JD^{-1}J^T)^{-1}(-\dot{X}_e^-) & \text{(2.64b)} \end{cases}$$

The results shown in (2.64) are identical to those derived by Zheng and Hemami (1984, 1985).

2.4.2.2 Rank-Deficient Jacobian Matrix

Two cases may cause Jacobian matrix J rank-deficient. The first case is that the number of contact constraints resulting from impact exceeds the degrees of freedom of the dynamic system. The second case is that the constraint equations themselves are linearly dependent. As J is rank-deficient, the number of unknowns is higher than the number of linear-independent equations shown by (2.62). Thus, extra equations are needed in order to solve the angular velocities, $\dot{q}^+$, and impulses, F_e. It will be shown next that there is only one solution of $\dot{q}^+$ to (2.62) when the Jacobian matrix is rank-deficient, and the solution of $\dot{q}^+$ can be solved explicitly without extra equations. The proof is carried out in two parts. Firstly, a matrix $\hat{J}$ in row-equivalent form (Schneider and Barker 1973) to J is constructed, which contains a full-ranked sub-matrix and a zero sub-matrix. By using the full-ranked sub-matrix and removing the null matrix from $\hat{J}$, a solution of the post impact velocities can be solved explicitly and a set of linear equations with unknown impulses can be obtained. Secondly, it has to be proven that all possible

solutions of $\dot{q}^+$ to (2.62) remain the same regardless of the extra equations. The detailed procedure is as follows.

The row-equivalent matrix $\hat{J}$ can be obtained by left-multiplying J by a transformation matrix T (Schneider and Barker 1973), where $T \in R^{2k\times 2k}$ and is invertible, such that the row vectors of $\hat{J}$ can be partitioned into r independent vectors and ($2k$-r) zero vectors in R^n space, i.e.,

$$\hat{J} = TJ = \begin{bmatrix} (\hat{J}_1)_{r\times n} \\ 0_{(2k-r)\times n} \end{bmatrix}. \tag{2.65}$$

Note that k is the number of the collision points. Furthermore, by multiplying both sides of (2.61b) by T, one has

$$TJ\dot{q}^+ = \hat{J}\dot{q}^+ = \begin{bmatrix} \hat{J}_{1\,r\times n} \\ 0_{(2k-r)\times n} \end{bmatrix}\dot{q}^+ = 0. \tag{2.66}$$

The second term on the left-hand side of (2.61a), $-J^T F_e$, can be rewritten as

$$-J^T F_e = -J^T T^T (T^T)^{-1} F_e = -(TJ)^T (T^T)^{-1} F_e = -\hat{J}^T (T^T)^{-1} F_e. \tag{2.67}$$

Thus, (2.62) can be modified as

$$\begin{bmatrix} D & \begin{bmatrix} -\hat{J}_1^T & 0 \end{bmatrix} \\ \begin{bmatrix} \hat{J}_1 \\ 0 \end{bmatrix} & 0 \end{bmatrix} \begin{bmatrix} \dot{q}^+ \\ (T^T)^{-1} F_e \end{bmatrix} = \begin{bmatrix} D\dot{q}^- \\ 0 \end{bmatrix}. \tag{2.68}$$

Denote

$$(T^T)^{-1} F_e = F_{Tr}(F_e) = \begin{bmatrix} F_{Tr1\,r\times 1} \\ F_{Tr2\,(2k-r)\times 1} \end{bmatrix}, \tag{2.69}$$

where F_{Tr1} and F_{Tr2} are the vectors of linear combinations of the external impulses. Equation (2.68) is rewritten as

$$\begin{bmatrix} D & -\hat{J}_1^T \\ \hat{J}_1 & 0 \end{bmatrix}\begin{bmatrix} \dot{q}^+ \\ F_{Tr1} \end{bmatrix}=\begin{bmatrix} D\dot{q}^- \\ 0 \end{bmatrix}. \tag{2.70}$$

Since $\hat{J}_1$ is a full-ranked matrix, the same procedure can be followed in case (i), and (2.70) is finally solved as

$$\begin{cases} F_{Tr1} = (\hat{J}_1 D^{-1} \hat{J}_1^T)^{-1}(-\hat{J}_1 \dot{q}^-) & \text{(2.71a)} \\ \dot{q}^+ = \dot{q}^- + D^{-1}\hat{J}_1^T(\hat{J}_1 D^{-1}\hat{J}_1^T)^{-1}(-\hat{J}_1\dot{q}^-) & \text{(2.71b)} \end{cases}$$

Note that in (2.71), although the external impulses can not be solved without extra equations, the post impact velocities are solved in an explicit form. It will be shown next that the solution of the post impact velocities, $\dot{q}^+$, shown in (2.71b), is independent of the row-equivalent matrix $\hat{J}$ and transformation matrix T, and therefore is unique.

Proof: Assuming that $\hat{J}_{1\_a}$ and $\hat{J}_{1\_b}$ are two arbitrary row-equivalent sub-matrices to J, then $\hat{J}_{1\_a}$ and $\hat{J}_{1\_b}$ are row-equivalent to each other (Schneider and Barker 1973), i.e., $\hat{J}_{1\_b} = M\hat{J}_{1\_a}$, where M is an $r \times r$ invertible transformation matrix. According to (2.71b), the solutions for $\dot{q}^+$ determined by $\hat{J}_{1\_a}$ and $\hat{J}_{1\_b}$ are,

$$\dot{q}_{Ja}^+ = \dot{q}^- + D^{-1}\hat{J}_{1\_a}^T(\hat{J}_{1\_a}D^{-1}\hat{J}_{1\_a}^T)^{-1}(-\hat{J}_{1\_a}\dot{q}^-), \tag{2.72a}$$

$$\dot{q}_{Jb}^+ = \dot{q}^- + D^{-1}\hat{J}_{1\_b}^T(\hat{J}_{1\_b}D^{-1}\hat{J}_{1\_b}^T)^{-1}(-\hat{J}_{1\_b}\dot{q}^-), \tag{2.72b}$$

respectively. Substituting $\hat{J}_{1\_b} = M\hat{J}_{1\_a}$ into (2.72b) gives

$$\begin{aligned} \dot{q}_{Jb}^+ &= \dot{q}^- + D^{-1}\hat{J}_{1\_b}^T(\hat{J}_{1\_b}D^{-1}\hat{J}_{1\_b}^T)^{-1}(-\hat{J}_{1\_b}\dot{q}^-) \\ &= \dot{q}^- + D^{-1}(M\hat{J}_{1\_a})^T\left[(M\hat{J}_{1\_a})D^{-1}(M\hat{J}_{1\_a})^T\right]^{-1}\left[-(M\hat{J}_{1\_a})\dot{q}^-\right] \\ &= \dot{q}^- + D^{-1}(\hat{J}_{1\_a}^T M^T)\left[(M^T)^{-1}(\hat{J}_{1\_a}D^{-1}\hat{J}_{1\_a}^T)^{-1}M^{-1}\right](-M\hat{J}_{1\_a}\dot{q}^-) \\ &= \dot{q}^- + D^{-1}\hat{J}_{1\_a}^T(\hat{J}_{1\_a}D^{-1}\hat{J}_{1\_a}^T)^{-1}(-\hat{J}_{1\_a}\dot{q}^-) \end{aligned} \tag{2.73}$$

Comparing (2.73) and (2.72a), finally,

$$\dot{q}_{Ja}^{+} = \dot{q}_{Jb}^{+}. \tag{2.74}$$

Remarks

(1) Equation (2.74) shows that regardless of the forms of the row-equivalent matrices $\hat{J}$, the solution of the angular velocities, $\dot{q}^{+}$ from (2.68), remains unchanged. Since (2.68) is equivalent to (2.62), the solution of the angular velocities, $\dot{q}^{+}$ from (2.62), is unique and can be solved explicitly in spite of the rank deficiency of the Jacobian matrix.

(2) Although various row-equivalent matrices $\hat{J}_1$ can be chosen, the row echelon form* is recommended here for its simplicity if only the solution of the post impact velocities is of interest.

Next, the effects of the forms of the row-equivalent matrices $\hat{J}$ on the equations for solving the external impulses are discussed. Equation (2.71a) is a set of linear equations with external impulses as unknowns. The number of impulses is higher than the number of equations. Thus, the impulses can only be solved uniquely when extra equations are provided. It is to be proven that the general solution of the external impulses is independent from the matrices $\hat{J}$ and transformation matrix T.

Proof: Assuming that $\hat{J}_{1\_a}$ and $\hat{J}_{1\_b}$ are two arbitrary row-equivalent sub-matrices to J, then $\hat{J}_{1\_b} = M\hat{J}_{1\_a}$, where M is an $r \times r$ invertible transformation matrix. According to (2.71a), the equations containing the external impulses F_e determined by $\hat{J}_{1\_a}$ and $\hat{J}_{1\_b}$, are,

---

*An m×n matrix A is said to be in row echelon form if and only if:
(1) The nonzero rows are at the top of the matrix;
(2) The leading entries move to the right as we go down the matrix;
(3) All leading entries are one;
(4) Any column that contains a leading entry has all other entries zero.

$$F_{Tr1\_Ja}(F_e) = (\hat{J}_{1\_a} D^{-1} \hat{J}_{1\_a}^T)^{-1} (-\hat{J}_{1\_a} \dot{q}^-), \tag{2.75a}$$

$$F_{Tr1\_Jb}(F_e) = (\hat{J}_{1\_b} D^{-1} \hat{J}_{1\_b}^T)^{-1} (-\hat{J}_{1\_b} \dot{q}^-). \tag{2.75b}$$

Substituting $\hat{J}_{1\_b} = M\hat{J}_{1\_a}$ into the right-hand side of (2.75b),

$$\begin{aligned} & (\hat{J}_{1\_b} D^{-1} \hat{J}_{1\_b}^T)^{-1} (-\hat{J}_{1\_b} \dot{q}^-) \\ &= \left[(M\hat{J}_{1\_a}) D^{-1} (M\hat{J}_{1\_a})^T \right]^{-1} \left[-(M\hat{J}_{1\_a}) \dot{q}^- \right] \\ &= \left[(M^T)^{-1} (\hat{J}_{1\_a} D^{-1} \hat{J}_{1\_a}^T)^{-1} M^{-1} \right] (-M\hat{J}_{1\_a} \dot{q}^-) \\ &= (M^T)^{-1} (\hat{J}_{1\_a} D^{-1} \hat{J}_{1\_a}^T)^{-1} (-\hat{J}_{1\_a} \dot{q}^-) \end{aligned} \tag{2.76}$$

From (2.67) and the definition of F_{Tr1} as shown in (2.69),

$$J^T F_e = \hat{J}^T F_{Tr} = \hat{J}_{1\_a}^T F_{Tr1\_Ja} = \hat{J}_{1\_b}^T F_{Tr1\_Jb}. \tag{2.77}$$

Substituting $\hat{J}_{1\_b} = M\hat{J}_{1\_a}$ into (2.77),

$$\hat{J}_{1\_a}^T F_{Tr1\_Ja} = \hat{J}_{1\_b}^T F_{Tr1\_Jb} = (M\hat{J}_{1\_a})^T F_{Tr1\_Jb} = \hat{J}_{1\_a}^T M^T F_{Tr1\_Jb}.$$

Since $\hat{J}_{1\_a}^T$ is full-ranked, one has

$$F_{Tr1\_Jb} = (M^T)^{-1} F_{Tr1\_Ja}. \tag{2.78}$$

Substituting (2.76) and (2.78) into (2.75b) gives

$$(M^T)^{-1} F_{Tr1\_Ja} = (M^T)^{-1} (\hat{J}_{1\_a} D^{-1} \hat{J}_{1\_a}^T)^{-1} (-\hat{J}_{1\_a} \dot{q}^-).$$

Since M^T is invertible, the above equation indicates that (2.75a) and (2.75b) are equivalent, i.e., with the same extra equations for impulses, the solution of the external impulses remains the same regardless of the choice of the row-equivalent matrices $\hat{J}$ and their associated transformation matrix T.

Remarks

(1) The equivalency of (2.75a) and (2.75b) indicates that the selection of the row-equivalent matrices $\hat{J}$ has no effects on the solution of the external impulses.

(2) For each specific row-equivalent matrix $\hat{J}$, its associated transformation matrix T is not necessarily unique. The unknown elements of T are solved from equation $T_{2k\times 2k} J_{2k\times n} = \hat{J}_{2k\times n}$, which has $2k\times 2k$ unknowns and $2k\times r$ independent equations, where r is the rank of the matrices $J_{2k\times n}$ and $\hat{J}_{2k\times n}$. Since $r<2k$ when J is rank-deficient, the elements of T have infinite solutions. There are $2k\times(2k-r)$ elements for T that can be chosen freely, e.g., some elements can be prescribed as zero for simplicity, provided that the transformation matrix T remains invertible.

2.4.3 Examples

For biped robot impact problems with full-ranked Jacobian matrices, Equation (2.64) can be used directly to solve the impact dynamics. Examples can be found such as the five-link single and double impact which has been shown in Section 2.3.3 and are not repeated here. As discussed in Section 2.4.2, rank-deficient Jacobian matrices may occur in two cases, *(i)* the number of constraint equations exceeds the system degrees of freedom prior to impact, and *(ii)* the constraint equations are not independent. For a rigid-link robot impact with at least one supporting point and more than one collision points, the number of contact constraints may exceed the system degrees of freedom prior to impact. Whereas if the supporting point and the collision point are located at one rigid link, for example, there may not be enough independent constraint functions that can be used to solve Equation (2.62). Both cases lead to rank-deficient Jacobian matrices. Two

typical examples of each case are presented next to demonstrate the method developed above.

Example 1: A three-link biped with two collision points

An example representing the first case is shown by Figure 2.6. A three-link biped robot is supported at *B* and collision happens at *C* and *E* simultaneously. After impact all tips on the biped, *b*, *c* and *e*, are assumed to rest on their contact surfaces at *B*, *C*, and *E*, respectively. The method, developed in Section 2.4.2, will be used to calculate the angular velocities after impact and to determine the equations for solving external impulses at collision points, *C* and *E*. The dynamic equation immediately before impact is presented by (2.47) with the matrices shown below:

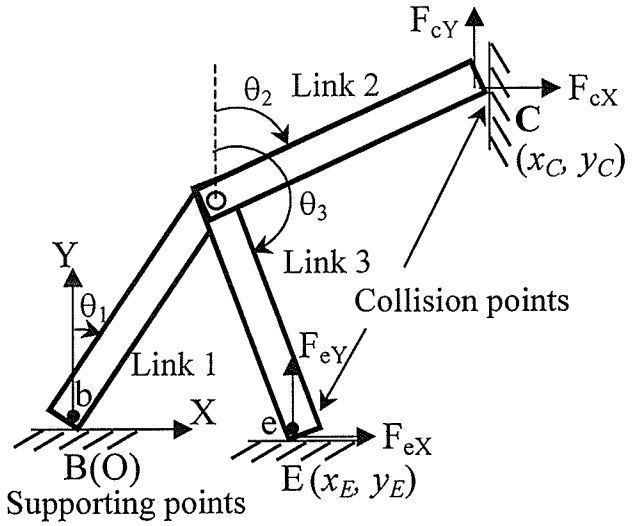

Figure 2.6 Biped robot mechanism with two collision points

$$D=\begin{bmatrix} I_1+m_1d_1^2+(m_2+m_3)l_1^2 & m_2l_1d_2C_{1-2} & m_3l_1d_3C_{1-3} \\ m_2l_1d_2C_{1-2} & I_2+m_2d_2^2 & 0 \\ m_3l_1d_3C_{1-3} & 0 & I_3+m_3d_3^2 \end{bmatrix},$$

$$H=\begin{bmatrix} 0 & m_2l_1d_2\dot{\theta}_2S_{1-2} & m_3l_1d_3\dot{\theta}_3S_{1-3} \\ -m_2l_1d_2\dot{\theta}_2S_{1-2} & 0 & 0 \\ -m_3l_1d_3\dot{\theta}_3S_{1-3} & 0 & 0 \end{bmatrix},$$

$$G=\begin{bmatrix} -(m_1d_1+2m_1l_1)gS_1 \\ -m_2d_2gS_2 \\ -m_3d_3gS_3 \end{bmatrix},$$

where θ_i is the segment angle of each link, and in abbreviated notation, $S_i=\sin\theta_i$; $S_{i-j}=\sin(\theta_i-\theta_j)$; $C_{i-j}=\cos(\theta_i-\theta_j)$. m_i, I_i and l_i are the mass, inertia and length of link i; d_i is the distance from the center of gravity of link i to the joint which connects link i and link i-1. The constraint functions are described as

$$\begin{bmatrix} f_1 \\ f_2 \\ f_3 \\ f_4 \end{bmatrix}=\begin{bmatrix} l_1\sin\theta_1+l_2\sin\theta_2-x_C \\ l_1\cos\theta_1+l_2\cos\theta_2-y_C \\ l_1\sin\theta_1+l_3\sin\theta_3-x_E \\ l_1\cos\theta_1+l_3\cos\theta_3-y_E \end{bmatrix}=0. \tag{2.79}$$

where $(x_C,\ y_C)$ and (x_E,y_E) are the coordinates of point C and E located at the environment. The Jacobian matrix is

$$J=\begin{bmatrix} l_1\cos\theta_1 & l_2\cos\theta_2 & 0 \\ -l_1\sin\theta_1 & -l_2\sin\theta_2 & 0 \\ l_1\cos\theta_1 & 0 & l_3\cos\theta_3 \\ -l_1\sin\theta_1 & 0 & -l_3\sin\theta_3 \end{bmatrix}. \tag{2.80}$$

The rank of the above Jacobian matrix is 3 and is rank-deficient. According to (2.62), there are six equations for the three-link bipedal system shown in Figure 2.6, and there are seven unknowns. Among them, three are angular velocities after impact, $\dot{\theta}_i^+$, and four

are impulse components at points C and E. The solutions cannot be determined based on Zheng and Hemami's (1984, 1985) work. By applying the above mentioned method, the row-equivalent Jacobian matrix $\hat{J}$ is chosen

$$\hat{J} = \begin{bmatrix} l_1 & 0 & 0 \\ 0 & l_2 & 0 \\ 0 & 0 & l_3 \\ 0 & 0 & 0 \end{bmatrix} = \begin{bmatrix} \hat{J}_1 \\ 0 \end{bmatrix}, \tag{2.81}$$

Consequently, the transformation matrix can be constructed as

$$T = \begin{bmatrix} 0 & 0 & \frac{S_3}{S_{3-1}} & \frac{C_3}{S_{3-1}} \\ \frac{1}{C_2} & 0 & -\frac{C_1 S_3}{C_2 S_{3-1}} & -\frac{C_1 C_3}{C_2 S_{3-1}} \\ 0 & 0 & -\frac{S_1 C_3}{C_3 S_{3-1}} & -\frac{C_1}{S_{3-1}} \\ -\frac{S_2 S_{3-1}}{C_3 S_{2-1}} & -\frac{C_2 S_{3-1}}{C_3 S_{2-1}} & \frac{1}{C_3} & \frac{1}{S_3} \end{bmatrix}, \tag{2.82}$$

where $C_i = \cos\theta_i$. Thus the post impact angular velocities can be solved by substituting the above $\hat{J}_1$ and T to (2.71b). If one impulse component can be obtained, for example that F_{EY} can be measured, the rest of impulse components, F_{EX}, F_{CX} and F_{CY} can be solved using (2.71a).

Example 2: A planar mobile robot with impact on the base

Figure 2.7 shows a planar mobile robot with a base and arms (Abo-Shanab and Sepehri 2001). When the base is rocking around contact point *b* toward *E* and colliding at *E*, point *b* may rest on the original position or lift up off the environment. If point *b* rests on the environment surface after impact, the degrees of freedom of the pre-impact system is *n*, representing *n* rotational joint angular displacements. The contact constraint function *f* can be written as

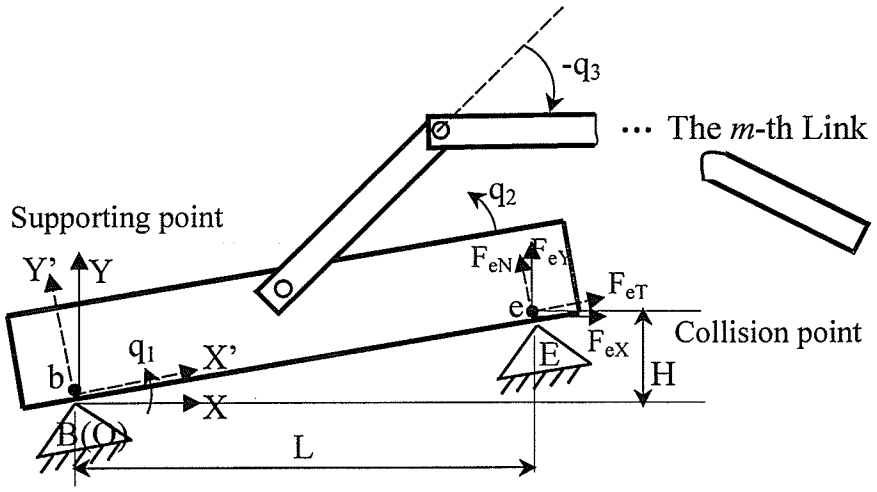

Figure 2.7 A planar mobile platform colliding at the base

$$\begin{bmatrix} f_1 \\ f_2 \end{bmatrix} = \begin{bmatrix} l_1 \cos q_1 - L \\ l_1 \sin q_1 - H \end{bmatrix} = \begin{bmatrix} 0 \\ 0 \end{bmatrix}. \tag{2.83}$$

Accordingly, Jacobian matrix is

$$J = \begin{bmatrix} -l_1 \sin q_1 & 0 & \dots & 0 \\ l_1 \cos q_1 & 0 & \dots & 0 \end{bmatrix}. \tag{2.84}$$

It is obvious that J is not full-ranked ($rank(J)=1$). From (2.62), there are $n+1$ equations but $n+2$ unknowns with n angular velocities after impact, $\dot{q}_i^+$, and two impulse components at point e. Through observations, a transformation matrix is constructed as

$$T = \begin{bmatrix} \cos q_1 & \sin q_1 \\ -\sin q_1 & \cos q_1 \end{bmatrix}, \tag{2.85}$$

to yield

$$\hat{J} = TJ = \begin{bmatrix} 0 & \dots & 0 \\ l_1 & \dots & 0 \end{bmatrix} = \begin{bmatrix} 0 \\ \hat{J}_1 \end{bmatrix}. \tag{2.86}$$

Note that $T=(T^T)^{-1}$, and T is also a matrix transforming an arbitrary vector in the coordinate system $O-xy$ into $O-x'y'$ by rotating an angle q_1. Thus, $F'_e=(T^T)^{-1}F_e=TF_e=\begin{bmatrix}F'_{eT} & F'_{eN}\end{bmatrix}^T$, where F'_{eT} and F'_{eN} represent the tangential and normal impulsive force at point e. Thus (2.70) becomes

$$\begin{bmatrix} D & -\hat{J}_1^T \\ \hat{J}_1 & 0 \end{bmatrix}\begin{bmatrix} \dot{q}^+ \\ F'_{eN} \end{bmatrix}=\begin{bmatrix} D\dot{q}^- \\ 0 \end{bmatrix}. \tag{2.87}$$

According to (2.71) and (2.86), (2.87) is finally solved as

$$\begin{cases} F'_{eN}=(\hat{J}_1D^{-1}\hat{J}_1^T)^{-1}(-l_1\dot{q}_1^-) & \text{(2.88a)} \\ \dot{q}^+=\dot{q}^-+D^{-1}\hat{J}_1^T(\hat{J}_1D^{-1}\hat{J}_1^T)^{-1}(-l_1\dot{q}_1^-) & \text{(2.88b)} \end{cases}$$

Equation (2.88a) shows that the normal impulse at the contact point E (e) can be solved explicitly without extra equations. However, the tangential impulse is not solvable due to the lack of one equation. Note that it is often of special interests in finding normal impulses in robotic collisions with the environment. Such normal impulses can be used to determine the type of impact (Hurmuzlu 1993).

Note that for both examples discussed above, the solutions presented are only valid when the supporting tip does not lift off the supporting surface after impact. If the supporting tip lifts up immediately after impact, the Jacobian matrices in the impact equations for both examples are actually full-ranked, and the "in the air" pre-impact dynamic model (Tzafestas *et al.*, 1996) should be employed.

2.5 Summary

A complete dynamic model to represent a planar five-link biped walking was developed in this chapter. The conventional definitions of certain physical parameters of the biped system have been modified for the kinematic analysis, and the dynamic

equations including the SSP, the DSP, single/double impact, and switching have been derived in detail. For the DSP, the biped model was first formulated as a robot system under holonomic constraints and then the hip position and trunk orientation were selected as independent generalized coordinates to describe the biped system in the reduced state space. The reduced space DSP dynamic model facilitates the biped motion regulation, which will be shown in Chapter 4.

The biped single and double impact equations were also developed by Newtonian approach. The post impact velocities and external impulses at contact point(s) were solved explicitly and they can be used conveniently to examine the validity of the solutions. Other equations were also formulated including the switching due to phase exchange, and transformation of the coordinates for facilitating control procedure. It has been shown that the whole dynamic modeling procedure was significantly improved and the detailed forms of those equations were greatly simplified comparing with conventional ones. This is due to the series kinematic chain model employed in this work.

Secondly, the impact dynamics of planar multi-link robotic collisions was extended and reformulated from previous literature, which can model both cases of full-ranked and rank-deficient Jacobian matrices. To solve the equations with the latter, row-equivalent matrices were constructed to apply to the model and the angular velocities immediately after impact can be solved explicitly without extra equations. Two robot collision problems with rank-deficient Jacobian matrices were presented to exemplify the impact problems and solution scheme.

It is the first time that the robotics impact dynamics was discussed and solved with Jacobian matrix being rank-deficient. It may fit into some special cases of biped impact

phenomena. As the impact model was generated from Lagrange mechanics, the system pre-impact dynamic equations can be directly incorporated into the model to solve the velocities after impact. In this work the impact dynamics was developed with an m-link rigid-body chain and detailed derivation of individual systems was not necessary. The proposed impact model and solution scheme contribute to research on impact phenomena of both biped robots and robot manipulators. Biped impact mechanics provides important information for the upcoming contact events (the SSP/DSP of next walking cycle or slippage of foot/feet). The related subject will be studied in detail in Chapter 5.

Chapter 3

Motion Planning

3.1 Introduction

Motion planning is a crucial step in the development of biped robots. Systematic methods for synthesizing biped gait are studied by researchers since 1980's (Miura and Shimoyama 1984, Pandy and Berme 1988, 1989, Shih and Churng 1990, Shih 1997, Channon *et al.* 1992, Hurmuzlu 1993a, Chevallereau and Aoustin 2001, Huang *et al.* 2001). Hurmuzlu (1993a,b) has presented an approach to develop objective functions that can be used in conjunction with controllers to regulate the motion of a planar five-link biped. The biped locomotion was designed in terms of step length, progression speed, maximum step height and the stance knee bias angle. According to his objective functions formulated for the motion planning, once the initial angles of each step are selected, the joint angular displacement profiles will be uniquely determined. However, in order to have continuous and repeatable gait, special requirements for the selection of initial joint angles, objective functions and their associated gait parameters are needed. These selections can be extremely challenging.

To solve such a problem, various numerical approximation methods, e.g., time polynomial functions (Red 2000, Chevallereau and Aoustin 2001) or periodic spline interpolations (Shih 1997, Huang *et al.* 2001) have been generated to approximate the biped joint angle profiles to the desired trajectories. Those methods can be conveniently used to find satisfactory or optimal joint angle profiles. A vast amount of literature was

found in biped motion planning by construction of polynomial functions to approximate biped joint angle positions (Chevallereau and Aoustin 2001, Channon *et al.*1992, Shih 1997). One advantage is its ability to satisfy some desired motion conditions, such as repeatability and gait optimization, etc. Disadvantages include a high computing load for large bipedal systems and the selection of the polynomials with improper orders may impose undesirable features to the joint angle profiles (Chevallereau and Aoustin 2001).

During bipedal locomotion, the upper body is in dynamic equilibrium, and the effect of hip motion in horizontal direction plays an important role for dynamically stable walking (Vukobratovic and Ekalo 1973, Thornton-Trump and Daher 1975). Chow and Jacobian (1971) studied the optimal biped locomotion and first drew attention to the hip motion and suggested that the hip trajectory be synthesized prior to joint angle profiles. The advantages include that it is easy to satisfy stability requirement and the gait synthesis procedure is also simplified. Although this method has been introduced to synthesize walking patterns for a seven-link biped (Huang *et al.* 2001), it has not attracted much attention.

From previous literature on biped gait generation, it has been noticed that several important issues need to be further investigated. Firstly, most studies have focused on the motion generation during SSP and the DSP has received less attention. The DSP plays an important role in keeping biped stable walking with a wide range of speeds, and should not be neglected. Thus it is important to synthesize the gait patterns that include both the SSP and DSP. Other important issues, which need to be considered in gait design, include requirements of continuity, repeatability and stability of the gait.

The objective of this chapter is to propose a method for synthesizing a cyclic gait for biped walking. The important issues, which have not been investigated properly in previous literature, will be considered. Compatible hip and swing limb tip trajectories will be designed first, which has the advantage of simplifying the problem by dividing the biped into three subsystems. The joint angle profiles for a full gait cycle including both the SSP and the DSP will be determined accordingly. The constraint functions and gait parameters are to be chosen such that repeatable gait will be generated. Smooth joint angle profiles will be generated at all times, including the transition between the SSP and the DSP, which also removes the velocity jump caused by impact. Certain gait parameters will be chosen such that the largest stability region during the DSP will be obtained.

3.2 Planning of Swing Limb and Hip Motion

3.2.1 Walking Cycle

It is desirable for the bipedal system to move steadily in the sagittal plane, that is, the cyclic biped motion is required to be continuous and repeatable. A complete step cycle (see Figure 3.1) under study is divided into a SSP and a DSP. The time period of the SSP is denoted as T_S and that of the DSP is denoted as T_D. In the successive step, the roles of the swing limb and stance limb are exchanged.

It has been noticed that the joint angle profiles can be determined if compatible trajectories for the hip and the tip of the swing limb can be prescribed. This approach has the advantage in that the biped is divided into the torso and two lower limbs, which significantly simplifies the problem. The compatible hip and swing limb trajectories should satisfy the condition that the distance between the hip and each lower limb tip is

less than the length of the whole limb and greater than the difference between the lengths of the shank and thigh at any time. This condition guarantees the existence of the joint angle profiles during the whole walking period. If it is further assumed that both knees can only bend in one direction, such as bending forward, the joint angle profile will be uniquely determined by the trajectories of the hip and swing limb.

From the viewpoint of natural human walking, it is desirable that the torso is kept directly upward or oscillates slightly around the upright position (Mitobe *et al.* 1997, Huang *et al.* 2001). Prescribing the trajectory $\theta_3(t) = 0$ in both the SSP and the DSP, the main task here is to synthesize the motion of the lower limbs. To satisfy the bipedal walking under various ground conditions, it is natural to design the trajectory for the swing limb tip first, followed by the design of compatible hip trajectory. Note that the solution is valid when the no-slip condition at the contact point is satisfied, *i.e.*, $|F_y/F_x| < \mu$, where μ is the friction coefficient between the lower limb tips and the ground.

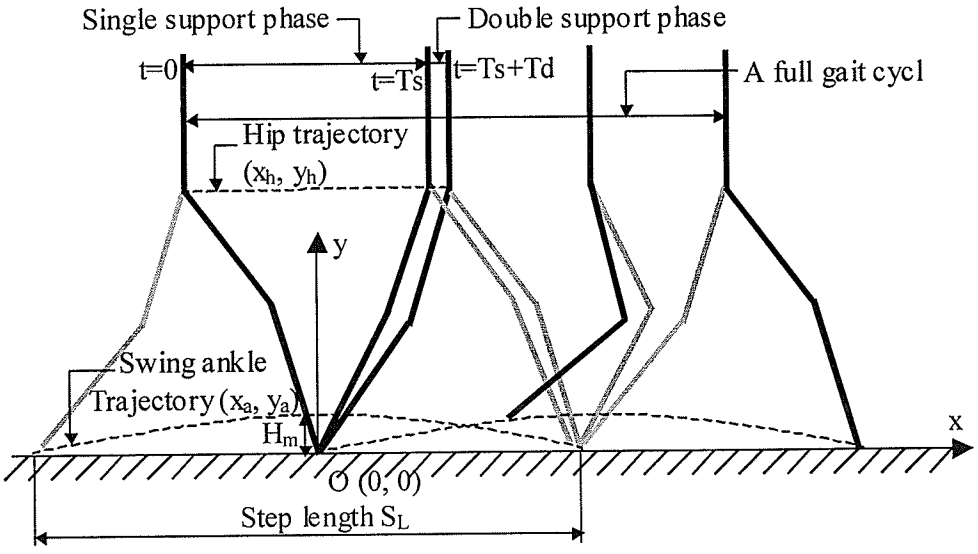

Figure 3.1 Full gait cycle of a five-link biped walking in sagittal plane

3.2.2 Design of the Trajectories of the Swing Limb Tip

The trajectory of the tip of the swing limb during the SSP is a significant factor in satisfying ground conditions. In this section, the constraint equations are developed for solving swing limb tip trajectories. The trajectory of the tip of the swing limb is denoted by the vector $X_a : (x_a(t), y_a(t))$, where $(x_a(t), y_a(t))$ is the coordinate of the swing limb tip position with the origin of the coordinate system located at the tip of the supporting limb (see Figure 3.1). There is a need to first outline how many constraint equations are required for the desired swing tip motion. The order of the polynomials can be determined accordingly so that the corresponding number of coefficients of the polynomials will be solved uniquely. Under this consideration, a total of 10 constraint equations will be needed to satisfy the requirements, which will be emphasized next. Accordingly, third-order and fifth-order time polynomial functions are chosen as the simplest form for the x_a and y_a, respectively. Although higher order polynomials can be employed, more constraints must be added and sometimes this may lead to improper orders resulting in undesirable features and oscillations (Chevallereau and Aoustin 2001). Thus the time polynomial functions for the coordinates of the swing limb tip is generated as

$$X_a : \begin{cases} x_a(t) = a_0 + a_1 t + a_2 t^2 + a_3 t^3, & 0 \le t \le T_S \quad (3.1a) \\ y_a(t) = b_0 + b_1 t + b_2 t^2 + b_3 t^3 + b_4 t^4 + b_5 t^5, & 0 \le t \le T_S \quad (3.1b) \end{cases}$$

In order to solve the coefficients a_i and b_j (i=0,...3 and j=0,...5), a set of constrained equations are required. These constrained equations come from the conditions of the desired motion. The gait patterns are cast in terms of four basic quantities: step length S_L, step period for the SSP T_S, maximum clearance of the swing limb H_m, and its location S_m. They are chosen from various biped walking gait requirements. Other constraints used for

designing the swing limb motion are the repeatability and continuity of the gait. The constraint relations are described as follows:

(1) ***Geometrical constraints*****:** The swing limb has to be lifted off the ground at the beginning of the step cycle and has to land back at the end of it. This condition must be enforced, which is shown by the following equations:

$$y_a(0) = 0, \tag{3.2}$$

$$y_a(T_s) = 0. \tag{3.3}$$

(2) ***Maximum clearance of the swing limb****:* During the swing phase, the tip of the swing limb has to stay clear off the ground to avoid accidental contact. In some previous work (Hurmuzlu 1993a, Cheng and Lin 2000) the parabolic relation between $x_a(t)$ and $y_a(t)$ has been assumed. Although this strategy has the advantage of being the simplest form that allows the prescription of the desired step length and the tip maximum clearance independently, it is unlikely to satisfy the requirement of repeatable gait. In this work, the swing limb trajectory is synthesized by setting the following relation:

$$x_a(T_m) = S_m, \tag{3.4}$$

$$y_a(T_m) = H_m, \tag{3.5}$$

$$\dot{y}_a(T_m) = 0, \tag{3.6}$$

Where H_m is the maximum clearance of the swing limb and S_m is the x-coordinate of the swing limb tip corresponding to the maximum clearance, which were mentioned as two of the four known basic quantities. T_m is the time instant when the tip of the swing limb reaches to the maximum clearance. Note that T_m is not prescribed.

(3) ***Repeatability of the gait:*** The requirement for repeatable gait imposes the initial posture and velocities to be identical to those at the end of each step. The posture

repeatability requires identical strides between the two lower tips at the beginning and end of the step. Furthermore, since during the DSP both tips are in contact with the ground and remain stationary, in order to keep velocity repeatability in the next cycle, the initial velocities of the swing tip in both horizontal and vertical direction must remain zero. Subsequently, the following relations must hold:

$$x_a(0) = -S_L/2, \tag{3.7}$$

$$x_a(T_S) = S_L/2, \tag{3.8}$$

$$\dot{x}_a(0) = 0, \tag{3.9}$$

$$\dot{y}_a(0) = 0. \tag{3.10}$$

(4) Continuity of the gait: The final state of the SSP and the initial state of the DSP should be continuous. Since the velocity of the leading tip at the beginning of the DSP is zero, the velocity of the swing tip immediately before contact should also be zero to satisfy the continuity condition. On the other hand, during biped locomotion, when the swing limb contacts the ground, impact occurs, which causes sudden changes in the joint angular velocities. It has been addressed in Chapter 2 that both the external impulses at contact points and the changes of angular velocities before and after impact are proportional to the change of swing tip linear velocity. The lower the magnitude of the swing tip velocity, the less impact effect is. By keeping the velocities of the swing limb zero before impact, the sudden jump in the joint angular velocities can be eliminated. The above conditions lead to:

$$\dot{x}_a(T_S) = 0, \tag{3.11}$$

$$\dot{y}_a(T_S) = 0. \tag{3.12}$$

Equations (3.2)-(3.12) can be used for solving ten polynomial coefficients a_i, b_j ($i=0,...3$ and $j=0,...5$) and T_m. The trajectory of the swing limb with the above coefficients satisfies the requirements, such as repeatable gait with no effect from the impact and with prescribed gait parameters.

3.2.3 Design of the Trajectories of Hip Motion

Hip motion has significant effect on the stability of the bipedal system. Here the trajectories of the hip are designed for the SSP and the DSP separately, which are denoted by the coordinate of the hip position as $X_{hS}:(x_{hS}(t),y_{hS}(t))$ in the SSP and $X_{hD}:(x_{hD}(t),y_{hD}(t))$ in the DSP. Similar to the procedure of the swing tip design, a third order polynomial function is used to describe both x_{hS} and x_{hD}. These chosen functions can adequately describe the desirable motion while keeping the simplest form of polynomials. The functions describing the coordinates of the hip position in the SSP and the DSP are shown below:

$$X_{hS}:\begin{cases} x_{hS}(t)=c_0+c_1t+c_2t^2+c_3t^3; & 0\le t\le T_S \quad (3.13a)\\ y_{hS}(t)=y_h(t)\,; & 0\le t\le T_S \quad (3.13b)\end{cases}$$

$$X_{hD}:\begin{cases} x_{hD}=d_0+d_1t+d_2t^2+d_3t^3; & 0\le t\le T_D \quad (3.13c)\\ y_{hD}(t)=y_h(t); & 0\le t\le T_D \quad (3.13d)\end{cases}$$

The next step involves formulating constrained equations, which include the additional quantities: positions of the hip at the beginning of the SSP and the DSP, S_{S0} and S_{D0}, step period for the DSP, T_D, and the height of the hip, H_h. Besides the constraints of repeatability and continuity of the gait, the stability of the bipedal walking during the DSP is also considered. The constraint relations are described as follows:

(1) ***Vertical hip motion:*** One desired feature of biped gait is to keep the minimum vertical oscillation of the gravity center, which requires minimum vertical motion of the hip. For the sake of simplicity, assuming y_{hS} and y_{hD} constant at any time during the whole gait cycle, *i.e.*,

$$y_{hS}(t) = H_h, \tag{3.14}$$

$$y_{hD}(t) = H_h. \tag{3.15}$$

(2) ***Repeatability of the gait:*** To keep the gait repeatable, the triangle constructed by the hip and the two lower tips must be identical to that at the beginning of the SSP and at the end of the DSP. Furthermore, the hip velocities at the beginning and the end of the step must be the same. Thus, the following relations must hold:

$$x_{hS}(0) = -S_{S0}, \tag{3.16}$$

$$\mathrm{x}_{\mathrm{hD}}(T_D) = S_L/2 - S_{S0}, \tag{3.17}$$

$$\dot{x}_{hS}(0) = V_{h1}, \tag{3.18}$$

$$\dot{x}_{hD}(T_D) = V_{h1}. \tag{3.19}$$

where V_{hl} is the hip velocity at the beginning of each step, which will be determined later.

(3) ***Continuity of the gait:*** The hip trajectory must be continuous during the whole gait cycle, *i.e.*, the horizontal displacements and velocities of the hip at the end of the SSP and the beginning of the DSP must be identical respectively, which leads to:

$$x_{hS}(T_S) = S_{D0}, \tag{3.20}$$

$$\mathrm{x}_{\mathrm{hD}}(0) = S_{D0}, \tag{3.21}$$

$$\dot{x}_{hS}(T_S) = V_{h2}, \tag{3.22}$$

$$\dot{x}_{hD}(0) = V_{h2}, \tag{3.23}$$

where V_{h2} will be determined later.

(4) Stability of the gait during the double support phase: The horizontal velocity of the hip is the main factor that affects the stability of a bipedal robot walking in a sagittal plane. As discussed in Section 3.1, some previous studies focused on deriving the hip trajectories to execute a desired ZMP. The disadvantages are that the hip acceleration may be very large and not all desired ZMP trajectories can be attained. In this work, the following procedure will be proposed to determine an optimal set of initial and final velocities of hip motion during the DSP: V_{h1} and V_{h2}:

(i) generate a series of smooth x_{hS} and x_{hD} by selecting various V_{h1} and V_{h2};

(ii) obtain a set of solutions of x_{hS} and x_{hD} with the largest stability margin.

Stability margin is defined here as the minimum distance between the ZMP and the boundary of the stable region, which is the line between the two tips of the supporting limbs. The Equations (3.16)-(3.23) and the stability constraints can be used to solve all eight coefficients, c_i *and* d_i *(i=0,...3)*. For each set of selected values of V_{h1} and V_{h2}, x_{hS} and x_{hD} can be solved uniquely and will be used to find out the ZMP trajectory. Through computer iterative calculation, a set of V_{h1} and V_{h2} can be easily obtained to solve the trajectories of x_{hS} and x_{hD} with the largest stability margin.

3.3 Biped Joint Angle Profiles of Angular Displacements

With the hip and swing limb tip trajectory design and the biped kinematic model, the joint angle profiles can be uniquely determined and expressed by the following equations:

$$\begin{cases} \theta_1(t) = \arcsin\left(\dfrac{A_1 C_1 + B_1\sqrt{A_1^2 + B_1^2 - C_1^2}}{A_1^2 + B_1^2}\right) \\ \theta_2(t) = \theta_1(t) + \arcsin\left(\dfrac{A_1\cos(\theta_1(t)) - B_1\sin(\theta_1(t))}{l_2}\right) \\ \theta_3(t) = 0 \\ \theta_4(t) = \arcsin\left(\dfrac{A_4 C_4 + B_4\sqrt{A_4^2 + B_4^2 - C_4^2}}{A_4^2 + B_4^2}\right) \\ \theta_5(t) = \theta_4(t) + \arcsin\left(\dfrac{A_4\cos(\theta_4(t)) - B_4\sin(\theta_4(t))}{l_5}\right) \end{cases} \tag{3.24}$$

where for the SSP,

$$A_1 = x_{hS}(t),\ B_1 = y_{hS}(t),\ C_1 = \frac{A_1^2 + B_1^2 + l_1^2 - l_2^2}{2l_1},$$

$$A_4 = x_{aS}(t) - x_{hS}(t),\ B_4 = y_{hS}(t) - y_{aS}(t),\ C_4 = \frac{A_4^2 + B_4^2 + l_4^2 - l_5^2}{2l_4}$$

For the DSP,

$$A_1 = x_{hD}(t),\ B_1 = y_{hD}(t),\ C_1 = \frac{A_1^2 + B_1^2 + l_1^2 - l_2^2}{2l_1}$$

$$A_4 = \frac{1}{2}S_L - x_{hD}(t),\ B_4 = y_{hD}(t),\ C_4 = \frac{A_4^2 + B_4^2 + l_4^2 - l_5^2}{2l_4}.$$

Note that the angles θ are defined as the angles between the link and the vertical position, "+" denotes the link right of the vertical and "-" left of the vertical. Equation (3.24) will be used as desired joint angle profiles in the control design shown in Chapter 4.

3.4 Simulation Verification

In this section, the hip and swing tip motion and joint angle profiles for a five-link biped walking on level ground with both the SSP and the DSP are simulated based on the

method discussed in Section 3.2 and Section 3.3. The physical parameters corresponding to the model used in this simulation are listed in Table 3.1. The walking speed is chosen approximately *1.0m/s* and the walking pattern is generated using the gait parameters S_L=*0.70m*, T_S=*0.6s*, T_D=*0.1s*, X_m=*(0, 0.05m)*.

Table 3.1 Biped physical parameters

Link No.	M_i (kg)	I_i (kgm^2)	L_i (m)	d_i (m)
1	2.23		0.332	0.189
2	5.28		0.302	0.236
3	14.79	0.033	0.486	0.282
4	5.28		0.302	0.066
5	2.23		0.332	0.143

Figure 3.2a shows the horizontal displacements of the hip and the tips of both the swing limb and stance limb versus time. Figure 3.2b shows the trajectories of motion of the tip of the swing limb in the x-y plane. It can be seen that all the trajectories are smooth, *i.e.,* all the velocities are continuous.

Figure 3.3 shows the joint angle profiles for two steps. Figure 3.3a shows the trajectories of the joint angles and Figure 3.3b is the angular velocities during the SSP and the DSP, respectively. It is seen that both joint angles and their angular velocities are repeatable, and the velocities are continuous at the instant of impact showing that the discontinuity of the angular velocities has been removed.

Figure 3.4 shows the horizontal displacements of the gravity centre of the biped, hip motion and ZMP trajectories during the DSP. The grey area is the stability region with the top and bottom lines representing the locations of the two feet. It can be seen that the gravity centre and the hip, especially the ZMP, remain approximately at the centre of the stability region, which ensures a large stability margin for DSP.

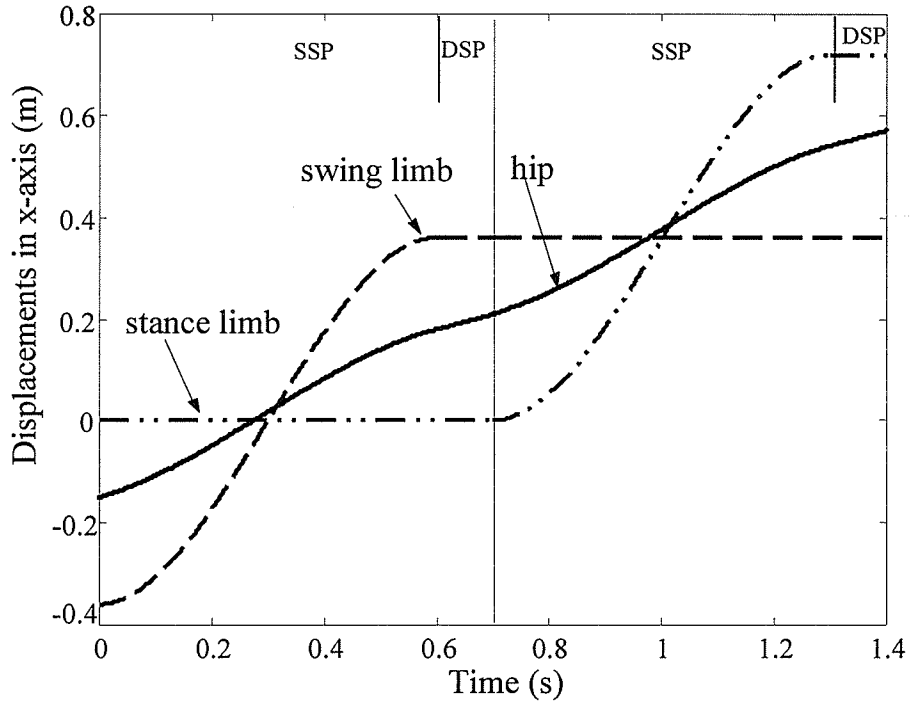

(a)

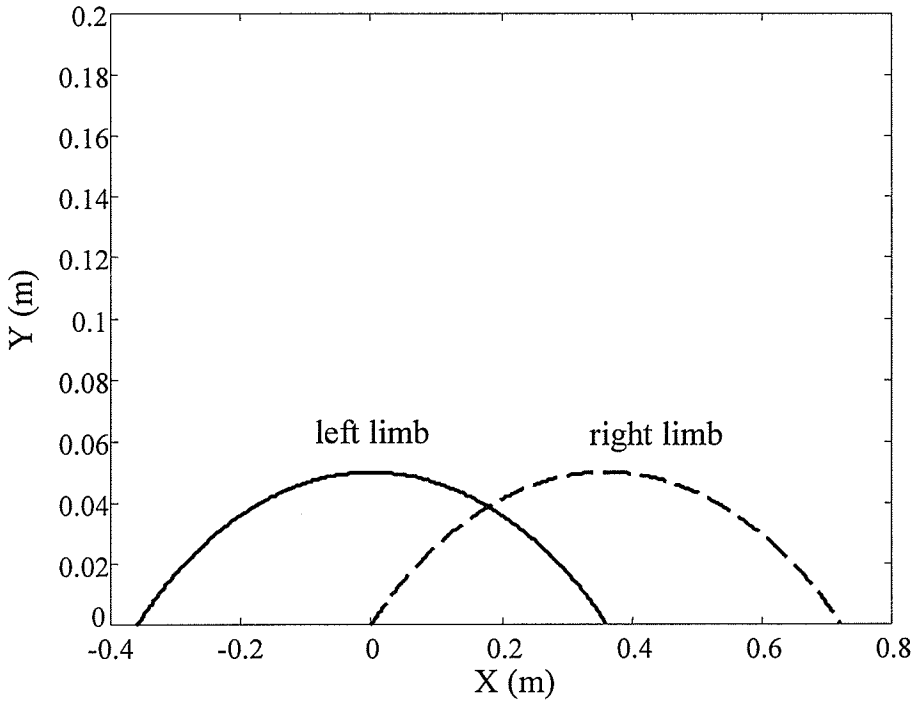

(b)

Figure 3.2 Designed movements of the hip and lower limb (a) *x-t* and (b) *y-x*

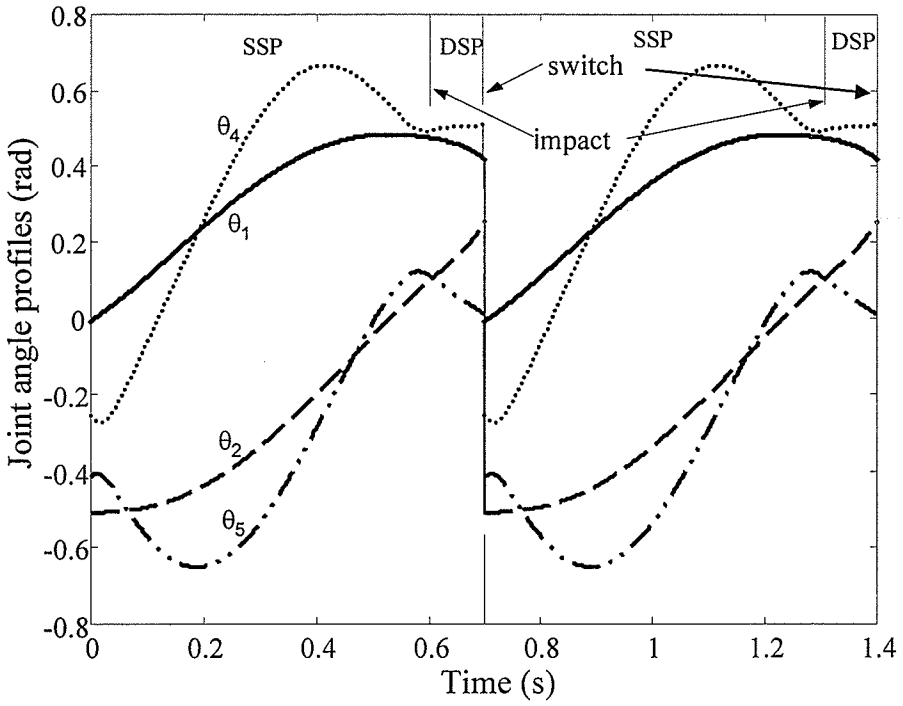

(a)

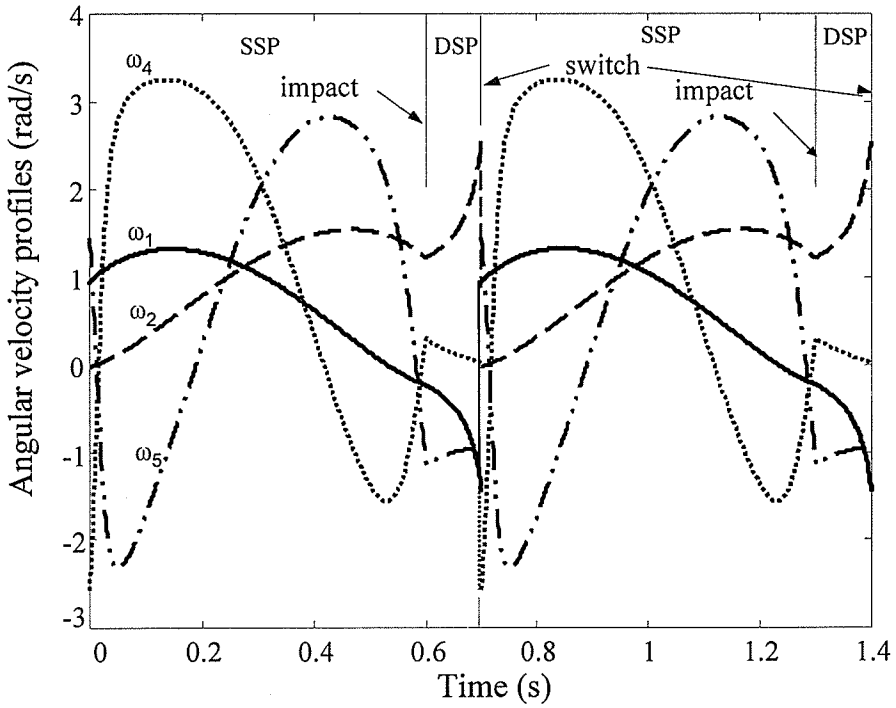

(b)

Figure 3.3 Joint profile design (a) joint angles, (b) angular velocities

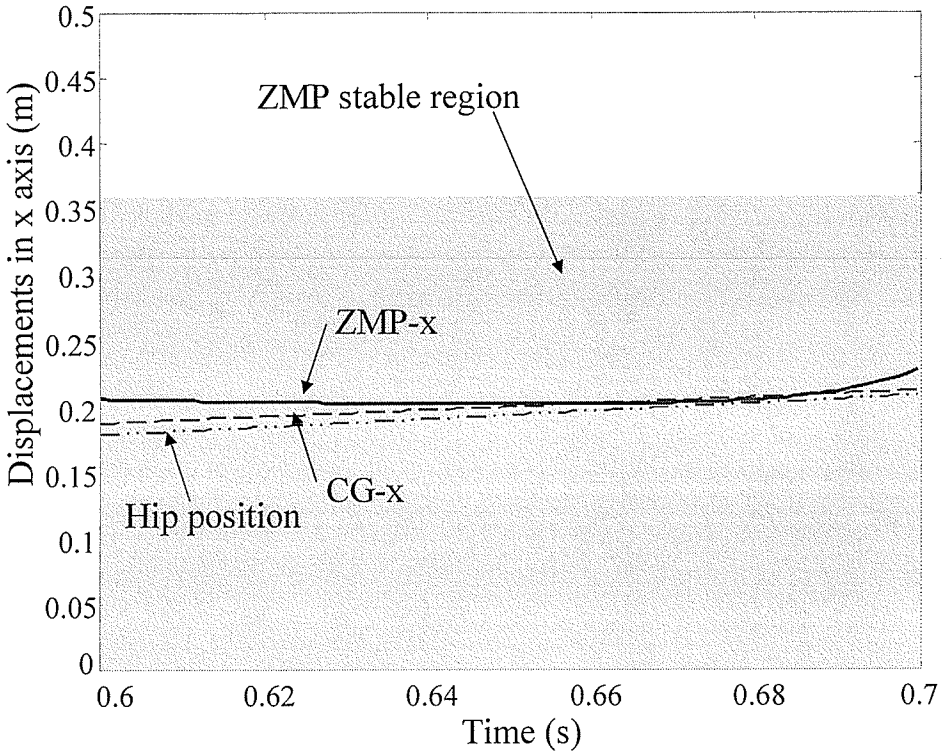

Figure 3.4 CG, hip and ZMP trajectories during the double support phase

Figure 3.5 shows the reaction forces exerted on the lower limbs obtained from simulations. For the above gait parameters, the vertical ground reaction forces are always upward showing that a firm contact without lifting is guaranteed. In addition, the no-slip condition can be guaranteed with a friction coefficient of 0.4 and higher.

Figure 3.6 is the stick diagram of the five-link biped walking on level ground. From this diagram, one can observe the overall motion of the biped during the SSP and the DSP. The solid lines represent the SSP while the dashed lines represent the DSP. The asterisk shows the CG of the biped during walking. The posture of the biped at the end of each step is close to that at the beginning of each step, and the displacement of CG trajectory is almost horizontal. Overall, Figure 3.5-3.6 show that the gait pattern design based on the proposed method is quite natural and the contact constraints between the lower limbs and the ground can be satisfied with a moderate friction coefficient.

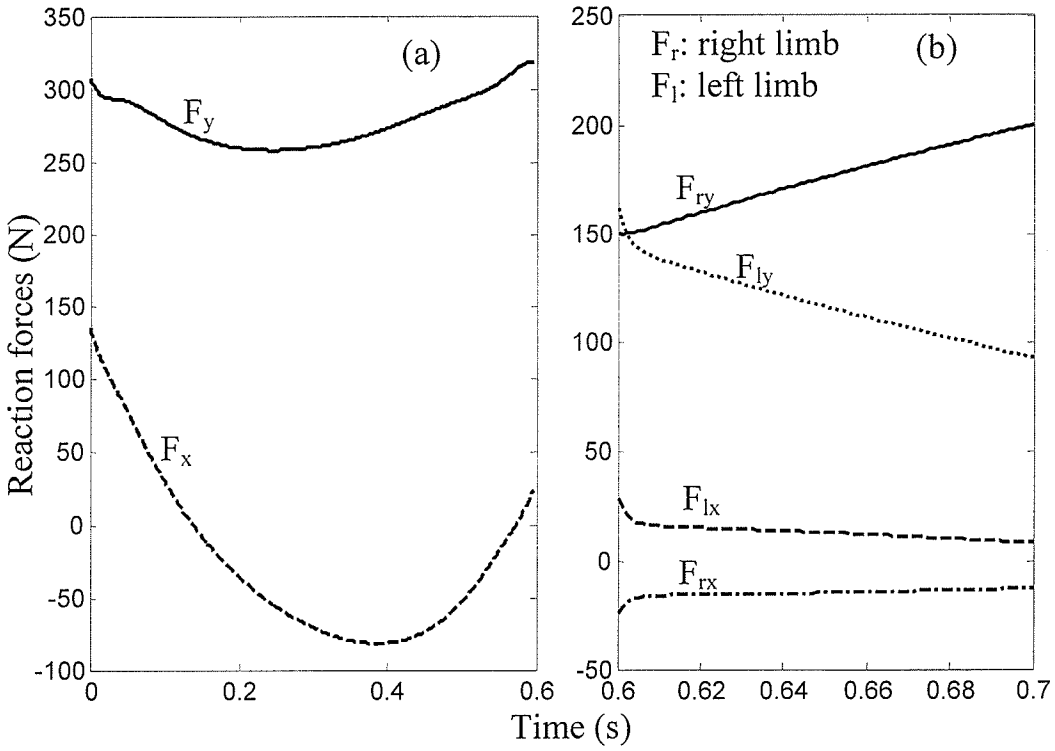

Figure 3.5 Reaction forces (a)SSP and (b)DSP

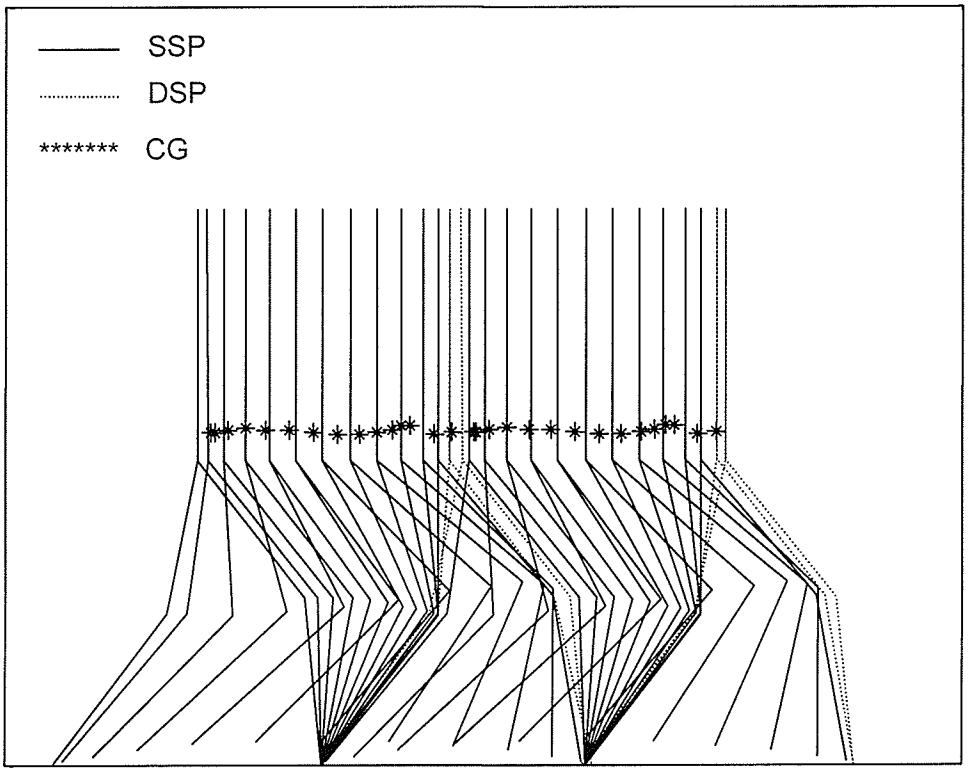

Figure 3.6 Stick diagram of a biped walking

3.5 Summary

In this chapter, a systematic approach was presented for gait synthesis for the five-link biped walking in the sagittal plane. Unlike most of the previous five-link biped work focusing on the SSP, the proposed motion planning included both the SSP and the DSP, which provided the biped a wide range of walking speeds and stable locomotion.

Although Chow and Jacobson (1971) have indicated the importance of the hip motion and suggested that the hip trajectory be synthesized prior to joint angle profiles, it was less attentive to present literature on biped motion planning and regulation. In this chapter, a method was developed by formulating the compatible trajectories for the hip and the swing limb instead of directly designing the joint angle profiles. This strategy has the advantage of dividing the biped into three subsystems, which significantly simplified the problem and made the calculation of joint angle profiles manageable.

Swing tip motion was first designed to satisfy the ground geometric conditions and speed requirement, etc. Hip motion was then generated to fulfil stability and continuity requirements, etc. The trajectories of the swing tip and the hip were approximated with time polynomial functions and their coefficients were solved using the constraint equations cast in terms of the step length, step period and maximum step clearance etc. Other important constraints introduced in this design contained the stability during the DSP and repeatability of the gait. The designed biped motion was also smooth during the full gait cycle.

Computer simulations were carried out to present the designed biped motion. The results showed that with all the above designed criteria satisfied, the gait pattern appears

natural and only moderate requirement on the friction coefficient of the ground is required to keep the contact constraints between the limbs and the ground.

The proposed strategies can provide a valuable tool for generating motion patterns of biped gait, which is crucial for biped motion control. The advantage of designing the hip and swing tip motion significantly simplifies the problem, which makes it feasible to generate other optimal gait patterns, such as energy efficient walking. It is also a stepping stone for using more complicated objective functions. The avoidance of impact occurring at heel strike to eliminate the sudden jump of the angular velocity and large impulsive forces to each joint reduces the control difficulty and enhances the system stability, which is the main concern in the development of bipedal walking machines.

Chapter 4

Motion Control

4.1 Introduction

One challenge in motion regulation of bipedal walking is the high nonlinearities of the dynamics and the inaccuracy of the parameters in biped models. Computed torque control as a classic nonlinear feedback control can be applied to biped locomotion to eliminate the nonlinear terms involved in the dynamic model and send feedback signals to track reference trajectories. Mitobe *et al.* have used computed torque control algorithms to a biped single support model (1995) and a double support model (1997). The main disadvantage of the computed torque control is that in practice the biped physical parameters and dynamic model are not available exactly but are only approximated. Therefore the computed torque control law may lead to unacceptable performance if the parameter uncertainties exist. In recent studies, the robust control or adaptive control techniques are utilized to deal with uncertain systems; specifically, the sliding mode control as one of the most often used robust control method has been applied in biped walking to counter the modeling uncertainties and stabilize the system. Tzafestas *et al.* (1996) used sliding mode control applied to a 5-link biped SSP and it is compared to computed torque control. They proved that the sliding mode controller performs much better with the superiority of its performance being strengthened as the degree of uncertainty increases.

Another challenge is the control of biped during DSP. Motion of a biped robot with DSP has the advantage that it is more convenient to realize the stable motion and can fulfill more tasks than that only walking with SSP. However it becomes more difficult when controlling a biped DSP than that of the SSP. Motion of a biped robot during DSP can be described as the motion of dynamic system under holonomic constraints. Vast literature was found for controlling such constraint systems in reduced state space or non-reduced space. The good reason to use non-reduced state space model is that the natural coordinate system is preserved for conceptual and computational reasons (Hemami and Wyman 1979a), however, these natural coordinates are actually not independent and if the controllers are not designed for perfectly tracking the reference signals, the constraint conditions may be violated (Mitobe *et al.* 1997). When the reduced state space model is applied to the constraint system, a set of independent generalized coordinates in a minimal dimension is introduced to adequately describe the constraint motion and to eliminate the constrained forces for the equation of motion (Goldstein 1980). However since the original coordinates are expressed as nonlinear functions of the new independent coordinates and when the system DOF is high, the explicit expression between the two coordinate systems can be very complicated in maping.

Many prevailing articles discussed the control algorithms of constraint biped systems (Hemami and Wyman 1979a and 1979b, Mitobe *et al.* 1997) or manipulators (Su *et al.* 1992, Mnif *et al.* 1995, Bartolini and Punta 2001), but only a few were found in the application of dynamic systems with DOF higher than three. Hemami and Wyman presented a modeling method and linear control law to a 3-link biped constrained system in the non-reduced state space, but for such a 3-DOF system with two constraints, the

method was only applicable for a swaying posture of the upper body in the vicinity of the vertical stance. Mitobe *et al.* (1997) discussed the motion of a 4-DOF biped robot during DSP and applied the computed torque control algorithm to the system. In their work, the position of center of gravity of the trunk were formulated as the reduced state space independent generalized coordinates, and the control problem was defined as a trajectory tracking problem which the body of the biped was controlled to track a desired trajectory. In their controller, the desired forces were needed as control input for controlling the constraint forces. From a careful literature review, no research was found using robust sliding mode control to a biped DSP. Especially in the 5-link biped double support model which has three independent coordinates and two holonomic constraints, the original coordinate system has to be reformulated with the independent ones by a 5×3 noninvertible transformation matrix, and pseudo-inverse matrices might be needed for designing controllers to distribute the joint torques. Furthermore, when the system parameter uncertainties are involved, the sliding mode controller can be very complicated to introduce to the model.

In the present research, the sliding mode controller is utilized in the 5-link biped SSP and DSP, provided that the upper boundaries of the system uncertainties are known. In controlling the biped double support motion, a set of independent generalized coordinates in reduced state space describing the hip position and trunk orientation is chosen and the controllers are designed to control the new generalized coordinates. The constraint forces are automatically solved from the dynamic equations as output of the system and also are the inputs for the controllers and it is not necessary to design the specific force controller to track some reference constraint forces.

4.2 Control Algorithm

For the system described by Equations (2.7) and (2.21), sliding mode control algorithms can be developed to stabilize the generalized coordinates, eliminate the effect of system parametric uncertainties, and maintain the constraint conditions (for DSP).

First, the following assumptions are made before establishing the control law:

1) The bounds of the parameter uncertainties of the biped system are known.

2) The state space variables are available for measurement.

"The parameters with uncertainties" are those physical parameters of the biped system, including mass (m), length (l) and the moment of inertial (I) of each link, as well as the position of the center of mass of each link with respect to its joint (d). A symbol φ_i is used to represent each physical parameter (m, l, I, d) and $E_i \times 100\%$ ($0 \leq E_i < 1$) represents their uncertainties in the upper bounds. The corresponding estimated values of each parameter are $\hat{\varphi}_i = (1 + E_i)\varphi_i$. Also, a symbol M_i is used to represent the matrices (D, H, G, J, etc) in the model of Equations (2.7) and (2.21), then, the estimated matrices are calculated by: $\hat{M}_i = \hat{M}_i(\hat{\varphi}_i) = M_i(\varphi_i) + \Delta M_i(E_i \varphi_i)$.

4.2.1 Control in Single Support Phase

In this second order differential system described by Equation (2.7), a time-varying sliding surface S is defined as $s(q,t) = 0$, where

$$s = \dot{e} + 2\Lambda e + \Lambda^2 \int_0^t e(\tau) d\tau , \tag{4.1}$$

where e and $\dot{e}$ are the vectors of tracking errors defined as

$$e = q - q_d$$
$$\dot{e} = \dot{q} - \dot{q}_d$$

Λ is a diagonal matrix standing for positive gains given by

$$\Lambda = diag[\Lambda_1 \quad \Lambda_2 \quad \Lambda_3 \quad \Lambda_4 \quad \Lambda_5],$$

Giving the PD controller with the form

$$u = \ddot{q}_d - K_D\dot{e} - K_P e, \tag{4.2}$$

where $K_P=\Lambda^2$ and $K_D=2\Lambda$ are the proportional and derivative gains.

As one has

$$\begin{aligned} u &= \ddot{q}_d - K_D\dot{e} - K_P e \\ &= \ddot{q} + (\ddot{q}_d - \ddot{q} - K_D\dot{e} - K_P e) \\ &= \ddot{q} + (-\ddot{e} - 2\Lambda\dot{e} - \Lambda^2 e) \\ &= \ddot{q} - \dot{s} \end{aligned}$$

the dynamic Equation (2.7) can be expressed as

$$D_q(\dot{s}+u) + H_q(s+v) + G_q = T_q,$$

where $v = \dot{q} - s = \dot{q}_d - 2\Lambda e - \Lambda^2\int_0^t e(\tau)d\tau$, i.e.,

$$D_q\dot{s} + H_q s = T_q - (D_q u + H_q v + G_q) \ . \tag{4.3}$$

The equivalent controller can be constructed as

$$\hat{T}_q = \hat{D}_q u + \hat{H}_q v + \hat{G}_q, \tag{4.4}$$

and the actuating torque is then generalized as

$$T_{qi} = \hat{T}_{qi} - (\eta_{Si} + \sigma_i)\,\mathrm{sgn}(s_i), \tag{4.5}$$

where $\eta_{Si} \in R^5$, $\eta_{Si} = abs\left\{\left[(\hat{D}_q - D_q)u + (\hat{H}_q - H_q)v + (\hat{G}_q - G_q)\right]_i\right\} \overset{\Delta}{=} abs(\Delta_{Si})$ is a vector of functions of those parameters with uncertainty boundaries and state space variables; σ is the positive constant vector used to satisfy the sliding condition which will be discussed later.

In general, control law (4.5) will be associated with a chattering problem because of the switching function in the controller. It is very undesirable and should be eliminated.

Slotting and Pastry (1983) suggested a solution to this problem by eliminating the discontinuities in a thin boundary layer neighbouring the switching surface (for n^{th} order system):

$$B(t) = \left\{x, \left| s(x;t) \le \Lambda^{n-1}\varepsilon \right| \right\}, \varepsilon > 0,$$

where ε is the boundary layer width. It is achieved by choosing the control law outside *B(t)* unchanged while replacing *sgn(s)* by $sat[s/(\Lambda^{n-1}\varepsilon)]$ inside *B(t)*, i.e. replace the switching function with a modified saturation function. Later researchers (Cai and Song 1993, Wu *et al.* 1998a) further smoothened the control law by a hyperbolic function *tanh(s)*. Here the smoothened controller is chosen using the latter,

$$T_{qi} = \hat{T}_{qi} - (\eta_{Si} + \sigma_i)\tanh(\gamma_i s_i), \tag{4.6}$$

where γ is positive constant 5×5 diagonal matrix for controlling the hyperbolic functions.

Instead of keeping trajectories on the sliding surface, the control algorithm maintains the trajectories close to the surface within a thin boundary layer. Once the system trajectories enter the boundary layer, they will remain inside. It is to be verified that with the smoothened controllers, the parameters γ can be found as some finite constants such that for any arbitrarily given thickness boundary layer neighbouring the sliding surface, the trajectories will be bounded. The verification is given below.

With the choice of Lyapunov function candidate given by $V = \frac{1}{2}s^T Ds$, the derivation of V along the trajectory of the solution of Equation (2.7) is given by

$$
\begin{aligned}
\dot{V} &= \tfrac{1}{2} s^T \dot{D} s + s^T D \dot{s} \\
&= \tfrac{1}{2} s^T \dot{D} s - s^T H s + s^T (D\dot{s} + Hs) \\
&= \tfrac{1}{2} s^T (\dot{D} - 2H) s + s^T \left[D(\ddot{q} - u) + H(q - v) \right] \\
&= 0 + s^T [T - (Du + Hv + G)] \\
&= s^T [\Delta_S - \tanh(\gamma s)(\eta_S + \sigma)]
\end{aligned}
\tag{4.7}
$$

Note that the term $\frac{1}{2} s^T (\dot{D} - 2H) s$ is zero because $\dot{D} - 2H$ is a skew-symmetric matrix (Koditschek 1985).

In order to guarantee $\dot{V} < 0$, the following condition must be satisfied

$$
\tanh(\gamma_i |s_i|) > \frac{\Delta_{Si}}{\eta_{Si} + \sigma_i} \stackrel{\Delta}{=} \mu_i \quad \text{i=1,2...5}, \tag{4.8}
$$

if the condition $\dot{V} < 0$ is held for all $|s_i| \geq \varepsilon_i$, the following condition must be held (See Appendix IV for detail)

$$
\gamma_i > \frac{1}{2\varepsilon_i} \ln\left(\frac{1 + \mu_i}{1 - \mu_i} \right). \tag{4.9}
$$

As σ_i is a positive constant, $-1 + \zeta < \mu_i < 1 - \zeta, 0 < \zeta < 1$ and thus $0 < \ln\left(\frac{1 + \mu_i}{1 - \mu_i} \right) < +\infty$, i.e. for any positive number ε_i denoting the width of the boundary layer, a positive γ_i can always be found. Thus the continuous sliding controller is realizable for an approximate trajectory tracking with the width of the boundary layer ε.

4.2.2 Control in Double Support Phase

In the second order differential system Equation (2.21), a time-varying sliding surface S is defined as $s(p,t) = 0$, where $s = \dot{e} + 2\Lambda e + \Lambda^2 \int_0^t e(\tau) d\tau$, and e and $\dot{e}$ are the vectors of tracking errors defined as

$$e = p - p_d$$
$$\dot{e} = \dot{p} - \dot{p}_d$$

Λ is a diagonal matrix standing for positive gains given by $\Lambda = diag[\Lambda_1 \quad \Lambda_2 \quad \Lambda_3]$.

By introducing the PD controller

$$u = \ddot{p}_d - K_D\dot{e} - K_P e, \tag{4.10}$$

Equation (2.21) can be written as:

$$\dot{s} = C(T - N) + B\dot{p} - u. \tag{4.11}$$

The equivalent controller can be constructed as

$$\hat{T} = \hat{C}^{-}u - \hat{C}^{-}\hat{B}\dot{p} + \hat{N}. \tag{4.12}$$

and the sliding controller is designed as

$$T_i = \hat{T}_i - \sum_{j=1}^{3}\left\{\hat{C}_{ij}^{-}\left[\text{sgn}(s_j)\sum_{k=1}^{5}\left(\left|\hat{C}_{jk}\right|\eta_{Dk} + \sigma_k\right)\right]\right\}, \quad i = 1,2...5, \tag{4.13}$$

where $\eta_D \in R^5$, $\eta_{Di} = abs\left\{\left|(\hat{C}^{-} - C^{-})\dot{u} - (\hat{C}^{-}\hat{B} - C^{-}B)\dot{p} + (\hat{N} - N)\right|_i\right\} = abs(\Delta_{Di})$ is a vector of functions of those parameters with uncertainty boundaries and state space variables; σ is the positive constant vector used to satisfy the sliding condition. $\hat{C}^{-}$ represents the pseudo-inverse matrix* of $\hat{C}$.

To eliminate the chattering problem due to the switching function, a smoothened controller is chosen as,

$$T_i = \hat{T}_i - \sum_{j=1}^{3}\left\{\hat{C}_{ij}^{-}\left[\tanh(\alpha_j s_j)\sum_{k=1}^{5}\left(\left|\hat{C}_{jk}\right|\eta_{Dk} + \sigma_k\right)\right]\right\}, \tag{4.14}$$

where α is a constant 3-dimentional vector for controlling the hyperbolic function.

The Lyapunov function candidate in the DSP is considered as $V = \frac{1}{2}s^T s$, and the

---

* Since $\hat{C}$ is not a square matrix, its 'inverse' form is solved by pseudo-inverse matrix defined by: $\hat{C}^{-} = C^T\left(\hat{C}C^T\right)^{-1}$.

derivation of V along the trajectory of the solution of Equation (2.21) is given by

$$\begin{aligned}\dot{V} &= s^T \dot{s} \\ &= s^T (\ddot{p} - u) \\ &= s^T (C\dot{T} + B\ddot{p} - C\dot{N} - u) \\ &= s^T \{C[\Delta - (\hat{C}^- \cdot \tanh(\alpha s))(abs(\hat{C})\eta + \sigma)]\end{aligned} \tag{4.15}$$

here $\left[abs(\hat{C})\right]_{ij} \triangleq |\hat{C}_{ij}|$ denotes a 3×5 matrix, each entry being the absolute value of that of matrix $\hat{C}$.

In practice, for parameter uncertainties to be less than 100%, $0 < K_{\min} < \sum_{k=1}^{5} C_{q\,ik} \hat{C}^{-}_{q\,kj} < K_{\max}$. In order to guarantee $\dot{V} < 0$, the following condition must hold

$$\tanh(\alpha_i |s_i|) > \frac{\sum_{k=1}^{5} |\hat{C}_{ik} \eta_{Dk}|}{k_{\min}\left(\sum_{k=1}^{5} |\hat{C}_{ik}| (|\eta_{Dk}| + \sigma_{ik})\right)} \triangleq \nu_i \quad i=1,2,3\,, \tag{4.16}$$

if $\dot{V} < 0$ holds for all $|s_i| \geq \varepsilon_i$, the following condition must also hold

$$\alpha_i > \frac{1}{2\varepsilon_i} \ln\left(\frac{1+\nu_i}{1-\nu_i}\right). \tag{4.17}$$

When the width of the boundary layer ε_i is selected, α_i can be chosen according to (4.17).

4.3 Simulation Results

The simulation is undertaken in three cases:

Case 1—no parameter uncertainty;

Case 2—with uncertainties of mass and moments of inertia e_m, e_I: 40%; length e_l, e_d: 10%;

Case 3— with uncertainties of mass and moments of inertia e_m, e_I: 100%; length e_l, e_d: 40%.

The joint angle profiles of a full gait cycle designed in Chapter 3 are used as reference trajectories in the simulation. The biped locomotion starts at a SSP with initial angles θ_i (deg) and initial angular velocities $\dot{\theta}_i$ (rad/s) shown in Table 4.1. The constants in the controllers in each case are chosen by trial and error and the values are listed in Table 4.2.

Table 4.1 Initial values of biped locomotion

Link No. (i)	θ_i (rad)	$\dot{\theta}_i$ (rad/s)
1	1.18	1.03
2	-31.29	-0.16
3	0	0
4	-10.19	-1.09
5	-28.14	0.1

Table 4.2 Values of controller constants

Cases	SSP			DSP		
	Λ	γ	σ	Λ	α	σ
1	25	1	2	10	5	10
2	100	2.5	2	10	10	35
3	80	2.5	2	30	5	10

Case 1:

Figure 4.1 shows the tracking errors of the relative angles in the SSP and hip position and trunk orientation in the DSP. Figure 4.2 shows the actuator joint torques in the SSP and the DSP. Figure 4.3 shows the stick diagram of the biped locomotion. Note that the time period of SSP and DSP can not be exactly the same as in the motion planning because of tracking errors, however they are close to each other.

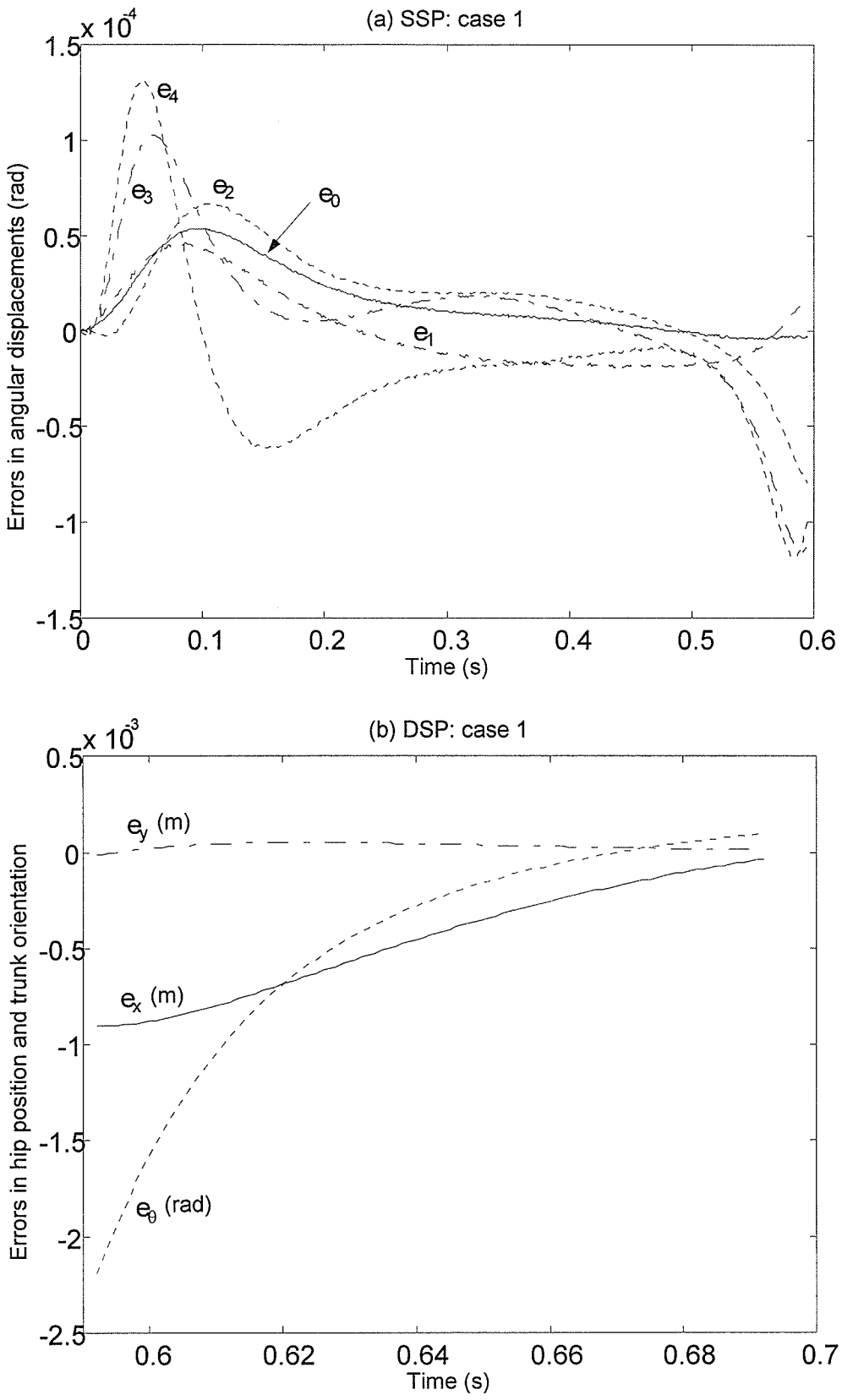

Figure 4.1 Tracking errors in (a) SSP and (b) DSP (case 1)

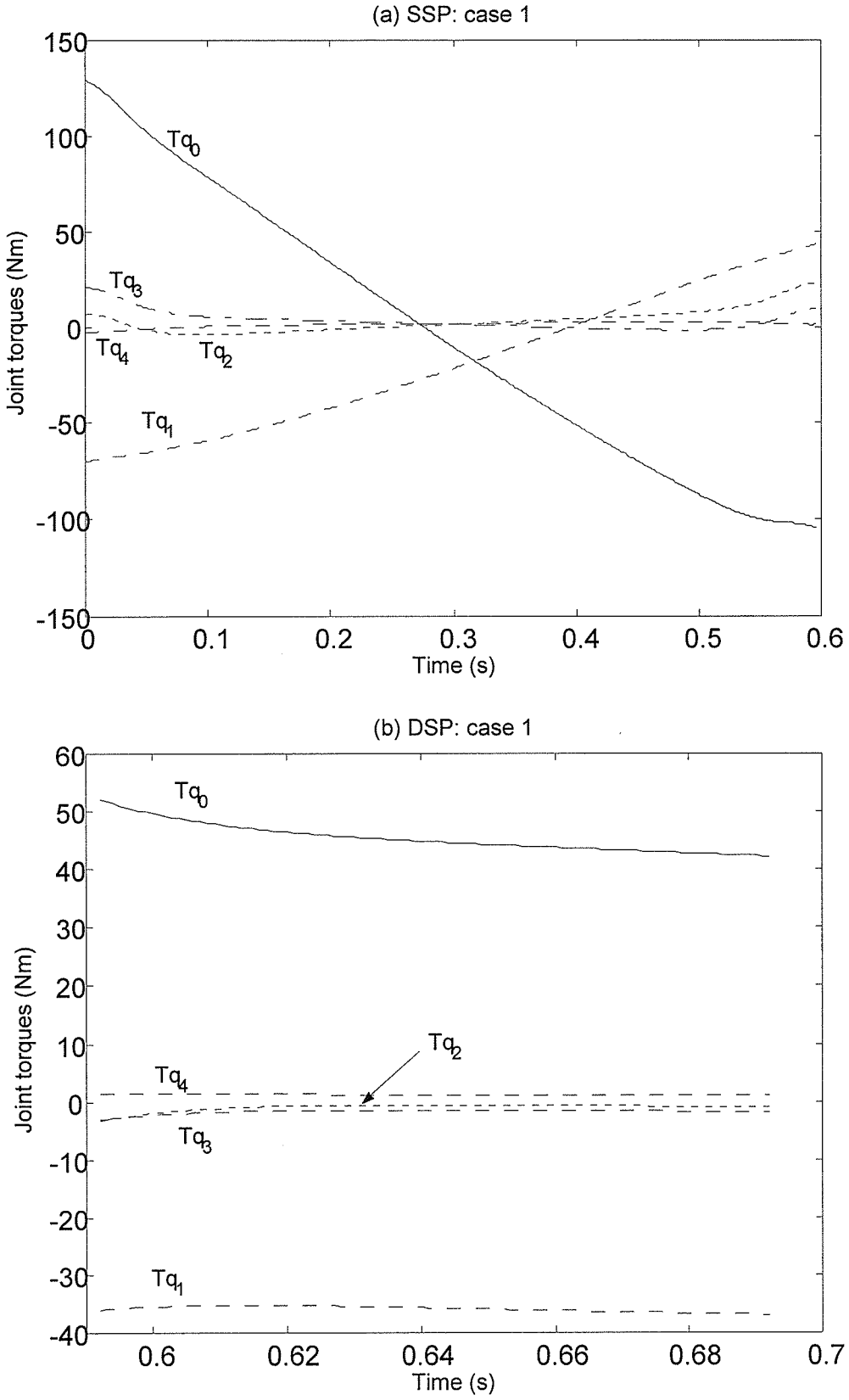

Figure 4.2 Actuator joint torques in (a) SSP and (b) DSP (case 1)

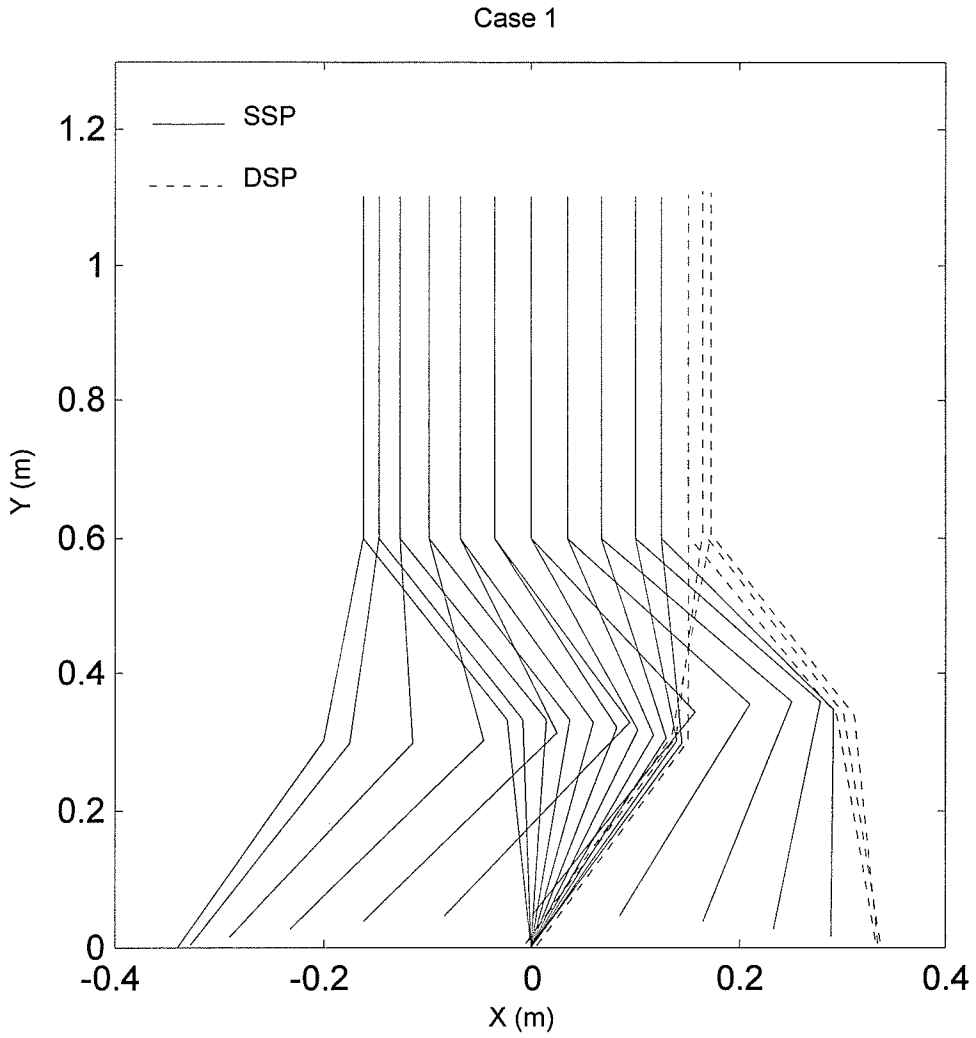

Figure 4.3 Stick diagram of biped walking (case1)

Case 2:

Figure 4.4 shows the tracking errors: (a) in the SSP and (b) in the DSP. Figure 4.5 is the actuator torques: (a) in the SSP and (b) in the DSP. Figure 4.6 shows the stick diagram of the biped locomotion in case 2.

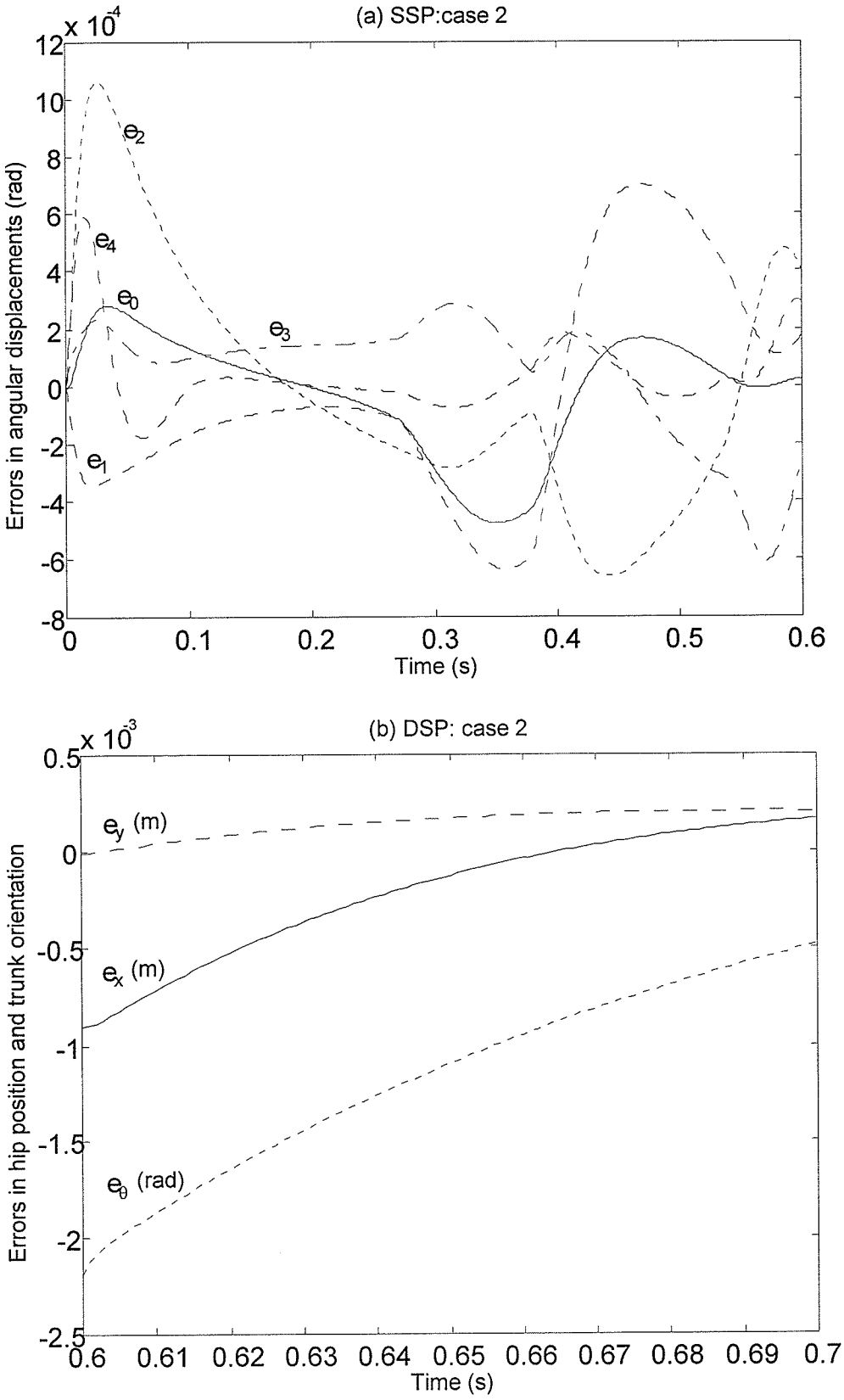

Figure 4.4 Tracking errors in SSP and DSP (case 2)

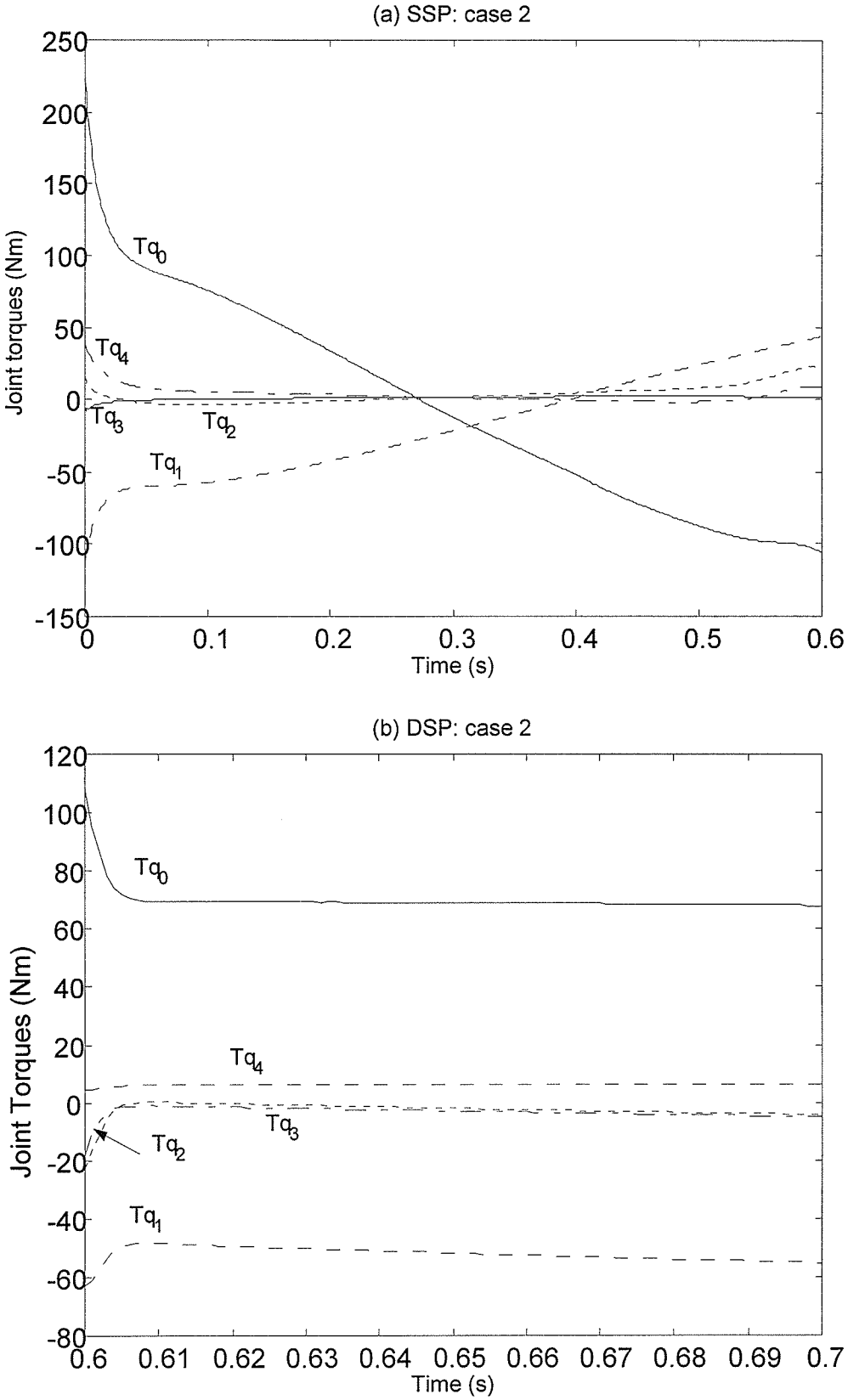

Figure 4.5 Actuator joint torques in SSP and DSP (case 2)

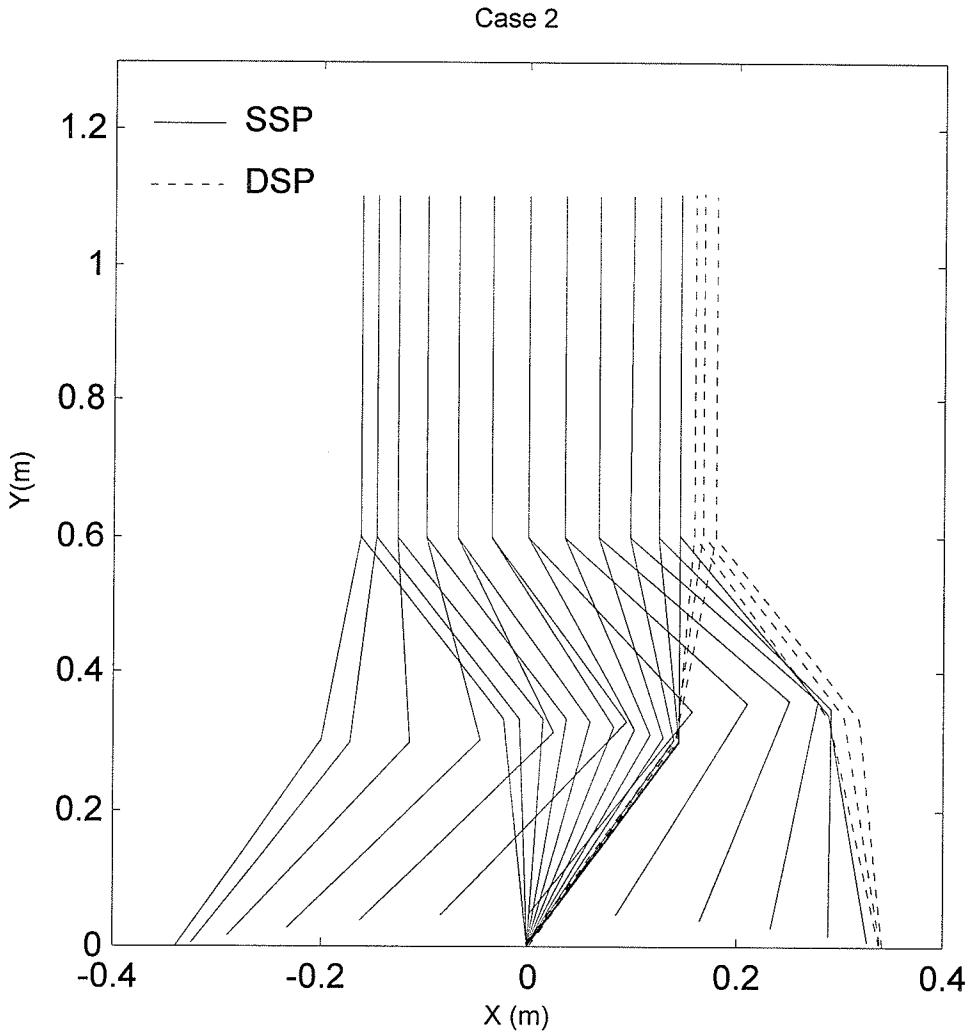

Figure 4.6 Stick diagram of biped walking (case 2)

Case 3:

Figure 4.7 shows the tracking errors with (a) in the SSP and (b) in the DSP. Figure 4.8 is the actuator torques: (a) in the SSP and (b) in the DSP. Figure 4.9 shows the stick diagram of the biped locomotion in case 3.

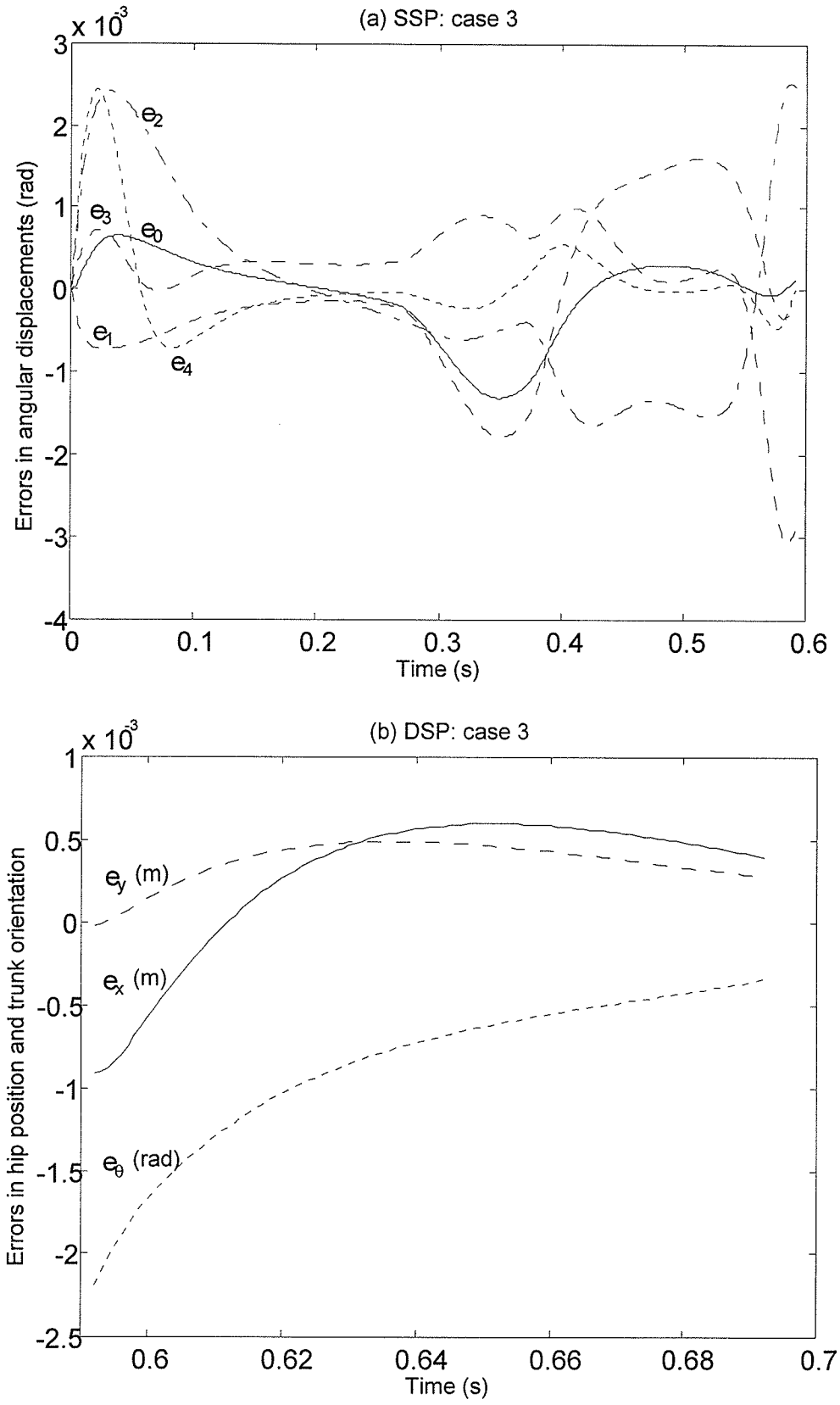

Figure 4.7 Tracking errors in SSP and DSP (case 3)

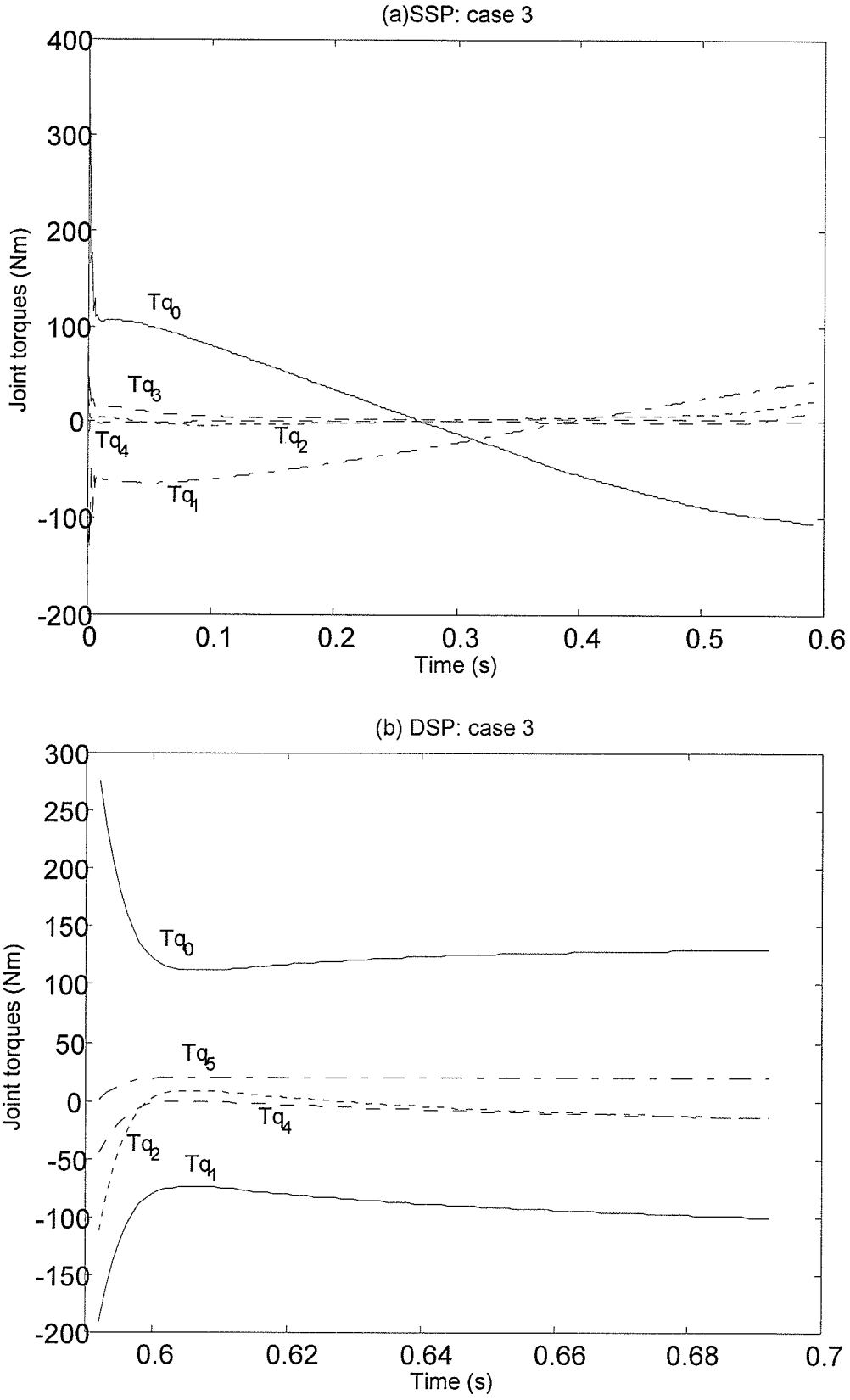

Figure 4.8 Actuator joint torques in SSP and DSP (case 3)

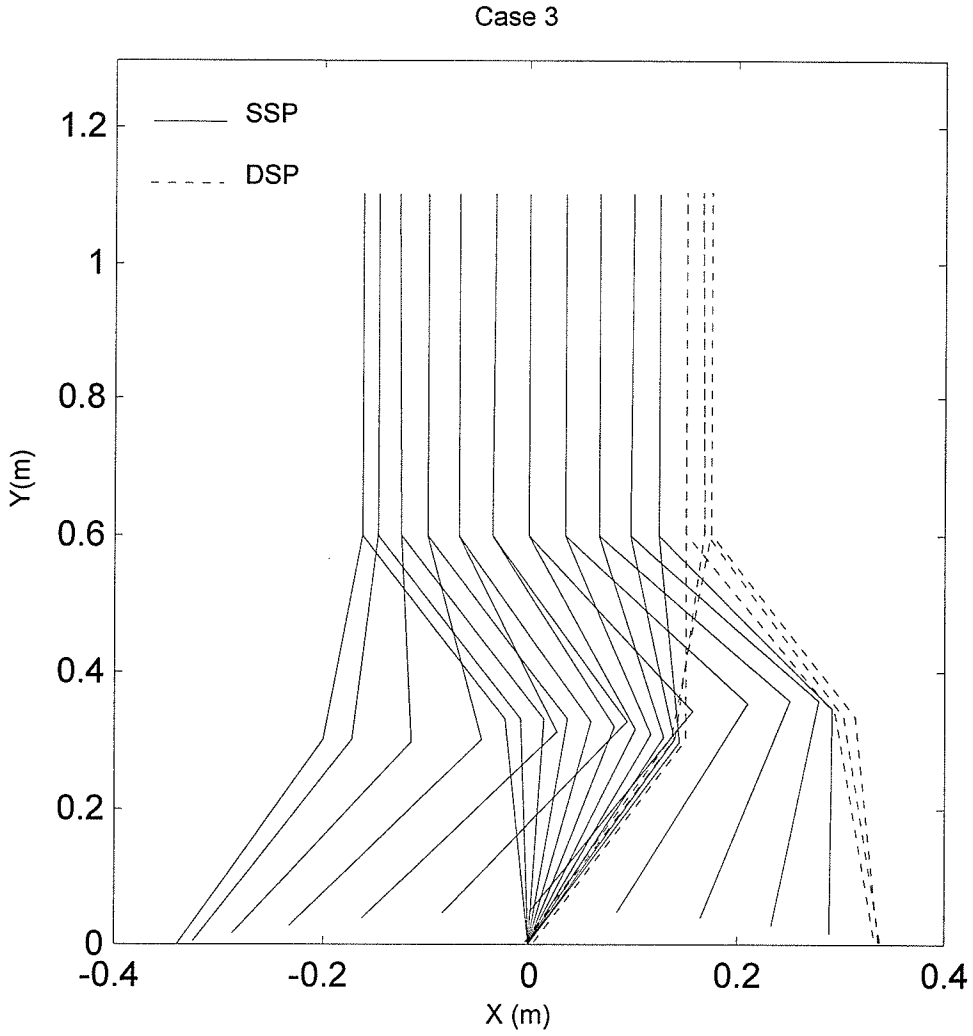

Figure 4.9 Stick diagram of biped walking (case3)

From Figure 4.1-4.9, one can see that the tracking errors are low and the actuator torques are acceptable in all three cases. For the SSP, the tracking errors are oscillating in a bounded range during the whole phase as the initial value is taken from the reference trajectories designed in Chapter 3. The tracking errors do not converge to zero because the tracking accuracy has been traded off by applying the smoothened controllers to remove the chattering problems and with such controllers the tracking errors will not

converge to zero but oscillate within a certain range around zero. While in the DSP, since there are initial errors, the controller will approach the reference input signals and because the time in the DSP is small, the oscillation of the tracking errors does not show. In Case 2 and Case 3 when there are parameter uncertainties in the model, both the average tracking errors and the actuator torques are slightly larger than those without uncertainties as in Case 1. But with the uncertainties the errors are still low and the controllers are realizable. The results presented above have shown the good performance of the sliding mode control for the situations where system parameter uncertainties exist.

4.4 Summary

An approach to the motion control of the five-link biped was presented in this chapter. Sliding mode technique was employed for the control design. For motion regulation during the DSP, the biped model was formulated as a robot system under holonomic constraints and the hip position and trunk orientation were selected as independent generalized coordinates to describe the biped system. A robust sliding mode control algorithm was developed by treating the biped as a redundant manipulator where the constraint of both limbs remaining in contact with the ground was assumed satisfied. The pseudo-inverse matrix was used as a performance function to distribute the control torques among the five joints. The control algorithm tracked the hip and trunk motion without force control and thus the control design was simplified by avoiding a separate force control law. To eliminate the chattering problem during the implementation of the sliding mode control, the smoothened control law was used to approximate the discontinuous controller. The simulation results showed that in spite of the presence of

system parameter uncertainties, the controller had a good performance in tracking reference signals with moderate control torques.

This work contributes to motion regulation of biped walking in that it provides an effective control scheme yet it is robust even with large system parameter uncertainties. The robust sliding mode control for biped DSP, to the best of the author's knowledge, has not been found in previous work. More importantly, the control strategy provides the flexibility to distribute the joint torques based on various performance functions.

Chapter 5

Contact Events and Parametric Analysis

5.1 Introduction

Biped locomotion is represented by the progression of the system with an upper body supported by two lower limbs alternately in contact with the ground. When a lower limb comes into contact with the ground, impact occurs. During impact the biped motion is interrupted and impulsive forces develop at the contact point(s) with the ground and at each joint. These impulses could cause damages to the biped and environment (Zheng and Hemami 1985). Furthermore, the joint angles remain unchanged but the angular velocities become discontinuous during impact. A quantitative relation between the impulses and other dynamic parameters will help analyze the severity of the collision, design physically reliable biped robots and synthesize reasonable biped gaits. The values of the joint angles and angular velocities after impact constitute the initial states for the forthcoming contact phase of walking (the SSP or the DSP), which are crucial for motion planning and regulation of biped locomotion. Chapter 2 has derived a set of single and double impact model for five-link biped robot and their solutions regarding the velocity changes and external impulses are also provided.

On the other hand, impact indicates the forthcoming contact event of the lower limbs with the ground, i.e., a SSP follows single impact and a DSP follows double impact (Hurmuzlu 1993). Note that the type of impact and its associated contact event occurring after impact are dictated by the nature of physics of the biped systems and the

environment. Thus, one aspect related to biped impact problems not discussed in Chapter 2 is how to correlate the type of impact with the system parameters and the states prior to impact. The correlation of pre-impact states and the type of impact can facilitate biped motion planning such that desired gait parameters are chosen to satisfy walking requirements. Research on this issue can also contribute to understanding the mechanics of biped locomotion. Such an understanding is important to the development of biped robots.

Literature related to the correlation of the type of impact with gait parameters and system states before impact is fairly limited. Hurmuzlu (1993) studied single and double impact and carried out a parametric analysis to correlate the outcome of the contact event with the gait parameters associated with the objective functions introduced in motion planning. The single and double impact regions in terms of specific gait parameters were presented in graphical form. The work is influential in biped study because the following contact phase arises as a direct consequence of the type of impact. However, the results of the parametric analysis were restricted to specific objective functions only. In view of the prevailing articles related to biped impact, there is a gap in seeking for a correlation among the general gait parameters and individual impact, which dictates the upcoming contact event of bipedal walking.

In this chapter, the explicit solutions to the biped impact and the conditions for their validity are revisited. The first objective is to establish a correlation of the contact events with biped system parameters and states via impact effects. The second objective is to perform a parametric analysis to associate the contact events with biped gait. The gait is not restricted to a specific motion design but related to the states immediately before

impact, thus it is generic. Results are provided in graphical form to show the relationship among the locomotion parameters and specific contact regions.

5.2 The Conditions for Contact Events

5.2.1 Double Impact Condition

Revisit Equations (2.30)

$$\begin{cases} \dot{\theta}^{+} = -W^{-1}J^{T}(JW^{-1}J^{T})^{-1}\dot{X}_{e}^{-} + \dot{\theta}^{-} & \text{(2.30a)} \\ P_{l} = (JW^{-1}J^{T})^{-1}\dot{X}_{e}^{-} & \text{(2.30b)} \\ P_{r} = -(I + VW^{-1}J^{T})(JW^{-1}J^{T})^{-1}\dot{X}_{e}^{-} & \text{(2.30c)} \end{cases}$$

and the conditions for the validity of the solution

$$1) \quad P_{lY} > 0, \tag{2.31a}$$

$$2) \quad \frac{|P_{lX}|}{|P_{lY}|} < \mu, \tag{2.31b}$$

$$3) \quad \frac{|P_{rX}|}{|P_{rY}|} < \mu. \tag{2.31c}$$

The explicit solutions expressed in Equation (2.30) can be used to gain some insights into the biped impact event. They can be associated with inequality (2.31) to determine the type of impact and to perform parametric studies. From Equation (2.30), it is observed that the angular velocity changes $\Delta\dot{\theta}$ and the external impulses at both contact points, P_l and P_r, are only dependent on biped system configuration θ^{-} and swing tip velocity $\dot{X}_e^{-}$. They are neither related to the trunk angular velocity $\dot{\theta}_3^{-}$ nor to the hip linear velocity $\dot{X}_h^{-}$ (refer to Figure 5.1). In addition, if the biped configuration is prescribed, these values are linearly proportional to the swing tip velocity before impact. It also implicitly indicates that the conditions that warrant double impact shown in (2.31), is dictated by the direction of the swing tip velocity before impact as proven below.

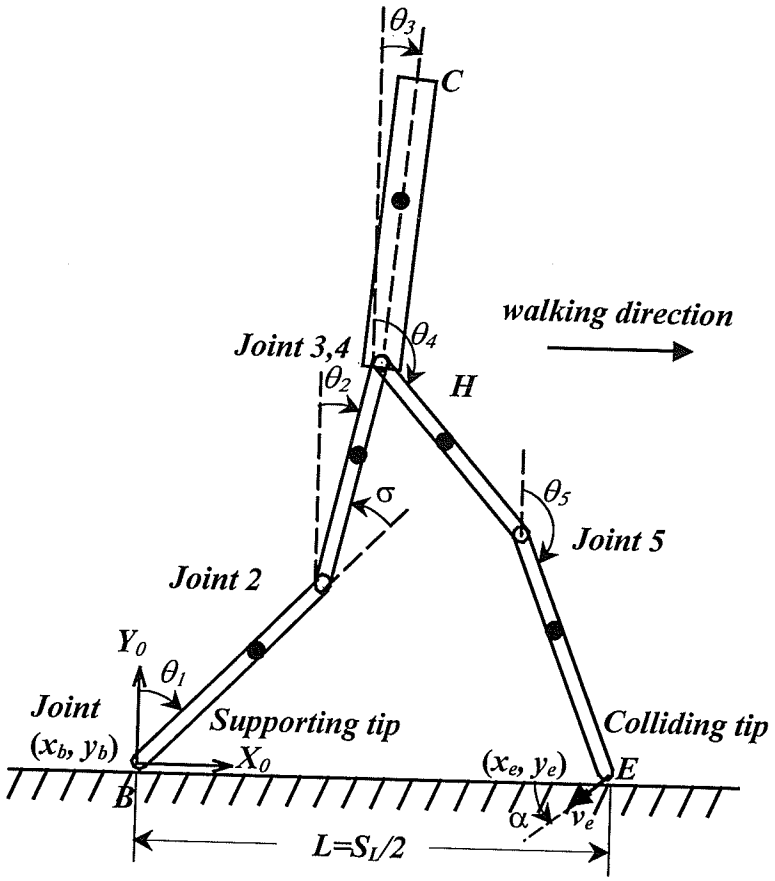

Figure 5.1 Five-link biped impact model

With abbreviated notations

$$M_{DL} = (JW^{-1}J^T)^{-1}, \tag{5.1a}$$

$$M_{DR} = -(I + VW^{-1}J^T)(JW^{-1}J^T)^{-1}. \tag{5.1b}$$

the impulses are expressed as $P_l = M_{DL}\dot{X}_e^-$ and $P_r = M_{DR}\dot{X}_e^-$ from Equations (2.30b) and (2.30c). The subscript '$_D$' denotes double impact, '$_L$' and '$_R$' denotes the left (trailing) and right (leading) limb tip. Then, the impulse components become

$$\begin{bmatrix} P_{lX} \\ P_{lY} \end{bmatrix} = \begin{bmatrix} (M_{DL})_{11}\dot{x}_e^- + (M_{DL})_{12}\dot{y}_e^- \\ (M_{DL})_{21}\dot{x}_e^- + (M_{DL})_{22}\dot{y}_e^- \end{bmatrix}, \tag{5.2a}$$

$$\begin{bmatrix} P_{rX} \\ P_{rY} \end{bmatrix} = \begin{bmatrix} (M_{DR})_{11}\dot{x}_e^- + (M_{DR})_{12}\dot{y}_e^- \\ (M_{DR})_{21}\dot{x}_e^- + (M_{DR})_{22}\dot{y}_e^- \end{bmatrix}. \quad (5.2b)$$

As the swing tip velocity $\dot{X}_e^- = \begin{bmatrix} \dot{x}_e^- & \dot{y}_e^- \end{bmatrix}^T$ can be expressed as a vector with magnitude $V_e = \|\dot{X}_e^-\|$ and direction angle $\alpha = \cot^{-1}(\dot{x}_e^- / \dot{y}_e^-)$, the following relation $\dot{x}_e^- = \cot(\alpha)\dot{y}_e^-$ is used for derivation. Note that the vertical swing tip velocity $\dot{y}_e^-$ must be downward. Thus, the above conditions shown by inequalities (2.31a)-(2.31c) become

$$\cot(\alpha)(M_{DL})_{21} < -(M_{DL})_{22}, \quad (5.3a)$$

$$\left|\cot(\alpha)(M_{DL})_{11} + (M_{DL})_{12}\right| < \mu\left|\cot(\alpha)(M_{DL})_{21} + (M_{DL})_{22}\right|, \quad (5.3b)$$

$$\left|\cot(\alpha)(M_{DR})_{11} + (M_{DR})_{12}\right| < \mu\left|\cot(\alpha)(M_{DR})_{21} + (M_{DR})_{22}\right|, \quad (5.3c)$$

Since M_{DL} and M_{DR} are functions of biped physical parameters and joint angles before impact, inequalities (5.3a)-(5.3c) indicate that the double impact conditions can be examined with the knowledge of the direction of the pre-impact swing tip velocity and the biped system configuration. It also indicates that, once the biped configuration immediately before impact is prescribed, the direction of the swing tip velocity before impact, denoted by α, plays an important role in the occurrence of double impact. This information can be used in biped motion regulation such that the direction of the swing tip velocity is controlled to ensure a desired contact event.

5.2.2 Single Impact Condition

Considering solutions for the single impact model

$$\begin{cases} \dot{\theta}^+ = (W - UJ)^{-1}U\dot{X}_e^- + \dot{\theta}^- & (2.36a) \\ \dot{X}_b^+ = -\left[I + J(W - UJ)^{-1}U\right]\dot{X}_e^- & (2.36b) \\ P_S = \left[(V - m_{sum}J)(W - UJ)^{-1}U - m_{sum}I\right]\dot{X}_e^- & (2.36c) \end{cases}$$

and the conditions

$$1)\quad \dot{y}_b^+ > 0, \tag{2.37a}$$

$$2)\quad \frac{|P_{SX}|}{|P_{SY}|} < \mu. \tag{2.37b}$$

Symbolically express Equations (2.36b) and (2.36c) as $\dot{X}_b^+ = M_{SL}\dot{X}_e^-$ and $P_S = M_{SR}\dot{X}_e^-$, where

$$M_{SL} = -\left[I + J(W - UJ)^{-1}U\right], \tag{5.4a}$$

$$M_{SR} = \left[(V - m_{sum}J)(W - UJ)^{-1}U - m_{sum}I\right]. \tag{5.4b}$$

The subscript '$_S$' denotes single impact, '$_L$' and '$_R$' represents the left and right limb tip as shown in Figure 5.1. Denote $\dot{x}_e^- = \cot(\alpha)\dot{y}_e^-$, where $\dot{y}_e^-$ is a negative number, the condition (2.37) can be rewritten as the following inequalities:

$$\cot(\alpha)(M_{SL})_{21} < (M_{SL})_{22}, \tag{5.5a}$$

$$\left|\cot(\alpha)(M_{SR})_{11} + (M_{SR})_{12}\right| < \mu\left|\cot(\alpha)(M_{SR})_{21} + (M_{SR})_{22}\right|. \tag{5.5b}$$

Similar to what has been found for double impact, inequalities (5.5) shows that the direction of the swing tip velocity before impact plays an important role in the validity of solutions to Equations (2.36). Thus the condition (5.5) can be examined through the direction angle of the swing tip velocity and pre-impact biped joint angles for the validity of the single impact model, shown in Equation (2.36).

Remarks

1) As shown in Equations (2.30) and (2.36), the angular velocity of the trunk $\dot{\theta}_3^-$ and the linear velocity of the hip $\dot{X}_h^-$ before impact do not affect the angular velocity changes and external impulses during impact. Thus, they do not play a role in determining the occurrence of single or double impact. This is because the contact constraints, shown in

Equation (2.23c), do not comprise the displacement of the trunk, and in addition, the trunk does not receive external forces from the environment. This conclusion is also valid for complicated upper body structures, which may include the head and arms.

2) Equations (2.30) and (2.36) reveal that the pre-impact swing tip velocity is the critical factor affecting the impulses and velocity changes. The magnitudes of velocity changes and external impulses are linearly proportional to the magnitude of the swing tip velocity. Thus the magnitude of the swing tip velocity before impact shows the severity of the collision. Inequalities (5.3) and (5.5) show that the direction of the swing tip velocity before impact plays a crucial role in the occurrence of the type of impact, which dictates the following contact phase.

3) The above remarks are obtained according to the biped impact model (Equations 2.23 and 2.32) derived by Newtonian approach shown in Chapter 2, Section 2.3.3. However, by utilizing the general rigid-link impact model (Equation 2.62) with Lagrange approach shown in Section 2.5, the same inferences can be achieved. It shows that these inferences also apply to multi-link rigid body system impact dynamics.

5.3 Parametric Study of the Contact Events

In this section, a parametric analysis is carried out using the results from Section 5.2 to identify the regions of the gait parameters that yield particular types of impact. The biped structure is taken from Figure 2.1 and the numerical values of the geometrical dimensions, masses, and moments of inertia that are used in the simulations are taken from Table 3.1.

As is seen from inequalities (5.3) and (5.5), the direction of the swing tip velocity and the biped configuration immediately before impact are the main factors to determine the

occurrence of the type of impact. Thus the direction angle of the pre-impact swing tip velocity, α, is chosen as one of the key parameters for the parametric study. The rest of the gait parameters are selected such that the biped configuration, described by joint/segment angles, is uniquely determined. In this work, as an example, choose the step length S_L and stance knee bias angle σ immediately before impact as the parameters for study. Both angles σ and α are shown in Figure 5.1, where $\sigma = \theta_1^- - \theta_2^-$ representing the joint angle at the knee of the trailing limb, $\alpha = \cot^{-1}(\dot{x}_e^- / \dot{y}_e^-)$ denoting the angle between the vector of the swing tip velocity and the negative x-axis since $\dot{y}_e^-$ is downward before contact. Two additional conditions, used in this work, are: *i*) immediately before impact, the upper body is upright, i.e. $\theta_3^- = 0$, and *ii*) the hip position in x-coordinate is centered with respect to the two lower limbs, i.e. $x_h^- = \frac{1}{4} S_L$. Note that all the parameters used in this study are measured right before impact and their values during each step are not required. This provides great flexibility for designing biped gait. Furthermore, the choice of the parameters that prescribe the biped posture before impact is not restrictive. Any objective functions can be used provided that the biped posture is uniquely defined. For example, one may choose hip height y_h instead of stance knee bias angle σ. However, it is preferable to use σ for parametric study since the range of y_h varies with different step lengths due to geometric constraints, which has been discussed in Chapter 3.

In previous work (Hurmuzlu 1993), double impact was believed guaranteed if the vertical impulse at the tip of the left limb, P_{lY}, is positive, where P_{lY} was calculated from the double impact model, and single impact was believed to occur if the vertical velocity

at the tip of the trailing limb after impact, $\dot{y}_b^+$, is positive, where $\dot{y}_b^+$ was calculated from the single impact model. However, positive P_{IY} alone does not ensure the occurrence of double impact because the conditions that warrant single impact ($\dot{y}_b^+ > 0$) can be satisfied simultaneously. Thus, in this work, both conditions for single impact and double impact are examined for each set of parameters, *i.e.*, the double impact occurs when $P_{IY} > 0$ and $\dot{y}_b^+ < 0$, and single impact occurs when $P_{IY} < 0$ and $\dot{y}_b^+ > 0$.

The regions of the parameter space that correspond to the single or the double impact cases and the impulse ratios describing the likelihood of slippage are presented in graphical form through the forthcoming simulations. In the simulations, the step length, S_L, is selected from 0 to 2m and stance knee bias angle, σ, from 0° to 60° excluding 0° as it is one of the singular points (Hurmuzlu 1993). The range of the direction angle of the swing tip velocity before impact, α, is from 0° to 180° indicating the swing tip velocity varying from backward to forward direction.

5.3.1 Single and Double Impact Regions

Figure 5.2 depicts the regions that represent different contact events in the parameter space. The friction coefficient between the biped and the ground is firstly assumed sufficiently high to prevent slippage. Surfaces A and B represent the post impact vertical velocity at the trailing tip, $\dot{y}_b^+$, is zero and surface C represents the vertical impulse at the trailing tip, P_{IY}, is zero. Regions I, II, III, bounded by the coordinate planes and surfaces A, B and C, respectively, contain the parameter values corresponding to positive impulse

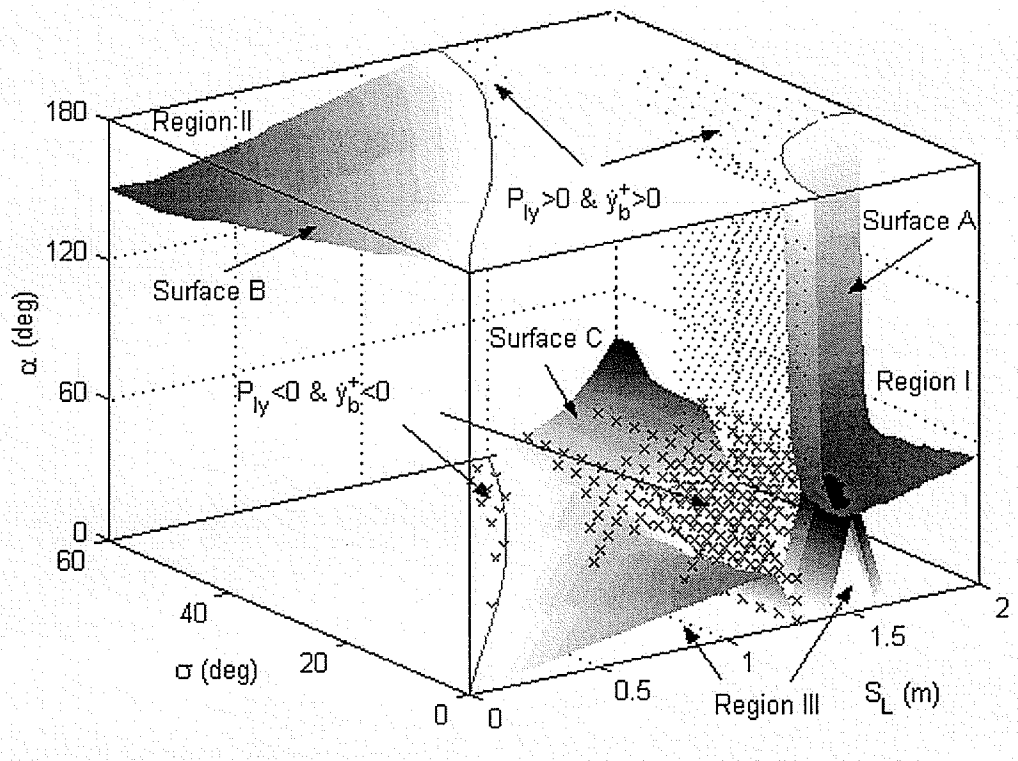

Figure 5.2 Five-link biped impact regions

(I, II, III ---double impact region;
× ---neither single impact nor double impact can happen
.. --- both single impact and double impact may happen
other---single impact region)

P_{IY} and negative velocity $\dot{y}_b^+$, which indicate double impact regions. The volumes neighboring regions I and II denoted by '.' represent the regions such that $\dot{y}_b > 0$ and $P_{IY} > 0$, i.e., both conditions that warrant single impact and double impact are satisfied, whereas those regions neighboring III denoted by '×' represent that $\dot{y}_b < 0$ and $P_{IY} < 0$, *i.e.*, neither single impact conditions nor double impact ones are satisfied. The blank area containing the parameter values corresponding to positive velocity $\dot{y}_b^+$ and negative impulse P_{IY}, indicates the single impact region. Figure 5.2 reveals the correlation between

the contact event and certain gait parameters before impact. The two regions shown by '.' and '×' have never been reported in the related literature, and they raise serious concerns about the validity of the impact criteria, shown in Equations (2.31) and (2.37), and assumptions that are often made when developing biped impact models.

5.3.2 Post Impact Velocity $\dot{y}_b^+$ and Impulse P_{lY} at the Tip of the Trailing Limb

Figure 5.3 depicts the vertical post impact velocity $\dot{y}_b^+$ and normal impulse P_{lY} both at the tip of the trailing limb versus the step length, S_L, stance knee bias angles, σ, and the direction of the swing tip velocity before impact, α. Figures 5.3(a) and 5.3(b) show the variations of $\dot{y}_b^+$ and P_{lY} versus S_L and α as the stance knee bias angle, σ, is taken as 15° and 30°, respectively. Figures 5.3(c) and 5.3(d) show the variations of $\dot{y}_b^+$ and P_{lY} versus σ and α as S_L is taken as 1m representing a relatively small step length and 1.8m representing a large step length. The gray surfaces represent the functions of $\dot{y}_b^+$ and the meshed surfaces represent P_{lY}. Figure 5.3 can also facilitate identifying the parameter regions where individual impact occurs as Figure 5.2. For example, Figure 5.3(a) shows that as the step length, S_L, varies between zero to 1.4m and the direction angle of the trailing tip velocity before impact, α, varies between 20° to 150°, $\dot{y}_b^+ > 0$ while $P_{lY} < 0$, indicating that only single impact can occur. In addition, one can observe the changes in both $\dot{y}_b^+$ and P_{lY} with respect to the selected parameters. For this purpose, only the surfaces above the zero-plane are examined since those below the zero-plane are invalid solutions. Figures 5.3(a) and 5.3(b) show that both positive $\dot{y}_b^+$ and P_{lY} decrease with the increase in S_L for small S_L (S_L<1.4m) and increase slightly for large S_L (S_L>1.4m). Figures

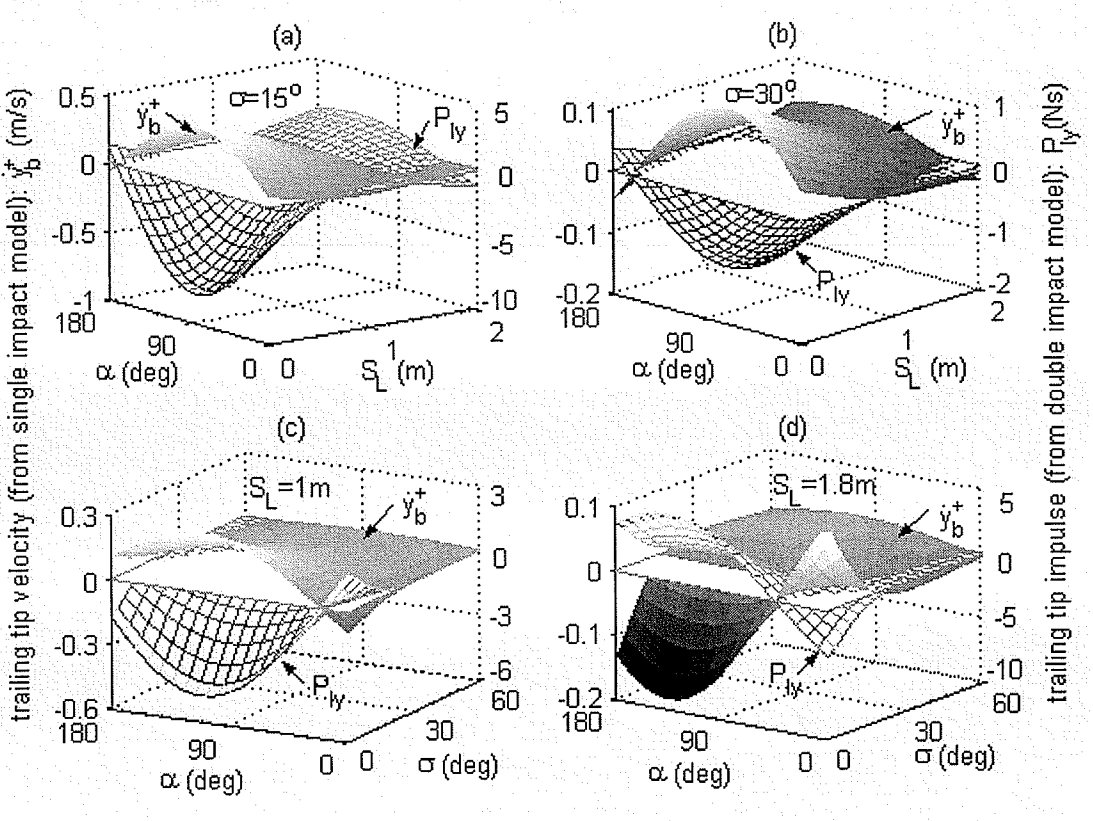

Figure 5.3 Vertical impulse and swing tip velocity after impact

(gray surface---post-impact trailing tip vertical velocity for single impact model
mesh surface---trailing tip vertical impulse for double impact model)

5.3(c) and 5.3(d) show that with the increase in the stance knee bias angle, σ, within the range of $\sigma < 20°$, both positive $\dot{y}_b^+$ and P_{IY} decrease no matter with small or large values of S_L, while in the region $20° < \sigma < 60°$, they are almost insensitive to the variations in σ. It can also be seen that for short step lengths (Figure 5.3(a), 5.3(b), 5.3(c)) the biped is more likely to encounter single impact except those α taking very large (approaching to 180°) or very small values (approaching to 0°), and for long step lengths (Figures 5.3(a) and 5.3(d)) double impact occurs with small values of σ ($\sigma < 20°$) within a relatively wide range of α ($40° < \alpha < 180°$).

5.3.3 Impulse Ratios

The double and single impact regions depicted in Figures 5.2 and 5.3 are studied with the assumption that friction coefficient is sufficiently high to prevent slippage. Now the effect of friction for the contact events is to be studied through a depiction of the impulse ratios in each region. Thus, if the friction coefficient μ between the feet and the ground is known, one can find the no-slip sub-regions in the parameter space by applying the inequalities (2.31b), (2.31c) and (2.37b), i.e. if both inequalities, $|\mu_L| = |P_{lX} / P_{lY}| < \mu$ and $|\mu_R| = |P_{rX} / P_{rY}| < \mu$, are satisfied, a no-slip double impact will be guaranteed; and if $|\mu_S| = |P_{SX} / P_{SY}| < \mu$, a no-slip single impact will be guaranteed. Here μ_L and μ_R denote the impulse ratios at the tips of left and right limbs during double impact, and μ_S is the impulse ratio at the collision tip during single impact.

The surfaces of impulse ratio μ_L and μ_R for double impact regions I, II, III (referring to Figure 5.2) are shown by Figures 5.4, 5.5 and 5.6, respectively. Each surface is depicted in S_L-α coordinates with a prescribed value of the stance knee bias angle, σ. In Figure 5.4, it is seen that for the values of long step length, S_L, dominated by region I (shown in Figure 5.2), μ_L increases with the increase of S_L and σ, but it is not sensitive to the changes in the direction angle of the leading tip velocity, α, before impact. The absolute values of μ_R are increasing with the increase of S_L and α, but it is not sensitive to the changes in stance knee bias angle, σ. These observations indicate that increasing the step length, S_L, makes both limbs more likely to slip, and increasing the stance knee bias angle, σ, increases the likelihood of the slippage of trailing limb without a significant effect on the leading limb, while increasing the direction angle of the leading tip velocity,

α (when $45^\circ < \alpha < 90^\circ$), increases the likelihood of the slippage of leading limb but not the trailing limb.

Figures 5.5(a) and 5.5(b) show the surfaces of μ_L and μ_R in S_L-α coordinates as the stance knee bias angle, $\sigma = 5^\circ, 25^\circ, 45^\circ$, for the double impact region II where the direction angle of the leading tip velocity, α, is large ($\alpha > 150^\circ$) and the step length, S_L, is small ($S_L < 1.4m$) as shown in Figure 5.2. One can see that both μ_L and μ_R increase with the increases in the stance knee bias angle σ. This observation indicates that a larger value of the stance knee bias angle makes it more likely to slip especially the leading limb. Figures 5.6(a-d) show μ_L and μ_R in S_L-α coordinates as $\sigma = 1^\circ, 20^\circ$ for the double impact region III as denoted in Figure 5.2. The curved surfaces represent the impulse ratio μ_L or μ_R taking the parameters in region III. The flat surfaces represent the region outside double impact region III which is not of the interests. Figures 5.5 and 5.6 show that the impulse ratio μ_L and μ_R increase significantly in the most part of the double impact Regions II and III, where the values of the parameters are uncommon, such as very low step lengths, S_L, very large and small direction angle of the leading tip velocity, α. Thus, it is not desirable to design gait with the parameters in such regions.

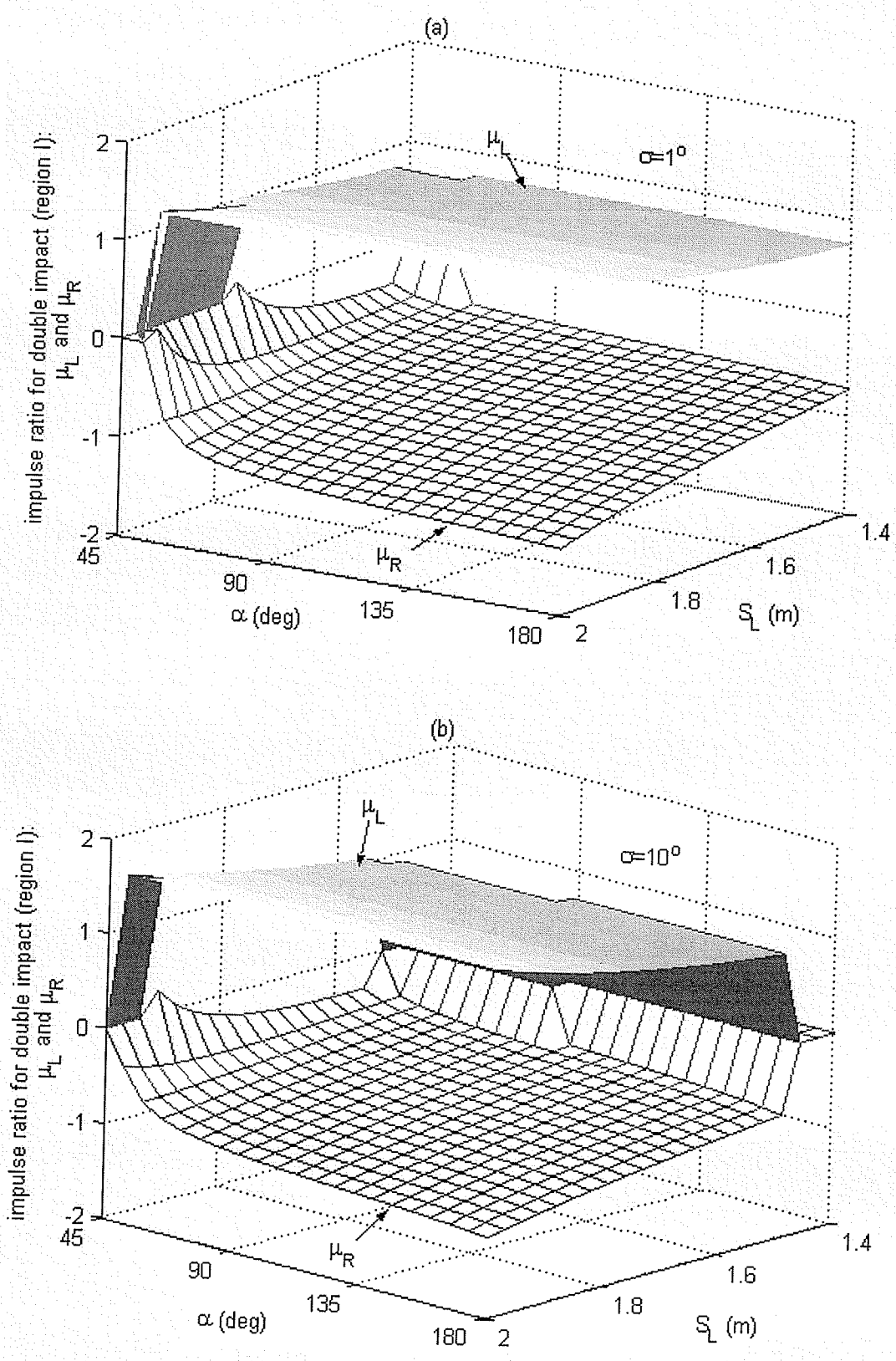

Figure 5.4 Impulse ratio for the double impact region (I)

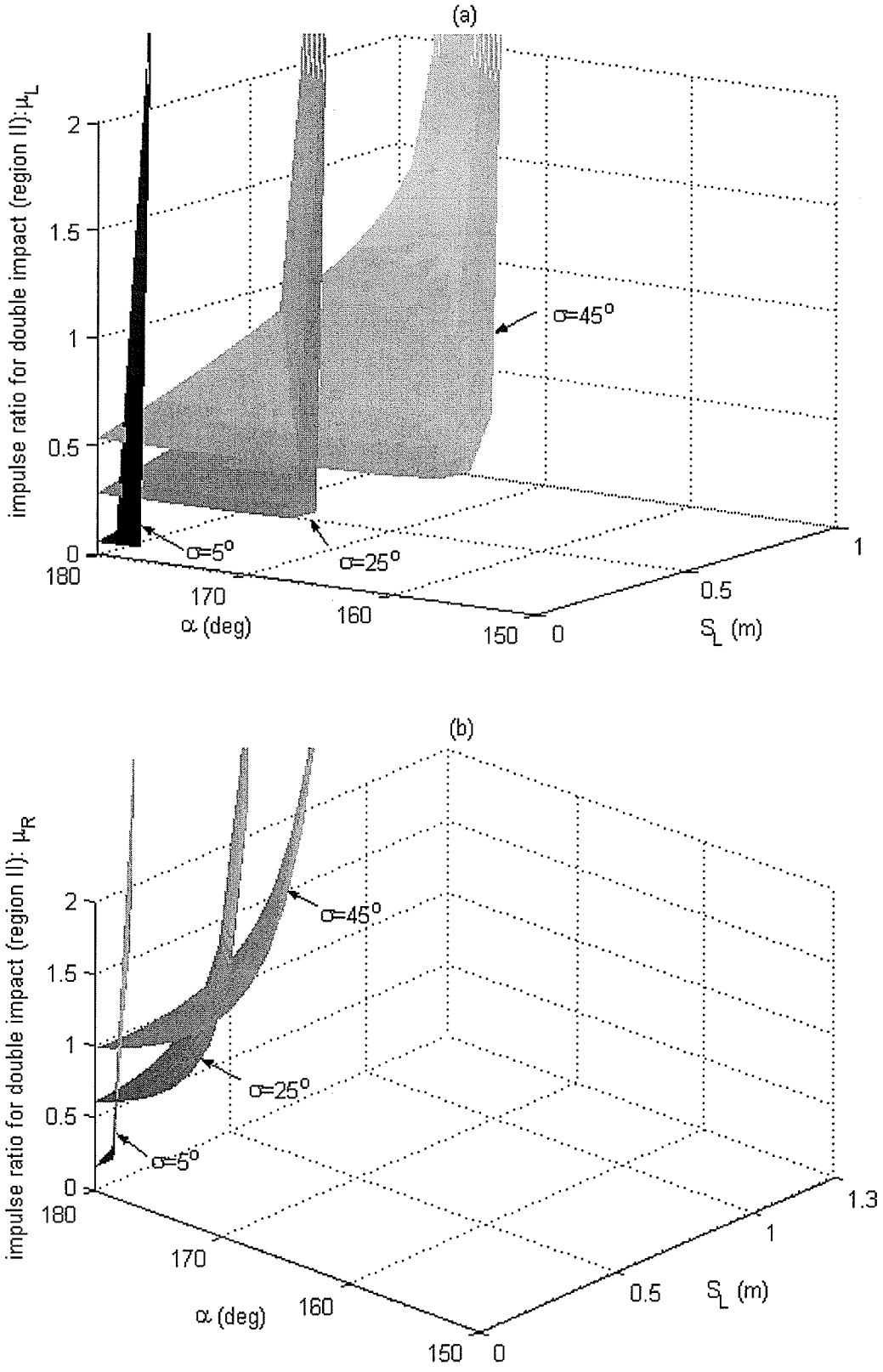

Figure 5.5 Impulse ratio for the double impact region (II)

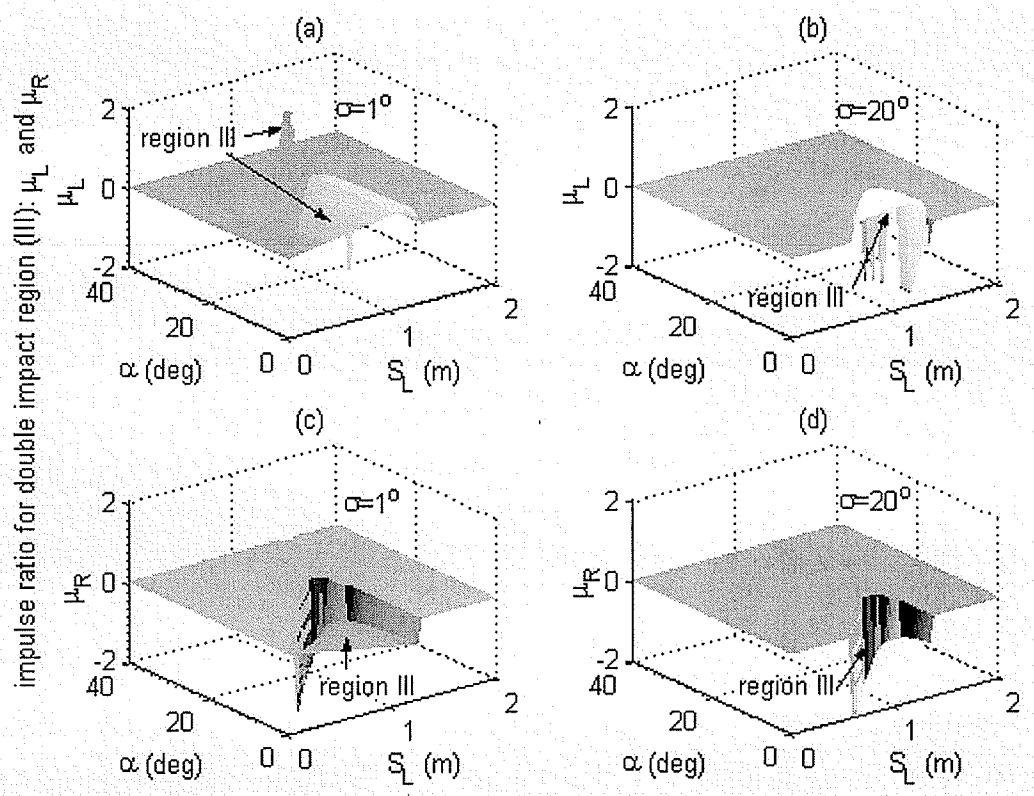

Figure 5.6 Impulse ratio for the double impact region (III)

Figure 5.7 shows the impulse ratio μ_S for single impact case. Surfaces are depicted with prescribed values of the stance knee bias angle, σ, where $\sigma = 1^{\circ}, 20^{\circ}, 40^{\circ}, 60^{\circ}$. From Figure 5.7 one can observe that all the surfaces are relatively flat in the area where the direction angle of the leading tip velocity, α, is between 50° and 140°, and the step length, S_L, is within 1.35m. The absolute value of μ_S increases slightly with the increase of S_L and the decrease of σ but under 0.5 in the overall region. This shows that for a moderate biped-ground friction condition, e.g., $\mu = 0.5$, the no-slip single impact region can be found within the above sub-region. However, the impulse ratio μ_S increases dramatically in the sub-region such that the direction angle of the leading tip velocity, α, being greater than 140° and the step length, S_L, is lower than 0.5m. Thus,

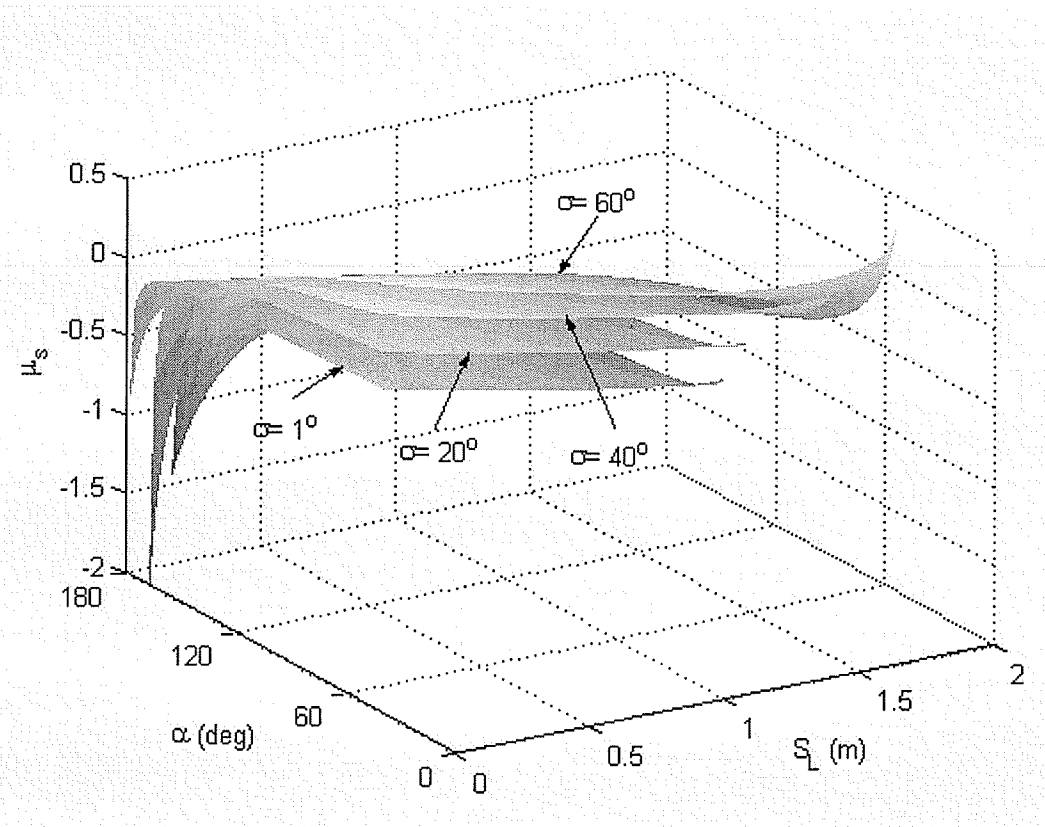

Figure 5.7 Impulse ratio for the single impact region

slippage is most likely to occur in this region.

The above observations are in agreement with those found in Hurmuzlu's work (1993). For example, it was inferred in Hurmuzlu's work (1993) that for small values of step length, the biped is more likely to encounter double impact with large values of stance knee bias angle and large values of direction angle of the swing tip velocity before impact, and for long step length within the double impact region, increasing the stance knee bias angle increases the likelihood of the slippage of the trailing limb without a significant effect in the leading limb, and increasing the step length makes both limbs more likely to slip. However, there are two major differences. Firstly, since the explicit solutions has shown that the direction angle of the swing tip velocity plays a crucial role

in the velocity changes and impulses during impact, in this work, the effects of the direction angle of the swing tip velocity on the type of impact are systematically investigated and reported. Other parameters can be selected freely provided that joint/segment angles before impact are uniquely determined. Secondly, the regions are identified where, based on the criteria shown in (2.31) and (2.37), either none of single impact and double impact can occur ($\dot{y}_b < 0$ and $P_{IY} < 0$) or both of them may occur ($\dot{y}_b > 0$ and $P_{IY} > 0$). Such regions have not been reported in (Hurmuzlu 1993). This finding raises serious concerns regarding the validity of the impact model, such as perfect plastic rigid body collision and of the conditions warranting each type of impact.

5.4 Summary

Some important aspects associated with impact during biped locomotion were studied in this chapter. The conditions that warrant single and double impact were evaluated using the explicit solutions of the post impact velocities and impulses derived in Chapter 2. The correlation between the specific type of impact and certain gait parameters prior to impact was also explored using these solutions.

It has been indicated that both the magnitude and the direction of the swing tip velocity plays a crucial role in impact dynamics of biped locomotion, and they can contribute to the development of biped robots in that the swing tip velocity can be regulated to obtain a desired gait with prescribed contact phase and to allow an acceptable collision.

A parametric analysis was then carried out to further explore the correlation between the type of impact and certain gait parameters. The results were illustrated in graphical form. The regions representing the biped contact events after impact were identified in

the parameter space. The effects of the direction of the swing tip velocity before impact were investigated and the impulse ratio indicating the likelihood of the slippage was also studied.

As compared with the previous parametric analysis (Hurmuzlu 1993), only the key parameters correlated with the direction of the swing tip velocity and the system configuration immediately before impact were chosen for study. These selections reflect both gait and dynamics information of biped walking. Another difference for the parametric analysis was that the regions were identified, for the first time in literature, where none of the two types of impact can occur or both types of impact may occur. This finding raises some serious concerns with the impact model. The related topics motivate further research on biped impact dynamics.

The explicit solutions of the changes in velocities before and after impact and the impulses introduced to the biped system during impact provide important insights into the effects of various gait parameters on the severity and the type of impact. Thus, the work enables one to gain better understanding of the impact dynamics for biped locomotion. The work also contributes directly to the development of bipedal robots in that the results can facilitate motion planning and motion regulation such that desired gait with prescribed contact events can be produced. Although the present study is focused on the biped contact events, the impact model and the method for the parametric analysis can be applied to other rigid body chain collision problems.

Chapter 6

Conclusions

6.1 Contributions of This Thesis

The locomotion of biped robots has been an extremely challenging problem and has attracted much attention over the past years. Understanding the dynamics and developing control law for stable walking are ongoing research issues in biped robot application. This thesis presents a systematic method for the dynamics and motion regulation of biped walking. From the work in this thesis, contributions have been made in the following aspects:

1) A complete dynamic model was developed to describe a five-link biped walking in the sagittal plane. The biped model was formulated with detailed equations including single support phase (SSP), double support phase (DSP), and impact. An improved kinematic model was constructed by modifying the definitions of some system parameters. The novelty of the definition was to treat the biped system as an open loop series chain, and consequently all the detailed dynamic equations and their derivation procedures can be significantly simplified. The associated computation and programming can thus be efficient and less prone to mistakes. The biped model for the DSP was first formulated as a robot system under holonomic constraints and then the hip position and trunk orientation were selected as independent generalized coordinates to describe the biped system in the reduced-state space. The model was used for the regulation of the biped during DSP. A general model to describe the impact dynamics of planar multi-link

robotic collisions was formulated, which can be used to solve the after-impact velocities and external impulses with both full-ranked and rank-deficient Jacobian matrices. Rank-deficient Jacobian matrices cause the impact equations to be undetermined. Special techniques were applied to solve the equations with Jacobian matrices being rank-deficient and proof is given that the solution of the post-impact velocities is unique and can be solved explicitly without extra equations. It is believed that, for the first time, the robotics impact dynamics involving rank-deficient Jacobian matrices was discussed and solved. The work contributes significantly to the research on impact dynamics of robots since impact occurs frequently when a robot interacts with the environment.

2) A complete biped gait cycle was synthesized for the biped motion planning. Swing tip motion was first designed followed by the design of hip motion. The trajectories of the motion are approximated with time polynomial functions. The advantages of the scheme include dividing the biped into subsystems which significantly simplifies the problem, and making it feasible to generate other optimal gait patterns such as energy efficient walking or using more complicated objective functions. The synthesized biped gait has the characteristics of repeatability in position and velocity, smoothness of joint movement and elimination of the physical impact occurring in the system. Stability condition was also considered during the DSP. The proposed strategies provide a valuable tool for generating motion patterns of biped gait, which is crucial for biped motion control.

3) The biped locomotion was regulated for a full gait cycle. Emphasis was given to the control of biped DSP. For motion regulation during the DSP, a sliding mode control algorithm was developed by treating the biped as a redundant manipulator where the constraint of both limbs remaining in contact with the ground is assumed satisfied. The

pseudo-inverse matrix was used as a performance function to distribute the control torques among the five joints. Simulation results showed the good performance obtained insensitively to the variation of biped system physical parameters. The robust sliding mode control for biped DSP, to the best of the author's knowledge, has not been found in previous work. The control strategy for the DSP by regulating the motion in reduced-state space may also provide the flexibility to distribute the joint torques based on various performance functions.

4) Some important aspects associated with impact dynamics during biped locomotion were studied. It was found that the direction of the pre-impact swing tip velocity plays a crucial role in determining the types of impact and consequently the type of the following supporting phase. Thus, it contributes to the development of biped robots by regulating the swing tip velocity such that desired gait with prescribed contact events can be produced. A parametric study was performed to investigate the correlation between the contact events (single impact, double impact or slippage of the foot/feet) and certain gait parameters. The regions representing the biped contact events were identified in the parameter space. Through the parametric analysis, the regions were identified, for the first time in literature, where none of the single or double impact can occur and both types of impact may occur. This finding raises serious concerns on the impact model and motivates further research on biped impact dynamics. The work provides important insights of the impact dynamics for biped locomotion. It also contributes directly to the development of bipedal robots in that the results can facilitate motion planning and motion regulation such that desired gait with prescribed contact events can be produced.

Overall, the complete dynamic model and motion regulation strategies developed in this work have provided a solid basis for the research on biped locomotion. The research has laid a framework for the future study on combining the model and robust control with stable walking conditions to realize practical biped locomotion. This work can also be expanded to other modeling and control problems involving the robot manipulators and the holonomic constraint systems.

6.2 Future Work

The results presented in this thesis are believed to be a further contribution to the development of a more practical biped walking. In particular, the planar five-link biped system can be extended to a model with seven or more links to include the dynamics of feet. Stability of the biped walking for the SSP may be also included in future analysis.

In addition, the finding in the parametric analysis, that the regions where none of the two types of impact can occur or both types of impact may occur, raises some serious concerns on the impact model used in this work and previous work (Hurmuzlu 1993, Tzafestas et al. 1996). One is whether it is possible for a physical biped system to have two possible contact events. If so, under what condition and which contact event will occur? Another concern is whether the impact conditions described previously are adequate. The third concern is whether the assumptions made in the impact model, such as perfect plastic rigid body collision, is valid. The related topic is interesting and further research on this issue is required.

References

Abo-Shanab, R.F. and Sepehri, N., "On Dynamic Stability of Manipulator Mounted on Mobile Platform", *Robotica* **19**, 439-449 (2001)

Borovac, B., Vukobratovic, M., and Surla, D., "An approach to Biped Control Synthesis", *Robotica* **7** 231-241 (1989)

Cabodevila, G. and Abba, G., "Quasi Optimal Gait for a Biped Robot Using Genetic Algorithm", *IEEE International Conference on Systems, Man, and Cybernetic—Computational Cybernetics and Simulation* **4**, 3960 –3965 (1997)

Cai, L and Song, G, "A Smooth Robust Nonlinear Controller for Robot Manipulators with Joint Stick-slip Friction", *Proceeding of IEEE International Conference on Robotics and Automation*, 449-455 (1993)

Caux, S. and Zapata, R. "Modeling and Control of Biped Robot Dynamics", *Robotica* **17**, 413-426 (1999)

Ceranowicz, A.Z., Wyman, B.F. and Hemami, "Control of Constrained Systems of Controllability Index Two", *IEEE Transactions on Automatic Control* **25**, 1102-1111 (1980)

Chan, C-Y.A., "Dynamic Modeling, Control and Simulation of a Planar Five-link Biped Walking System", *University of Manitoba Master Degree Thesis*, (2000)

Chang T-H., Hurmuzlu, Y., "Sliding Control Without Reaching Phase and Its Application to Biped Locomotion", *Journal of Dynamic Systems, Measurement, and Control* **115**, 447-455 (1993)

Channon, P.H., Hopkins, S.H. and Phan, D.T., "Derivation of Optimal Walking Motions for a Biped Walking Robot", *Robotica* **10** 165-172 (1992)

Chatterjee, A. and Ruina, A., "Two Interpretations of Rigidity in Rigid-Body Collisions," *Journal of Applied Mechanics* **65**, 894-900 (1998)

Cheng, M-Y. and Lin, C-S. "Dynamic Biped Robot Locomotion on Less Structured Surfaces", *Robotica* **18**, 163-170 (2000)

Chen, B-R., Hines, M and Hemami, H, "Dynamic Modeling for Implementation of a right Turn in Bipedal Walking", *Journal of Biomechanics* **19**, 195-206 (1986)

Chi, C-T. and Shih, C-L., "Inverted Pendulum-Like Walking Pattern for a Five-Link Biped Robot", *Journal of The Chinese Institute of Electrical Engineering* **7**, 287-298 (2000)

Chevallereau, C. Formal'sky, A. and Perrin, B., "Low Energy Cost Reference Trajectories for a Biped Robot", *Proceedings of IEEE International Conference on Robotics and Automation* **3**, 1398-1404 (1998)

Chevallereau, C., Aoustin, Y., and Formal'sky, "Optimal Walking Trajectories for a Biped", *Proceedings of the First Workshop on Robot Motion and Control*, 171-176 (1999)

Chevallereau, C. and Aoustin, Y., "Optimal Reference Trajectories for Walking and Running of a Biped Robot", *Robotica* **19**, 557-569 (2001)

Chow, C.K. and Jacobson, D.H., "Studies of Human Locomotion via Optimal Programming", *Mathematical biosciences* **10**, 239-306 (1971)

Chow, C.K. and Jacobson, D.H., "Further Studies of Human Locomotion: Postural Stability and Control", *Mathematical biosciences* **15**, 93-108 (1972).

Dinneen, J.A. and Hemami, H., "Stability and Movement of a One-Link Neuromusculoskeletal Sagittal Arm", *IEEE Transactions on Biomedical Engineering* **40**, 541-548 (1993)

Dorf, R.C. and Bishop, R.H., "Modern Control Systems", Addison Wesley Longman, Inc. 8th ed., (1998)

Furusho, J. and Masubuchi, M., "Control of a Dynamical Biped Locomotion System for Steady Walking", *Journal of Dynamic Systems, Measurement, and Control* **108**, 111-118 (1986)

Furusho, J. and Masubuchi, M. "A Theoretically Motivated Reduced Order Model for the Control of Dynamic Biped Locomotion", *Journal of Dynamic Systems, Measurement, and Control* **109**, 155-163 (1987).

Furusho, J. and Sano, A. "Sensor-Based Control of a Nine-Link Biped", *International Journal of Robotics Research* **9**, 83-98 (1990)

Gienger, M., Loffler, K. and Pfeiffer, F., "Toward the Design of a Biped Jogging Robot", *Proceedings of the 2001 IEEE International Conference on Robotics & Automation*, 4140-4145 (2001)

Goddard, R., Hemami, H. and Weimer, F., "Biped side step in the frontal plane", *IEEE Transaction of Automation Control* **28**, 179-187 (1983)

Goldsmith, W., *Impact, the Theory and Physical Behaviour of Colliding Solids*, London Edward Arnold Publishers LTD., London (1960)

Goldstein, H., Classical Mechanics, 2nd edition, Addison-Wesley Publishing Company, Reading, Massachusetts (1980)

Golliday, C.L., and Hemami, H. "Postural Stability of the Two-Degree-of-freedom biped by General Linear Feedback", *IEEE Transactions on Automatic Control* **21**, 74-79 (1976)

Golliday, C.L., and Hemami, H. "An Approach to Analyzing Biped Locomotion Dynamics and Designing Robot Locomotion Controls", *IEEE Transactions on Automatic Control* **22**, 963-972 (1977)

Goswami, A., "Postural Stability of Biped Robots and the Foot-Rotation Indicator Point", *International Journal of Robotics Research* **18** No 6 523-533 (1999)

Hardt, D.E. and Mann, R.W., "A Five Body-Three Dimensional Dynamic Analysis of Walking", *Journal of Biomechanics* **13**, 455-457 (1980)

Hardt, M., Kreutz-Delgado, K., and Helton J.W. "Optimal Biped Walking with a Complete Dynamic Model", *Proceedings of the 38th Conference on Decision & Control*, 2999-3004 (1999)

Hemami, H., Weimer, F.C. and Koozekanani, S.H., "Some Aspects of the Inverted Pendulum Problem for Modeling of Locomotion Systems", *IEEE Transactions on Automatic Control*, 658-661 (1973)

Hemami, H. and Camana, P.C., "Nonlinear Feedback in simple Locomotion systems", *IEEE Transactions on Automatic Control*, 835-860 (1976)

Hemami, H. and Golliday, C.Jr. "The Inverted Pendulum and Biped stability", *Mathematical Bioscience* **34**, 95-110 (1977)

Hemami, H. and Cvetkovic, V.S., "Postural Stability of Two Biped Models via Lyapunov Second Method", *IEEE Transactions on Automatic Control*, 66-70 (1977)

Hemami, H. and Farnsworth, R.L. "Postural and Gait Stability of a Planar Five Link biped by Simulation", *IEEE Transactions on Automatic Control*, 452-458 (1977)

Hemami, H., Weimer, F.C., Robinson, C.S., Stockwell, C.W. an Cvetkovic, V.S., "Biped Stability Considerations with Vestibular Model", *IEEE Transactions on Automatioc Control* **23**, 1074-1079 (1978)

Hemami, H. and Wyman, B.F., "Modeling and Control of Constrained Dynamic Systems with Application to Biped Locomotion in the Frontal Plane", *IEEE Transactions on Automatic Control* **24**, 526-535 (1979a)

Hemami, H. and Wyman, B.F., "Indirect Control of the Forces of Constraint in Dynamic Systems", *Journal of Dynamic Systems, measurement, and Control* **l**, 335-360 (1979b)

Hemami, H., "A Feedback On-Off Model of Biped Dynamics", *IEEE Transactions on Systems, Man and Cybernetic,* **10**, 376-383 (1980)

Hirai, K., Hirose, M., Haikawa, Y. and Takenaka, T., "The Development of Honda Humanoid robot", *Proc. IEEE International Conference on Robotics and Automation,* 1321-1326 (1998)

Honda Motor Co., Ltd, http://world.honda.com/ASIMO/ (2004)

Hu, J-J, Pratt J. and Pratt G. "Stable Adaptive Control of a Biped Walking Robot with CMAC Neural Networks", *Proceedings of IEEE International Conference on Robotics & Automation*, 1050-1056 (1999)

Huang, Q., Yokoi, K., Kajita, S., Kaneko, K., Arai, H., Koyachi, N. and Tanie, K., "Planning Walking Patterns for a Biped Robot", *IEEE Transactions on Robotics and Automation* **17**, 280-289 (2001).

Hurmuzlu, Y. and Moskowitz, "The Role of Impact in the Stability of Bipedal Locomotion", *Dynamics and Stability of Systems* **1** 217-234 (1986)

Hurmuzlu, Y. and Moskowitz, "Bipedal Locomotion Stabilized by Impact and Switching: I. Two- and Three-dimensional, Three-element Models", *Dynamics and Stability of Systems* **2** 75-96 (1987a)

Hurmuzlu, Y. and Moskowitz, "Bipedal Locomotion Stabilized by Impact and Switching: II. Structural Stability Analysis of a Four-element Bipedal Locomotion Model", *Dynamics and Stability of Systems* **2** 98-112 (1987b)

Hurmuzlu, Y. and Chang, T.-H., 1992, "Rigid Body Collisions of a Special Class of Planar Kinematic Chains", *IEEE Transactions on Systems, Man and Cybernetics* **22**, No. 5, pp. 964-971

Hurmuzlu, Y., "Dynamics of Bipedal Gait: Part I - Objective Functions and the Contact Event of a Planar Five-Link Biped", *Journal of Applied Mechanics* **60**, 331-336 (1993a)

Hurmuzlu, Y., "Dynamics of Bipedal Gait: Part II – Stability Analysis of a Planar Five-Link Biped", *Journal of Applied Mechanics* **60**, 337-343 (1993b)

Iqbal, K, Hemami, H. and Sheldon, S. "Stability and Control of a Frontal Four-Link biped System", *IEEE Transactions on Biomedical Engineering* **40**, 1007-1017 (1993)

Ivanov, A.P., "On Multiple Impact," *Journal of Applied Mathematics and Mechanics* **59**, 887-902 (1995)

Kagami, S., Nishiwaki, K., Sugihara, T., Kuffner, J.J., Inaba, M. and Inoue, H., "Design and Implementation of Software Research Platform for Humanoid Robotics: H6", *Proceedings of International Conference on Robotics and Automation (ICRA'01)*, pp. 2431-2436 (2001)

Kajita, S. and Tanie, K., "Study of Dynamic Biped Locomotion on Rugged Terrain", *IEEE Proceedings of 1991 International Conference on Robotics and Automation*, 1405-1411 (1991)

Kajita, S., Yamaura, T. and Kobayashi, A., "Dynamic Walking Control of a Biped Robot Along a Potential Energy Conserving Orbit", *IEEE Transactions on Robotics and Automation* **8**, 431-438 (1992)

Kane, T.T. And Scher, M.F., "Human Self-Rotation by Means of Limb Movements", *Journal of Biomechanics* **3**, 39-49 (1970)

Kawato, M., Furukawa, K. and Suzuki, R., "A Hierarchical Neural Network Model for Control and Learning of Voluntary Movement", *Biological Cybernetics* **57**, 169-185 (1987)

Kawato, M., Uno, Y., Isobe, M. and Suzuki, R., "Hierarchical Neural Network Model for Voluntary Movement with Application to Robotics", *IEEE Control Systems Magazine* **8**, 8-15 (1988)

Kerr, J. and Roth, B., "Analysis of Multifingered Hands", *International Journal of robotics Research* **4**, 3-16 (1986)

Kim J and Hemami, H., "Coordinated Three-Dimensional Motion of the Head and Torso by Dynamic Neural Networks" IEEE Transactions on System, Man and Cybernetics, part B **5**, 653-666 (1998)

Koditschek, D., "Nature Motion of Robot Arms", *IEEE Proceedings of International Conference on Decision and Control*, (1985)

Koopman, B., Barin, K., McGhee, R.B. and Chang, H.T., "A Recursive Free-Body Approach to Reconstruction and Prediction of Bipedal Walking", *Journal of Biomechanics* **28**, 1025-1036 (1995)

Lin, Y. and Song, S., "Learning Hybrid Position/Force Control of a Quadruped Walking Machine Using a CMAC Neural Network", *Journal of Robotic Systems* **14**, 483-499 (1997)

Lum, H.K., Zribi, M. and Soh, Y.C., "Planning and Control of a Biped Robot", *International Journal of Engineering Science* **37**, 1319-1349, (1999)

Ma, B. and Wu, Q., "Parametric Study of Repeatable Gait for a Planar Five-Link Biped", *Robotica* **20** 493-498 (2002)

Marchese S., Muscate G. and Virk G.S., "Dynamically Stable Trajectory Synthesis for a Biped Robot during the Single-Support Phase", *IEEE/ASME International Conference on Advanced Intelligent Mechatronics Proceedings*, 953-958 (2001)

Marghitu D.B., and Hurmuzlu, Y., "Three-Dimensional Rigid-Body Collisions with Multiple Contact Points," *Journal of Applied Mechanics*, **62**, 725-732 (1995)

McCown-McClintick, B.E. and Moskowitz, G.D., "The Behavior of a Biped Walking Gait on Irregular Terrain", *The International Journal of Robotics Research* **17**, 43-55 (1998)

McGeer, T., "Passive Biped Walking", *International Journal of Robotics Research* **9** 62-82 (1990a)

McGeer, T., "Passive Walking with Knees", *Proceedings of IEEE International Conference on Robotics and Automation* 1640-1645 (1990b)

Mitobe, K., Mori, N., Aida, K. and Nasu, Y., "Nonlinear Feedback Control of a Biped Walking Robot", *Proceedings of IEEE International Conference on Robotics and Automation*, 2865-2870 (1995)

Mitobe, K., Mori, N., Nasu, Y. and Adachi, N., "Control of a Biped Walking Robot during the Double Support Phase", *Autonomous Robots* **4**, 287-296 (1997)

Miura, H. and Shimoyama, I. "Dynamic Walking of a Biped Locomotion", *The International Journal of Robotics Research* **3**, 60-74 (1984)

Miyazaki, F. and Arimoto, S., "A Control Theoretic Study on Dynamical Biped Locomotion", *Journal of Dynamic Systems, Measurement, and Control* **102** 233-239 (1980)

Mnif, F., Saad, M. and Boukas, E. K., "A Robust Adaptive Approach for Force/Motion Control of Manipulators under Holonomic Constraints", *Canadian Congress in electric genius and data processing*, 334-7, (1995)

Onyshko, S. and Winter, D.A., "A Mathematical Model for the Dynamics of Human Locomotion", *Journal of Biomechanics* **13**, 361-368 (1980)

Pandy, M.G. and Berme, N., "Synthesis of Human Walking: A Planar Model for Single Support", *Journal of Biomechanics* **21**, 1053-1060 (1988)

Pandy, M.G. and Berme, N., "Quantitative Assessment of Gait Determinants During Single Stance via a Three-Dimensional Model-Part I. Normal Gait", *Journal of Biomechanics* **22**, 717-724 (1989)

Pandy, M.G., Zajac, F.E. and Levine, W.S., "An Optimal Control Model for Maximum Height Human Jumping", *Journal of Biomechanics* **23** 1185-1198 (1990)

Park, J.H. and Chung, H., "Hybrid Control of Biped Robots to Increase Stability in Locomotion", *Journal of Robotic Systems* **17**, No. 4, pp. 187-197 (2000)

Park, I-G. and Kim, J-G., "Robust Control for Dynamic Walking of a Biped Robot with Ground Contacting Condition", *ISIE*, 2067-2072 (2001)

Paradopoulos, E.G. and Rey, D.A., "A New Measurement of Tipover Stability Margin for Mobile Manipulator", *Proceedings of the IEEE International Conference on Robotics and Automation*, 3111-3116 (1996)

Pestel, E.C. and Thomson, W.T., *Dynamics*, McGraw-Hill Book Company, New York, 172-177 (1968)

Raibert, M.H. and Brown, H.B., "Experiments in Balance with a 2D One-Legged Hopping Machine", *ASME Journal of Dynamic Systems, Measurement, and Control* **106**, 75-81 (1984)

Raibert, M.G., "Running with Symmetry", *International Journal of Robotics Research* **5** 3-19 (1986)

Red, E., "A Dynamic Optimal Trajectory Generator for Cartesian Path Following", *Robotica* **18**, 451-458 (2000)

Reisinger, K.D. and Moskowitz, G.D., "Bipedal Locomotion: Stopping and the Standing/Balance Gait", *The International Journal of robotics Research* **18**, 333-343 (1999)

Rostami, M. and Bessonnet, G. "Impactless Sagittal Gait of a Biped Robot During the Single Support Phase", *Proceedings of IEEE International Conference on Robotics and Automation* 1385-1391 (1998)

Roussel, l., Canudas-de-Wit, C. and Goswami, A., "Generation of Energy Optimal Complete Gait Cycles for Biped Robots", *Proceedings of IEEE International Conference on Robotics and Automation* 2036-2041 (1998)

Schneider, H. and Barker, G.P., *Matrices and Linear Algebra*, second edition, Hopt, Rinehart and Winston, Inc. New York (1973)

Seo, Y-J and Yoon Y-S, "Design of a Robust Dynamic Gait of the Biped Using the Concept of Dynamic Stability Margin", *Robotica* **13**, 461-468 (1995)

Shih, C.L., Churng, S., Lee, T.T. and Gruver, W.A., "Trajectory Synthesis and Physical Admissibility for a Biped Robot During the Single-Support Phase", *Proceedings of IEEE International Conference on Robotics and Automation*, 1646-1651 (1990).

Shih, C-L., "The Dynamics and Control of a Biped Walking Robot with Seven Degrees of Freedom", *Journal of Dynamic Systems, Measurement, and Control* **118**, 683-690 (1996)

Shih, C-L., "Gait Synthesis for a Biped Robot", *Robotica* **15**, 599-607 (1997)

Silva, F.M., and Machado, J.A.T., "Goal-Oriented Biped Walking Based on Froce Interaction Control", *Proceedings of the IEEE International Conference on Robotics and Automation*, 4122-4127, (2001)

Slotine, J.J. and Sastry, S.S., "Tracking Control of Non-Linear Systems using Sliding Surface, with Application to Robot Manipulators", *International Journal of Control* **40**, 421-434 (1983)

Slotine, J.J., "sliding Mode Controller Design for Non-Linear Systems", *International Journal of Control* **40**, 421-434 (1984)

Slotine, J.J. and Li, W., "Applied Nonlinear Control", Prentice Hall, New Jersey (1991)

Song, J., Low, K.H., and Guo, W. "A Simplified Hybrid Force/Position controller Method for the walking robots", *Robotica* **17**, 583-589 (1999)

Sonoda, N., Murakami, T. and Ohnishi, K. "An Approach to Biped Robot Control Utilized Redundancy in Double Support Phase", *23rd International Conference on Industrial Electronics, Control & Instrumentation* **3,** 1332-1336 (1997)

Stojic, R. and Chevallereau, C., "On the Stability of Biped with Point Foot-Ground Contact", *IEEE International Conference on Robotics and Automation*, **4**, 3340-3345 (2000)

Su, C-Y, Leung, T-P, an Zhou Q-J, "Force/Motion Control of Constrained Robots Using Sliding Mode", *IEEE Transactions on Automatic Control*, **37 (5)**, 668-672 (1992)

Suzuki, S., Furuta, K., Pan, Y. and Hatakeyama, S., "Biped Walking Robot Control with Passive Walker Model by New VSC servo", *Proceedings of the American Control Conference*, 25-27 (2001)

Tagawa, Y., and Yamashita, T., "Characteristics of Multi-Body Model for Human Level Walking", *Biomechanics* **VIII B** 1005-1010 (1981)

Thornto-Trump, A.B., and Daher, R., "The Prediction of Reaction Forces From Gait Date", *Journal of Biomechanics* **8**, 173-178 (1975)

Tzafestas, S., Raibert, M. and Tzafestas, C. "Robust Sling-Mode Control Applied to a 5-Link Biped Robot", *Journal of Intelligenct and Robotic Systems* **15**, 67-133 (1996)

Vanel, O. and Gorce, P., "A New Approach to Dynamic Posture Control", *Robotica* **15**, 449-459 (1997)

Vukobratovic, M. and Juricic, D., "Contribution to the Synthesis of Biped Gait", *IEEE Transactions on Bio-medical Engineering* **16**, 1-6 (1969)

Vukobratovic, M., Frank, A.A. and Juricic, D., "On the Stability of biped Locomotion", *IEEE Transactions on Bio-medical Engineering* **17**, 25-36 (1970)

Vukobratovic, M. and Ekalo, Y., "Mathematical Model of General Anthropomorphic Systems", *Mathematical biosciences* **17**, 191-242 (1973)

Vukobratovic, M., Borovac, B., Surla, D. and Stokic, D., "Biped Locomotion: Dynamics, Stability, Control and Application", *Scientific Fundamentals of Robotics* **7** (Springer-Verlag, New York) (1990)

Whittaker, E.T., "A Treatise on the Analytical Dynamics of Particles and Rigid Bodies", Ed.4, New York: Dover Publications, Inc. (1944)

Wu, Q., "Lyapunov Stability Analysis of a class of Base-Excited Inverted Pendulums with Application to Bipedal Locomotion Systems", *University of Manitoba Ph.D. Thesis*, (1996)

Wu, Q., Thornton-Trump, A.B. and Sepehri, N., "Lyapunov Stability Control of Inverted Pendulums with General Base Point Motion", *International Journal of Non-Linear Mechanics* **33**, 801-818 (1998a)

Wu, Q., Sepehri, N., Thornton-Trump, A.B., and Alexander, M., "Stability and Control of Human Trunk Movement during Walking", *Computer Methods in Biomechanics and Biomedical Engineering* **1** 247-259 (1998b)

Wu, Q., and Swain R. "A mathematical model of the stability control of human thorax and pelvis movements during walking", *Computer Methods in Biomechanics and Biomedical Engineering* **5**, 67-74 (2002)

Wu, Q., and Chan, C.Y.A., "Design of energy efficient joint profiles for a planar five-link biped robot", *Proceedings of 2001 IEEE International Symposium on Computational Intelligence in Robotics and Automation*, 35-40, (2001)

Yang, J-S. and Shahabuddin, A., "Trajectory Planning and Control, for a Five-Degree-of-Freedom Biped Locomotion System", *Proceedings of the American Control Conference* 3105-3109 (1994)

Yi, K.Y., "Walking of a Biped Robot with Passive Ankle Joint", *Proceedings of International Conference of Control Applications*, 484-489 (1999)

Zarrugh, M.Y. and Radcliffe, C.W. "Computer Generation of Human Gait Kinematics", *Journal of Biomechanics,* **12**, 99-111 (1979)

Zheng, Y.F. and Hamami, H., "Impact Effect of Biped Contact with the Environment", *IEEE Transactions on Systems, man and Cybernetics* **3**, 437-443 (1984)

Zheng, Y.F. and Hamami, H., "Mathematic Modeling of a Robot Collision with its Environment", *Robotics Systems* **2**, 289-307 (1985)

Zheng, Y.F., "Acceleration Compensation for biped Robots to Reject External Disturbance ", *IEEE Transactions on Systems, Man and Cybernetics* **19,** 74-84 (1989)

Zheng, Y.F. and Shen, J., "Gait Synthesis for the SD-2 biped Robot to Climb Sloping Surface", *IEEE Transactions on Robotics and Automation* **6**, 86-96 (1990)

Zeng, G. and Hemami, A., "An Overview of Robot force Control", Robotica 15, 473-482 (1997)

Appendix I Derivation of the Biped Dynamic Model (2.7)

The single support phase dynamic equation (2.7) is derived by applying the Lagrange equation (2.6). The total potential energy and kinetic energy of the biped has been given in equation (2.3) and (2.4). From (2.3)-(2.5) one obtains

$$\frac{\partial P}{\partial \theta_i} = -\left[m_i d_i + \left(\sum_{k=i+1}^{5} m_k \right) a_i l_i \right] g \sin\theta_i \,, \tag{A1}$$

$$\begin{aligned} \frac{\partial K}{\partial \theta_i} = & -\sum_{j=1}^{i-1} \left\{ \left[m_i d_i + \left(\sum_{k=i+1}^{5} m_k \right) a_i l_i \right] a_j l_j \sin(\theta_i - \theta_j) \dot{\theta}_i \dot{\theta}_j \right\} \\ & - \sum_{j=i+1}^{5} \left\{ \left[m_j d_j + \left(\sum_{k=j+1}^{5} m_k \right) a_j l_j \right] a_i l_i \sin(\theta_i - \theta_j) \dot{\theta}_i \dot{\theta}_j \right\} \end{aligned} \tag{A2}$$

$$\begin{aligned} \frac{\partial K}{\partial \dot{\theta}_i} = & \left[I_i + m_i d_i^2 + \left(\sum_{k=i+1}^{5} m_k \right) a_i l_i^2 \right] \dot{\theta}_i \\ & + \sum_{j=1}^{i-1} \left\{ \left[m_i d_i + \left(\sum_{k=i+1}^{5} m_k \right) a_i l_i \right] a_j l_j \cos(\theta_i - \theta_j) \dot{\theta}_j \right\} \\ & + \sum_{j=i+1}^{5} \left\{ \left[m_j d_j + \left(\sum_{k=j+1}^{5} m_k \right) a_j l_j \right] a_i l_i \cos(\theta_i - \theta_j) \dot{\theta}_j \right\} \end{aligned} \tag{A3}$$

$$\begin{aligned} \frac{d}{dt}\left(\frac{\partial K}{\partial \dot{\theta}_i} \right) = & \left[I_i + m_i d_i^2 + \left(\sum_{k=i+1}^{5} m_k \right) a_i l_i^2 \right] \ddot{\theta}_i \\ & + \sum_{j=1}^{i-1} \left\{ \left[m_i d_i + \left(\sum_{k=i+1}^{5} m_k \right) a_i l_i \right] a_j l_j \cos(\theta_i - \theta_j) \ddot{\theta}_j \right\} \\ & + \sum_{j=i+1}^{5} \left\{ \left[m_j d_j + \left(\sum_{k=j+1}^{5} m_k \right) a_j l_j \right] a_i l_i \cos(\theta_i - \theta_j) \ddot{\theta}_j \right\} \\ & + \sum_{j=1}^{i-1} \left\{ \left[m_i d_i + \left(\sum_{k=i+1}^{5} m_k \right) a_i l_i \right] a_j l_j \sin(\theta_i - \theta_j) \dot{\theta}_j (\dot{\theta}_j - \dot{\theta}_i) \right\} \\ & + \sum_{j=i+1}^{5} \left\{ \left[m_j d_j + \left(\sum_{k=j+1}^{5} m_k \right) a_j l_j \right] a_i l_i \sin(\theta_i - \theta_j) \dot{\theta}_j (\dot{\theta}_j - \dot{\theta}_i) \right\} \end{aligned} \tag{A4}$$

Substituting (A1-A4) into (2.6), one obtains the desired model (2.7) in detailed forms.

Appendix II Derivation of the Double Impact Model (2.23)

For each of the five separate links shown in Figure (2.3), one has the following equations:

$$m_i \Delta \dot{x}_{ci} = m_i \left[\sum_{j=1}^{i-1} \left(a_j l_j \cos\theta_j \Delta\dot{\theta}_j \right) + d_i \cos\theta_i \Delta\dot{\theta}_i \right] = P_{xi} - P_{xi-1}, \tag{A5}$$

$$m_i \Delta \dot{y}_{ci} = -m_i \left[\sum_{j=1}^{i-1} \left(a_j l_j \sin\theta_j \Delta\dot{\theta}_j \right) - d_i \sin\theta_i \Delta\dot{\theta}_i \right] = P_{yi} - P_{yi-1}, \tag{A6}$$

$$I_i \Delta\dot{\theta}_i = P_{xi}(a_i l_i - d_i)\cos\theta_i + P_{xi-1} d_i \cos\theta_i - P_{yi}(a_i l_i - d_i)\sin\theta_i - P_{yi-1} d_i \sin\theta_i . \tag{A7}$$

Because the two legs are in contact with ground during double support phase, the linear velocities of the two lower leg tips are zero and thus the following constraint conditions are held at the end of the double impact:

$$\dot{x}_e^+ = \sum_{i=1}^{5} a_i l_i \cos\theta_i \dot{\theta}_i^+ + \dot{x}_b^+ = \sum_{i=1}^{5} a_i l_i \cos\theta_i \dot{\theta}_i^+ = 0, \tag{A8}$$

$$\dot{y}_e^+ = -\sum_{i=1}^{5} a_i l_i \sin\theta_i \dot{\theta}_i^+ - \dot{y}_b^+ = -\sum_{i=1}^{5} a_i l_i \sin\theta_i \dot{\theta}_i^+ = 0 . \tag{A9}$$

Equations (A5-A7) can be simplified for the following i (i=1,2...5) equations by cancelling the internal impulses:

$$\sum_{j=1}^{i} \left[w_{ij} \cos(\theta_i - \theta_j) \Delta\dot{\theta}_j \right] = P_{x0} l_i \cos\theta_i - P_{y0} l_i \sin\theta_i , \tag{A10}$$

where w_{ij} are some inertial terms:

$$w_{ij} = \begin{cases} I_i - m_i d_i (a_i l_i - d_i) & j = i \\ -\left[a_i m_j d_j l_i + a_j m_i (a_i l_i - d_i) l_j + a_i a_j \left(\sum_{k=j+1}^{i-1} m_k \right) l_i l_j \right] & j < i \\ 0 & j > i \end{cases} \tag{A11}$$

It is obviously that equation (A10) and (A8-A9) can be written as the following equations in vector forms:

$$W\dot{\theta}^{+} = W\dot{\theta}^{-} + J^{T}\underline{P}_{0}, \tag{A12a}$$

$$J\dot{\theta}^{+} = 0, \tag{A12b}$$

where $P_0 = \begin{bmatrix} P_{x0} & P_{y0} \end{bmatrix}^T$, and J is the Jacobian matrix.

Combining equation (A12a) and (A12b), one obtains the double impact model (2.23).

Appendix III Derivation of the Dynamic Model Using Traditional Biped Kinematics

According to the kinematic model shown by Figure (2.4), the coordinates of the mass center of each link are

$$
\begin{aligned}
xc_1 &= d_1 \sin\theta_1 \\
yc_1 &= d_1 \cos\theta_1 \\
xc_2 &= \ell_1 \sin\theta_1 + d_2 \sin\theta_2 \\
yc_2 &= \ell_1 \cos\theta_1 + d_2 \cos\theta_2 \\
xc_3 &= \ell_1 \sin\theta_1 + \ell_2 \sin\theta_2 + d_3 \sin\theta_3 \\
yc_3 &= \ell_1 \cos\theta_1 + \ell_2 \cos\theta_2 + d_3 \cos\theta_3 \\
xc_4 &= \ell_1 \sin\theta_1 + \ell_2 \sin\theta_2 + (\ell_4 - d_4)\sin\theta_4 \\
yc_4 &= \ell_1 \cos\theta_1 + \ell_2 \cos\theta_2 - (\ell_4 - d_4)\cos\theta_4 \\
xc_5 &= \ell_1 \sin\theta_1 + \ell_2 \sin\theta_2 + \ell_4 \sin\theta_4 + (\ell_5 - d_5)\sin\theta_5 \\
yc_5 &= \ell_1 \cos\theta_1 + \ell_2 \cos\theta_2 - \ell_4 \cos\theta_4 - (\ell_5 - d_5)\cos\theta_5
\end{aligned}
\tag{A13a}
$$

$$
\begin{aligned}
\dot{x}_{c1} &= d_1 \cos\theta_1\dot{\theta}_1 + \dot{x}_b \\
\dot{y}_{c1} &= -d_1 \sin\theta_1\dot{\theta}_1 + \dot{y}_b \\
\\
\dot{x}_{c2} &= l_1 \cos\theta_1\dot{\theta}_1 + d_2 \cos\theta_2\dot{\theta}_2 + \dot{x}_b \\
\dot{y}_{c2} &= -l_1 \sin\theta_1\dot{\theta}_1 - d_2 \sin\theta_2\dot{\theta}_2 + \dot{y}_b \\
\\
\dot{x}_{c3} &= l_1 \cos\theta_1\dot{\theta}_1 + l_2 \cos\theta_2\dot{\theta}_2 + d_3 \cos\theta_3\dot{\theta}_3 + \dot{x}_b \\
\dot{y}_{c3} &= -l_1 \sin\theta_1\dot{\theta}_1 - l_2 \sin\theta_2\dot{\theta}_2 - d_3 \sin\theta_3\dot{\theta}_3 + \dot{y}_b \\
\\
\dot{x}_{c4} &= l_1 \cos\theta_1\dot{\theta}_1 + l_2 \cos\theta_2\dot{\theta}_2 + (l_4 - d_4)\cos\theta_4\dot{\theta}_4 + \dot{x}_b \\
\dot{y}_{c4} &= -l_1 \sin\theta_1\dot{\theta}_1 - l_2 \sin\theta_2\dot{\theta}_2 + (l_4 - d_4)\sin\theta_4\dot{\theta}_4 + \dot{y}_b \\
\\
\dot{x}_{c5} &= l_1 \cos\theta_1\dot{\theta}_1 + l_2 \cos\theta_2\dot{\theta}_2 + l_4 \cos\theta_4\dot{\theta}_4 + (l_5 - d_5)\cos\theta_5\dot{\theta}_5 + \dot{x}_b \\
\dot{y}_{c5} &= -l_1 \sin\theta_1\dot{\theta}_1 - l_2 \sin\theta_2\dot{\theta}_2 + l_4 \sin\theta_4\dot{\theta}_4 + (l_5 - d_5)\sin\theta_5\dot{\theta}_5 + \dot{y}_b
\end{aligned}
\tag{A13b}
$$

and thus the kinetic and potential energy of each link are

$$
\begin{aligned}
K_1 &= \frac{1}{2}(I_1 + m_1 d_1^{\,2})\dot{\theta}_1^{\,2} \\
P_1 &= m_1 g d_1 \cos\theta_1
\end{aligned}
$$

$$K_2 = \frac{1}{2}\left[I_2 + m_2 d_2{}^2\right]\dot{\theta}_2{}^2 + \frac{1}{2} m_2 \ell_1{}^2 \dot{\theta}_1{}^2 + m_2 \ell_1 d_2 \cos(\theta_1 - \theta_2)\dot{\theta}_1\dot{\theta}_2$$
$$P_2 = m_2 g(\ell_1 \cos\theta_1 + d_2 \cos\theta_2)$$

$$K_3 = \frac{1}{2}\left[I_3 + m_3 d_3{}^2\right]\dot{\theta}_3{}^2 + \frac{1}{2} m_3 [\ell_1{}^2 \dot{\theta}_1{}^2 + \ell_2{}^2 \dot{\theta}_2{}^2 + 2\ell_1 \ell_2 \cos(\theta_1 - \theta_2)\dot{\theta}_1\dot{\theta}_2$$
$$+ 2\ell_1 d_3 \cos(\theta_1 - \theta_3)\dot{\theta}_1\dot{\theta}_3 + 2\ell_2 d_3 \cos(\theta_2 - \theta_3)\dot{\theta}_2\dot{\theta}_3]$$
$$P_3 = m_3 g(\ell_1 \cos\theta_1 + \ell_2 \cos\theta_2 + d_3 \cos\theta_3)$$

$$K_4 = \frac{1}{2}\left[I_4 + m_4(\ell_4 - d_4)\right]\dot{\theta}_4{}^2 + \frac{1}{2} m_4 [\ell_1{}^2 \dot{\theta}_1{}^2 + \ell_2{}^2 \dot{\theta}_2{}^2 + 2\ell_1 \ell_2 \cos(\theta_1 - \theta_2)\dot{\theta}_1\dot{\theta}_2$$
$$+ 2\ell_1(\ell_4 - d_4)\cos(\theta_1 + \theta_4)\dot{\theta}_1\dot{\theta}_4 + 2\ell_2(\ell_4 - d_4)\cos(\theta_2 + \theta_4)\dot{\theta}_2\dot{\theta}_4]$$
$$P_4 = m_4 g(l_1 \cos\theta_1 + l_2 \cos\theta_2 - (\ell_4 - d_4)\cos\theta_4)$$

$$K_5 = \frac{1}{2}\left[I_5 + m_5(\ell_5 - d_5)^2\right]\dot{\theta}_5{}^2 + \frac{1}{2} m_5 [\ell_1{}^2 \dot{\theta}_1{}^2 + \ell_2{}^2 \dot{\theta}_2{}^2 + \ell_4{}^2 \dot{\theta}_4{}^2 + 2\ell_1 \ell_2 \cos(\theta_1 - \theta_2)\dot{\theta}_1\dot{\theta}_2$$
$$+ 2\ell_1 \ell_4 \cos(\theta_1 + \theta_4)\dot{\theta}_1\dot{\theta}_4 + 2\ell_1(\ell_5 - d_5)\cos(\theta_1 + \theta_5)\dot{\theta}_1\dot{\theta}_5 + 2\ell_2 \ell_4 \cos(\theta_2 + \theta_4)\dot{\theta}_2\dot{\theta}_4$$
$$2\ell_2(\ell_5 - d_5)\cos(\theta_2 + \theta_5)\dot{\theta}_2\dot{\theta}_5 + 2\ell_4(\ell_5 - d_5)\cos(\theta_4 - \theta_5)\dot{\theta}_4\dot{\theta}_5]$$
$$P_5 = m_5 g(\ell_1 \cos\theta_1 + \ell_2 \cos\theta_2 - \ell_4 \cos\theta_4 - (\ell_5 - d_5)\cos\theta_5)$$

(A14)

From (A13) and (A14), one obtains,

$$\frac{\partial P}{\partial \theta_1} = -[m_1 d_1 + m_2 \ell_1 + m_3 \ell_1 + m_4 \ell_1 + m_5 \ell_1] g \sin\theta_1$$
$$\frac{\partial P}{\partial \theta_2} = -[m_2 d_2 + m_3 \ell_2 + m_4 \ell_2 + m_5 \ell_2] g \sin\theta_2$$
$$\frac{\partial P}{\partial \theta_3} = -[m_3 d_3] g \sin\theta_3 \qquad \text{(A15)}$$
$$\frac{\partial P}{\partial \theta_4} = [m_4(\ell_4 - d_4) + m_5 \ell_4] g \sin\theta_4$$
$$\frac{\partial P}{\partial \theta_5} = [m_5(\ell_5 - d_5)] g \sin\theta_5$$

$$\frac{\partial K}{\partial \theta_1} = -[m_2 \ell_1 d_2 + m_3 \ell_1 \ell_2 + m_4 \ell_1 \ell_2 + m_5 \ell_1 \ell_2]\sin(\theta_1 - \theta_2)\dot{\theta}_1\dot{\theta}_2$$
$$-[m_3 \ell_1 d_3]\sin(\theta_1 - \theta_3)\dot{\theta}_1\dot{\theta}_3 - [m_4 \ell_1(\ell_4 - d_4) + m_5 \ell_1 \ell_4]\sin(\theta_1 + \theta_4)\dot{\theta}_1\dot{\theta}_4$$
$$-[m_5 \ell_1(\ell_5 - d_5)]\sin(\theta_1 + \theta_5)\dot{\theta}_1\dot{\theta}_5$$

$$\frac{\partial K}{\partial \theta_2} = -[m_2\ell_1 d_2 + m_3\ell_1\ell_2 + m_4\ell_1\ell_2 + m_5\ell_1\ell_2]\sin(\theta_1-\theta_2)\dot{\theta}_1\dot{\theta}_2$$
$$-[m_3\ell_2 d_3]\sin(\theta_2-\theta_3)\dot{\theta}_2\dot{\theta}_3 - [m_4\ell_2(\ell_4-d_4)+m_5\ell_2\ell_4]\sin(\theta_2+\theta_4)\dot{\theta}_2\dot{\theta}_4$$
$$-[m_5\ell_2(\ell_5-d_5)]\sin(\theta_2+\theta_5)\dot{\theta}_2\dot{\theta}_5$$

$$\frac{\partial K}{\partial \theta_3} = -[m_3\ell_1 d_3]\sin(\theta_1-\theta_3)\dot{\theta}_1\dot{\theta}_3 + [m_3\ell_2 d_3]\sin(\theta_2-\theta_3)\dot{\theta}_2\dot{\theta}_3$$

$$\frac{\partial K}{\partial \theta_4} = -[m_4\ell_1(\ell_4-d_4)+m_5\ell_1\ell_4]\sin(\theta_1+\theta_4)\dot{\theta}_1\dot{\theta}_4$$
$$-[m_4\ell_2(\ell_4-d_4)+m_5\ell_2\ell_4]\sin(\theta_2+\theta_4)\dot{\theta}_2\dot{\theta}_4$$
$$-[m_5\ell_4(\ell_5-d_5)]\sin(\theta_4-\theta_5)\dot{\theta}_4\dot{\theta}_5$$

$$\frac{\partial K}{\partial \theta_5} = -[m_5\ell_1(\ell_5-d_5)]\sin(\theta_1+\theta_5)\dot{\theta}_1\dot{\theta}_5$$
$$-[m_5\ell_2(\ell_5-d_5)]\sin(\theta_2+\theta_5)\dot{\theta}_2\dot{\theta}_5 \qquad \text{(A16)}$$
$$+[m_5\ell_4(\ell_5-d_5)]\sin(\theta_4-\theta_5)\dot{\theta}_4\dot{\theta}_5$$

$$\frac{\partial k}{\partial \dot{\theta}_1} = (I_1 + m_1 d_1^2 + (m_2+m_3+m_4+m_5)l_1^2)\dot{\theta}_1$$
$$+(m_2 l_1 d_2 + (m_3+m_4+m_5)l_1 l_2)\cos(\theta_1-\theta_2)\dot{\theta}_2 + m_3 l_1 d_3\cos(\theta_i-\theta_3)\dot{\theta}_3$$
$$+(m_4 l_1(l_4-d_4)+m_5 l_1 l_4)\cos(\theta_1+\theta_4)\dot{\theta}_4 + m_5 l_1(l_5-d_5)\cos(\theta_1+\theta_5)\dot{\theta}_5$$

$$\frac{\partial k}{\partial \dot{\theta}_2} = (m_2 l_1 d_2 + (m_3+m_4+m_5)l_1 l_2)\cos(\theta_1-\theta_2)\dot{\theta}_1$$
$$+(I_2 + m_2 d_2^2 + (m_3+m_4+m_5)l_2^2)\dot{\theta}_2 + m_3 l_2 d_3\cos(\theta_2-\theta_3)\dot{\theta}_3$$
$$+(m_4 l_2(l_4-d_4)+m_5 l_2 l_4)\cos(\theta_2+\theta_4)\dot{\theta}_4 + m_5 l_2(l_5-d_5)\cos(\theta_2+\theta_5)\dot{\theta}_5$$

$$\frac{\partial k}{\partial \dot{\theta}_3} = m_3 l_1 d_3\cos(\theta_1-\theta_3)\dot{\theta}_1 + m_3 l_2 d_3\cos(\theta_2-\theta_3)\dot{\theta}_2 + (I_3 + m_3 d_3^2)\dot{\theta}_3$$

$$\frac{\partial k}{\partial \dot{\theta}_4} = (m_4 l_1(l_4-d_4)+m_5 l_1 l_4)\cos(\theta_1+\theta_4)\dot{\theta}_1 + (m_4 l_2(l_4-d_4)+m_5 l_2 l_4)\cos(\theta_2+\theta_4)\dot{\theta}_2$$
$$+(I_4 + m_4(l_4-d_4)^2 + m_5 l_4^2)\dot{\theta}_4 + m_5 l_4(l_5-d_5)\cos(\theta_4-\theta_5)\dot{\theta}_5$$

$$\frac{\partial k}{\partial \dot{\theta}_5} = m_5 l_1(l_5-d_5)\cos(\theta_1+\theta_5)\dot{\theta}_1 + m_5 l_2(l_5-d_5)\cos(\theta_2+\theta_5)\dot{\theta}_2 \qquad \text{(A17)}$$
$$+m_5 l_4(l_5-d_5)\cos(\theta_4-\theta_5)\dot{\theta}_4 + (I_5 + m_5(l_5-d_5)^2)\dot{\theta}_5$$

$$\frac{d}{dt}\left(\frac{\partial K}{\partial \dot{\theta}_1}\right) = [I_1 + m_1 d_1^{\,2} + m_2 \ell_1^{\,2} + m_3 \ell_1^{\,2} + m_4 \ell_1^{\,2} + m_5 \ell_1^{\,2}]\ddot{\theta}_1$$
$$+ [m_2 \ell_1 d_2 + m_3 \ell_1 \ell_2 + m_4 \ell_1 \ell_2 + m_5 \ell_1 \ell_2]\cos(\theta_1 - \theta_2)\ddot{\theta}_2$$
$$+ [m_3 \ell_1 d_3]\cos(\theta_1 - \theta_3)\ddot{\theta}_3$$
$$+ [m_4 \ell_1 (\ell_4 - d_4) + m_5 \ell_1 \ell_4]\cos(\theta_1 + \theta_4)\ddot{\theta}_4$$
$$+ [m_5 \ell_1 (\ell_5 - d_5)]\cos(\theta_1 + \theta_5)\ddot{\theta}_5$$
$$- [m_2 \ell_1 d_2 + m_3 \ell_1 \ell_2 + m_4 \ell_1 \ell_2 + m_5 \ell_1 \ell_2]\sin(\theta_1 - \theta_2)\dot{\theta}_1\dot{\theta}_2$$
$$+ [m_2 \ell_1 d_2 + m_3 \ell_1 \ell_2 + m_4 \ell_1 \ell_2 + m_5 \ell_1 \ell_2]\sin(\theta_1 - \theta_2)\dot{\theta}_2^{\,2}$$
$$- [m_3 \ell_1 d_3]\sin(\theta_1 - \theta_3)\dot{\theta}_1\dot{\theta}_3 + [m_3 \ell_1 d_3]\sin(\theta_1 - \theta_3)\dot{\theta}_3^{\,2}$$
$$- [m_4 \ell_1 (\ell_4 - d_4) + m_5 \ell_1 \ell_4]\sin(\theta_1 + \theta_4)\dot{\theta}_1\dot{\theta}_4$$
$$- [m_4 \ell_1 (\ell_4 - d_4) + m_5 \ell_1 \ell_4]\sin(\theta_1 + \theta_4)\dot{\theta}_4^{\,2}$$
$$- [m_5 \ell_1 (\ell_5 - d_5)]\sin(\theta_1 + \theta_5)\dot{\theta}_1\dot{\theta}_5 - [m_5 \ell_1 (\ell_5 - d_5)]\sin(\theta_1 + \theta_5)\dot{\theta}_5^{\,2}$$

$$\frac{d}{dt}\left(\frac{\partial K}{\partial \dot{\theta}_2}\right) = [I_2 + m_2 d_2^{\,2} + m_3 \ell_2^{\,2} + m_4 \ell_2^{\,2} + m_5 \ell_2^{\,2}]\ddot{\theta}_2$$
$$+ [m_2 \ell_1 d_2 + m_3 \ell_1 \ell_2 + m_4 \ell_1 \ell_2 + m_5 \ell_1 \ell_2]\cos(\theta_1 - \theta_2)\ddot{\theta}_1$$
$$+ [m_3 \ell_2 d_3]\cos(\theta_2 - \theta_3)\ddot{\theta}_3$$
$$+ [m_4 \ell_2 (\ell_4 - d_4) + m_5 \ell_2 \ell_4]\cos(\theta_2 + \theta_4)\ddot{\theta}_4$$
$$+ [m_5 \ell_2 (\ell_5 - d_5)]\cos(\theta_2 + \theta_5)\ddot{\theta}_5$$
$$+ [m_2 \ell_1 d_2 + m_3 \ell_1 \ell_2 + m_4 \ell_1 \ell_2 + m_5 \ell_1 \ell_2]\sin(\theta_1 - \theta_2)\dot{\theta}_1\dot{\theta}_2$$
$$- [m_2 \ell_1 d_2 + m_3 \ell_1 \ell_2 + m_4 \ell_1 \ell_2 + m_5 \ell_1 \ell_2]\sin(\theta_1 - \theta_2)\dot{\theta}_2^{\,2}$$
$$- [m_3 \ell_2 d_3]\sin(\theta_2 - \theta_3)\dot{\theta}_2\dot{\theta}_3 + [m_3 \ell_2 d_3]\sin(\theta_2 - \theta_3)\dot{\theta}_3^{\,2}$$
$$- [m_4 \ell_2 (\ell_4 - d_4) + m_5 \ell_2 \ell_4]\sin(\theta_2 + \theta_4)\dot{\theta}_2\dot{\theta}_4$$
$$- [m_4 \ell_2 (\ell_4 - d_4) + m_5 \ell_2 \ell_4]\sin(\theta_2 + \theta_4)\dot{\theta}_4^{\,2}$$
$$- [m_5 \ell_2 (\ell_5 - d_5)]\sin(\theta_2 + \theta_5)\dot{\theta}_2\dot{\theta}_5 - [m_5 \ell_2 (\ell_5 - d_5)]\sin(\theta_2 + \theta_5)\dot{\theta}_5^{\,2}$$

$$\frac{d}{dt}\left(\frac{\partial K}{\partial \dot{\theta}_3}\right) = [I_3 + m_3 d_3^{\,2}]\ddot{\theta}_3 + [m_3 \ell_1 d_3]\cos(\theta_1 - \theta_3)\ddot{\theta}_1 + [m_3 \ell_2 d_3]\cos(\theta_2 - \theta_3)\ddot{\theta}_2$$
$$+ [m_3 \ell_1 d_3]\sin(\theta_1 - \theta_3)\dot{\theta}_1\dot{\theta}_3 - [m_3 \ell_1 d_3]\sin(\theta_1 - \theta_3)\dot{\theta}_1^{\,2}$$
$$+ [m_3 \ell_2 d_3]\sin(\theta_2 - \theta_3)\dot{\theta}_2\dot{\theta}_3 - [m_3 \ell_2 d_3]\sin(\theta_2 - \theta_3)\dot{\theta}_2^{\,2}$$

$$\frac{d}{dt}\left(\frac{\partial K}{\partial \dot{\theta}_4}\right) = [I_4 + m_4(\ell_4 - d_4)^2 + m_5\ell_4{}^2]\ddot{\theta}_4 + [m_4\ell_1(\ell_4 - d_4) + m_5\ell_1\ell_4]\cos(\theta_1 + \theta_4)\ddot{\theta}_1$$
$$+ [m_4\ell_2(\ell_4 - d_4) + m_5\ell_2\ell_4]\cos(\theta_2 + \theta_4)\ddot{\theta}_2 + [m_5\ell_4(\ell_5 - d_5)]\cos(\theta_4 - \theta_5)\ddot{\theta}_5$$
$$- [m_4\ell_1(\ell_4 - d_4) + m_5\ell_1\ell_4]\sin(\theta_1 + \theta_4)\dot{\theta}_1\dot{\theta}_4$$
$$- [m_4\ell_1(\ell_4 - d_4) + m_5\ell_1\ell_4]\sin(\theta_1 + \theta_4)\dot{\theta}_1{}^2$$
$$- [m_4\ell_2(\ell_4 - d_4) + m_5\ell_2\ell_4]\sin(\theta_2 + \theta_4)\dot{\theta}_2\dot{\theta}_4$$
$$- [m_4\ell_2(\ell_4 - d_4) + m_5\ell_2\ell_4]\sin(\theta_2 + \theta_4)\dot{\theta}_2{}^2$$
$$- [m_5\ell_4(\ell_5 - d_5)]\sin(\theta_4 - \theta_5)\dot{\theta}_4\dot{\theta}_5 + [m_5\ell_4(\ell_5 - d_5)]\sin(\theta_4 - \theta_5)\dot{\theta}_5{}^2$$

$$\frac{d}{dt}\left(\frac{\partial K}{\partial \dot{\theta}_5}\right) = [I_5 + m_5(\ell_5 - d_5)^2]\ddot{\theta}_5 + [m_5\ell_1(\ell_5 - d_5)]\cos(\theta_1 + \theta_5)\ddot{\theta}_1$$
$$+ [m_5\ell_2(\ell_5 - d_5)]\cos(\theta_2 + \theta\ )\ddot{\theta}_2 + [m_5\ell_4(\ell_5 - d_5)]\cos(\theta_4 - \theta_5)\ddot{\theta}_4$$
$$- [m_5\ell_1(\ell_5 - d_5)]\sin(\theta_1 + \theta_5)\dot{\theta}_1\dot{\theta}_5 - [m_5\ell_1(\ell_5 - d_5)]\sin(\theta_1 + \theta_5)\dot{\theta}_1{}^2 \qquad \text{(A18)}$$
$$- [m_5\ell_2(\ell_5 - d_5)]\sin(\theta_2 + \theta_5)\dot{\theta}_2\dot{\theta}_5 - [m_5\ell_2(\ell_5 - d_5)]\sin(\theta_2 + \theta_5)\dot{\theta}_2{}^2$$
$$+ [m_5\ell_4(\ell_5 - d_5)]\sin(\theta_4 - \theta_5)\dot{\theta}_4\dot{\theta}_5 - [m_5\ell_4(\ell_5 - d_5)]\sin(\theta_4 - \theta_5)\dot{\theta}_4{}^2$$

By applying (A15)-(A18) to the Lagrangian equation of motion, the dynamic model is derived as (2.7) with the following detailed form:

$$\underline{D}(\underline{\theta}) = D_{ij}(\underline{\theta}) \quad (i, j = 1,2,\ldots 5)$$

$$D_{11} = I_1 + m_1 d_1{}^2 + (m_2 + m_3 + m_4 + m_5)\ell_1{}^2$$
$$D_{12} = [m_2\ell_1 d_2 + (m_3 + m_4 + m_5)\ell_1\ell_2]\cos(\theta_1 - \theta_2)$$
$$D_{13} = [m_3\ell_1 d_3]\cos(\theta_1 - \theta_3)$$
$$D_{14} = [m_4\ell_1(\ell_4 - d_4) + m_5\ell_1\ell_4]\cos(\theta_1 + \theta_4)$$
$$D_{15} = [m_5\ell_1(\ell_5 - d_5)]\cos(\theta_1 + \theta_5)$$

$$D_{21} = D_{12}$$
$$D_{22} = I_2 + m_2 d_2{}^2 + (m_3 + m_4 + m_5)\ell_2{}^2$$
$$D_{23} = [m_3\ell_2 d_3]\cos(\theta_2 - \theta_3)$$
$$D_{24} = [m_4\ell_2(\ell_4 - d_4) + m_5\ell_2\ell_4]\cos(\theta_2 + \theta_4)$$
$$D_{25} = [m_5\ell_2(\ell_5 - d_5)]\cos(\theta_2 + \theta_5)$$

$$D_{31} = D_{13}$$
$$D_{32} = D_{23}$$
$$D_{33} = I_3 + m_3 d_3^{\,2}$$
$$D_{34} = D_{35} = 0$$

$$D_{41} = D_{14}$$
$$D_{42} = D_{24}$$
$$D_{43} = D_{34}$$
$$D_{44} = I_4 + m_4(\ell_4 - d_4)^2 + m_5 \ell_4^{\,2}$$
$$D_{45} = [m_5 \ell_4 (\ell_5 - d_5)]\cos(\theta_4 - \theta_5)$$

$$D_{51} = D_{15}$$
$$D_{52} = D_{25}$$
$$D_{53} = D_{35}$$
$$D_{54} = D_{45}$$
$$D_{55} = I_5 + m_5(\ell_5 - d_5)^2$$

$$\underline{h}(\underline{\theta}, \dot{\underline{\theta}})\dot{\underline{\theta}} = col\left[\sum_{\substack{j=1 \\ j \neq i}}^{5} h_{ijj}\dot{\theta}_j^{\,2}\right] \qquad (i, j = 1,2,\ldots 5)$$

$$h_{122} = [m_2 \ell_1 d_2 + (m_3 + m_4 + m_5)\ell_1 \ell_2]\sin(\theta_1 - \theta_2)$$
$$h_{133} = [m_3 \ell_1 d_3]\sin(\theta_1 - \theta_3)$$
$$h_{144} = -[m_4 \ell_1 (\ell_4 - d_4) + m_5 \ell_1 \ell_4]\sin(\theta_1 + \theta_4)$$
$$h_{155} = -[m_5 \ell_1 (\ell_5 - d_5)]\sin(\theta_1 + \theta_5)$$

$$h_{211} = -h_{122}$$
$$h_{233} = [m_3 \ell_2 d_3]\sin(\theta_2 - \theta_3)$$
$$h_{244} = -[m_4 \ell_2 (\ell_4 - d_4) + m_5 \ell_2 \ell_4]\sin(\theta_2 + \theta_4)$$
$$h_{255} = -[m_5 \ell_2 (\ell_5 - d_5)]\sin(\theta_2 + \theta_5)$$

$$h_{311} = -h_{133}$$
$$h_{322} = h_{233}$$
$$h_{344} = h_{355} = 0$$

$$h_{411} = h_{144}$$
$$h_{422} = h_{244}$$
$$h_{433} = 0$$
$$\mathrm{h}_{455} = [m_5 \ell_4 (\ell_5 - d_5)] \sin(\theta_4 - \theta_5)$$

$$h_{511} = h_{155}$$
$$h_{522} = h_{255}$$
$$h_{533} = 0$$
$$h_{544} = -h_{455}$$

$$\underline{G}(\underline{\theta}) = G_i(\underline{\theta}) \quad (i = 1,2,\ldots 5)$$

$$G_1 = -[m_1 d_1 + m_2 \ell_1 + m_3 \ell_1 + m_4 \ell_1 + m_5 \ell_1] g \sin\theta_1$$
$$G_2 = -[m_2 d_2 + m_3 \ell_2 + m_4 \ell_2 + m_5 \ell_2] g \sin\theta_2$$
$$G_3 = -[m_3 d_3] g \sin\theta_3$$
$$G_4 = [m_4 (\ell_4 - d_4) + m_5 \ell_4] g \sin\theta_4$$
$$G_5 = [m_5 (\ell_5 - d_5)] g \sin\theta_5$$

Appendix IV Derivation of the Inequality (4.9)

Inequality (4.8) gives

$$\tanh(\gamma_i|s_i|) > \mu_i .$$

Since

$$\tanh(\gamma_i|s_i|) = \frac{e^{\gamma_i|s_i|} - e^{-\gamma_i|s_i|}}{e^{\gamma_i|s_i|} + e^{-\gamma_i|s_i|}}, \tag{A19}$$

thus

$$\frac{e^{\gamma_i|s_i|} - e^{-\gamma_i|s_i|}}{e^{\gamma_i|s_i|} + e^{-\gamma_i|s_i|}} > \mu_i , \tag{A20}$$

i.e.,

$$\frac{1-\mu_i}{1+\mu_i} > e^{-2\gamma_i|s_i|}, \tag{A21}$$

or

$$\ln\left(\frac{1-\mu_i}{1+\mu_i}\right) > -2\gamma_i|s_i| . \tag{A22}$$

Thus we have

$$\gamma_i > \frac{1}{2|s_i|}\ln\left(\frac{1-\mu_i}{1+\mu_i}\right). \tag{A23}$$

For all $|s_i| \geq \varepsilon_i$, the following inequality is held

$$\gamma_i > \frac{1}{2\varepsilon_i}\ln\left(\frac{1-\mu_i}{1+\mu_i}\right) \tag{4.9}$$